NUWC-NPT Technical Report 11,043
31 August 1995

# A Three-Dimensional Dynamic Elasticity Solution for Wave Propagation in a Two-Layered Infinite Viscoelastic Solid Cylinder With Outer Fluid Loading

**Mark S. Peloquin**
**Submarine Sonar Department**

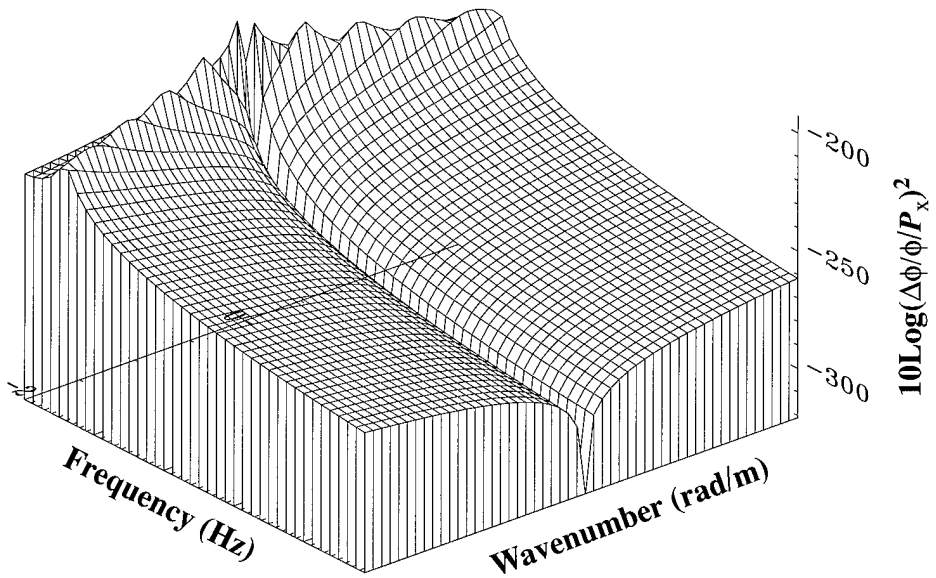




**Naval Undersea Warfare Center Division**
**Newport, Rhode Island**

## PREFACE

The research presented in this report was prepared under two sponsorships. The first was the Ocean, Atmosphere, and Space S&T Department, Sensing and Systems Division, of the Office of Naval Research (ONR), Program Element 0602314N. The ONR Program Manager for Sensors, Sources, and Arrays is K. G. Dial (ONR 321SS). The second sponsor was the NUWC Division Newport Independent Research (IR) Program, Project No. B10008, *Analysis of the First Directly Measured Wall Pressure k-ω Spectra Under a Cylindrical Turbulent Boundary Layer.* The IR program is funded by ONR; the NUWC Division Newport program manager is Dr. S. C. Dickinson (Code 102).

The technical reviewer for this report was Dr. S. A. Austin (Code 2141) of NUWC Detachment New London. The author gratefully acknowledges Dr. Austin for his careful review of the manuscript.

The author wishes to thank Karen Holt (Code 0251) of NUWC Detachment New London for her meticulous technical editing.

**Reviewed And Approved: 31 August 1995**

**R. J. Martin**
**Acting Head, Submarine Sonar Department**

# DISCLAIMER NOTICE

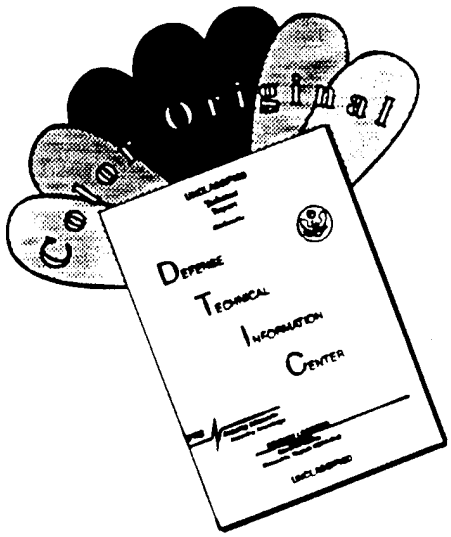


THIS DOCUMENT IS BEST QUALITY AVAILABLE. THE COPY FURNISHED TO DTIC CONTAINED A SIGNIFICANT NUMBER OF COLOR PAGES WHICH DO NOT REPRODUCE LEGIBLY ON BLACK AND WHITE MICROFICHE.

# REPORT DOCUMENTATION PAGE

*Form Approved*
*OMB No. 0704-0188*



| 1. AGENCY USE ONLY (Leave Blank) | 2. REPORT DATE | 3. REPORT TYPE AND DATES COVERED |
|---|---|---|
| | 31 August 1995 | Final |

4. TITLE AND SUBTITLE

**A Three-Dimensional Dynamic Elasticity Solution for Wave Propagation in a Two-Layered Infinite Viscoelastic Solid Cylinder With Outer Fluid Loading**

5. FUNDING NUMBERS

6. AUTHOR(S)

Mark S. Peloquin

7. PERFORMING ORGANIZATION NAME(S) AND ADDRESS(ES)

Naval Undersea Warfare Center
Detachment New London
New London, Connecticut 06320

8. PERFORMING ORGANIZATION REPORT NUMBER

TR 11,043

9. SPONSORING/MONITORING AGENCY NAME(S) AND ADDRESS(ES)

Office of Naval Research
800 North Quincy Street
Arlington, VA 22217-5000

Independent Research Program
Naval Undersea Warfare Center
Division Newport
Newport, RI 02841-5047

10. SPONSORING/MONITORING AGENCY REPORT NUMBER

11. SUPPLEMENTARY NOTES

12a. DISTRIBUTION/AVAILABILITY STATEMENT

Approved for public release; distribution is unlimited.

12b. DISTRIBUTION CODE

13. ABSTRACT (Maximum 200 words)

The research presented in this report provides an exact closed form solution to the problem of a two-layered viscoelastic solid infinite cylinder immersed in an infinite ideal inviscid fluid. Damping is incorporated by the use of a complex modulus of elasticity. The composite system is subject to forced harmonic vibration at the solid/fluid interface. The response to both axisymmetric and nonaxisymmetric excitations is derived. A three-dimensional dynamic elasticity solution is obtained. Nonaxisymmetric excitation is described in terms of circumferential order number $n$. For circumferential order numbers $n = 0$ and $n = 1$, simulations are performed for excitations $P_o$ and $P_x$ applied to the single-layer and two-layer cylinders. For excitation $P_\theta$, simulations are performed at $n = 1$ applied to the two-layer cylinder. Simulations are displayed as response transfer surfaces in the longitudinal wavenumber-frequency plane. Material properties consistent with those of an optical fiber and ALCRYN were chosen for the simulations. The strain and optical phase sensitivity of the optical fiber to longitudinal shear stress is 30 to 110 dB greater than the optical fiber sensitivity to radial pressure excitation. In the ALCRYN-coated case, a comparison between the optical phase sensitivity to radial pressure and longitudinal shear stress reveals a shear stress response that is 50 to 70 dB greater than the radial pressure response. This result is consistent with that for the bare optical fiber.

14. SUBJECT TERMS

Dynamic Elasticity Solution, Fluid Loading, Nonaxisymmetric Vibration, Viscoelastic Solid Cylinder, Wave Propagation

15. NUMBER OF PAGES
118

16. PRICE CODE

| 17. SECURITY CLASSIFICATION OF REPORT | 18. SECURITY CLASSIFICATION OF THIS PAGE | 19. SECURITY CLASSIFICATION OF ABSTRACT | 20. LIMITATION OF ABSTRACT |
|---|---|---|---|
| UNCLASSIFIED | UNCLASSIFIED | UNCLASSIFIED | SAR |

# TABLE OF CONTENTS

# TABLE OF CONTENTS (CONT'D)

# LIST OF ILLUSTRATIONS

# LIST OF ILLUSTRATIONS (CONT'D)

# LIST OF ILLUSTRATIONS (CONT'D)

# LIST OF ILLUSTRATIONS (CONT'D)

# LIST OF ILLUSTRATIONS (CONT'D)

## LIST OF ILLUSTRATIONS (CONT'D)



## LIST OF TABLES

# LIST OF SYMBOLS

## Cylinder

$a$ = Outer radius of cylinder 1

$b$ = Outer radius of cylinder 2

$c_e$ = Extensional wave speed

$c_l$ = Dilatational wave speed

$c_t$ = Shear or transverse wave speed

$k_e$ = Extensional wavenumber

$L_e$ = Extensional wavelength

$r$ = Radial coordinate

$x$ = Axial coordinate

$\theta$ = Angular coordinate

$E_c$ = General Young's modulus

$E_j^*$ = Complex Young's modulus

$\mu_c$ = General shear modulus

$\lambda_c$ = General Lame constant

$\nu_c$ = General Poisson ratio

$\rho_c$ = General density

$\rho_1$ = Density of cylinder 1

$\zeta_1$ = Structural loss factor for cylinder 1

$\lambda_1$ = Lame constant of cylinder 1

$\nu_1$ = Poisson ratio of cylinder 1

$\rho_2$ = Density of cylinder 2

$\zeta_2$ = Structural loss factor for cylinder 2

$\lambda_2$ = Lame constant of cylinder 2

$\nu_2$ = Poisson ratio of cylinder 2

$\tau_{ij}$ = Components of the stress tensor

$\varepsilon_{ij}$ = Components of the strain tensor

$\boldsymbol{u}$ = Displacement vector

$u_i$ = Components of the displacement vector

$\ddot{u}_i$ = Components of the acceleration vector = $\dfrac{\partial^2 u_i}{\partial t^2}$

$f_i$ = Body forces

$\varphi$ = Scalar displacement potential = $\varphi(r, \theta, x, t)$

$\psi$ = Vector displacement potential = $\psi(r, \theta, x, t)$

$\psi_r, \psi_\theta, \psi_x$ = Components of the vector displacement potential

$u_c, v_c, w_c$ = Radial, tangential, and longitudinal displacement of a general cylinder (field quantity)

$u_c^{C1}, v_c^{C1}, w_c^{C1}$ = Radial, tangential, and longitudinal displacement of cylinder 1 (field quantity)

$u_c^{C2}, v_c^{C2}, w_c^{C2}$ = Radial, tangential, and longitudinal displacement of cylinder 2 (field quantity)

$A_1^{C1}, B_1^{C1}, C_1^{C1}$ = Arbitrary constants for cylinder 1

$A_1^{C2}, A_2^{C2}, B_1^{C2}, B_2^{C2}, C_1^{C2}, C_2^{C2}$ = Arbitrary constants for cylinder 2

## Fluid

$\beta$ = Bulk modulus

$c_f$ = Speed of sound in a general fluid

$c_s$ = Speed of sound in the outer fluid

$k_s$ = Outer fluid wavenumber

$L_s$ = Wavelength in the outer fluid

$k_r$ = Radial wavenumber

$\rho_f$ = General fluid density

$\rho_s$ = Outer fluid density

$\varphi_f$ = General fluid displacement potential

$\varphi_s$ = Outer fluid displacement potential

$u_f$ = Particle displacement of a general fluid

$u_s$ = Particle displacement of the outer fluid

$p_f$ = General fluid pressure field

$p_s$ = Outer fluid pressure field

# LIST OF SYMBOLS (CONT'D)

$P_o$ = Amplitude of the normal pressure excitation field

$P_x$ = Amplitude of the axial shear stress excitation field

$P_\theta$ = Amplitude of the circumferential shear stress excitation

$\lambda_f$ = Lame constant

$\mu_f$ = Lame constant (shear modulus)

$\sigma_{ij}$ = Components of the stress tensor for the fluid

$\varepsilon_{kk}$ = Components of the strain tensor for the fluid

$\delta_{ij}$ = Kronecker delta

$H, M$ = Fluid velocity potential field constants

## Cylinder and Fluid

$\alpha$ = Angle relative to radial coordinate $r$

$\omega$ = Angular frequency

$t$ = Time

$k$ = Axial wavenumber ($2\pi/L$)

$L$ = Axial wavelength

$i$ = $\sqrt{-1}$

$n$ = Circumferential order number

$u_{int}$ = Radial displacement at the cylinder/fluid interface

$J_n$ = Bessel function of the first kind

$Y_n$ = Bessel function of the second kind

$I_n$ = Modified Bessel function

$K_n$ = Modified Bessel function

$H_n^{(1)}$ = Hankel function of the first kind

$r_1$ = Calculation radius

## Optical Fiber Properties

$r_c$ = Radius of the optic fiber core

$n_o$ = Optical index of refraction

$\phi$ = Optical phase

$\Delta\phi$ = Change in optical phase

$P_{11}, P_{12}$ = Pockel coefficients

# A THREE-DIMENSIONAL DYNAMIC ELASTICITY SOLUTION FOR WAVE PROPAGATION IN A TWO-LAYERED INFINITE VISCOELASTIC SOLID CYLINDER WITH OUTER FLUID LOADING

## INTRODUCTION

This research, which is a precursor to the case of a two-layered cylinder with inner and outer fluid loading, treats the two-layered solid cylinder subject to forced harmonic vibration within the scope of the linearized theory of dynamic elasticity. In previous efforts, the statically loaded solid cylinder was documented by numerous authors, and the forced vibration response of the solid cylinder was investigated by Holden,[1] Kaul and McCoy,[2] and others.

In the theoretical development presented in this report, the case of nonaxisymmetric vibration is discussed in terms of circumferential order number $n$. Results are presented for the first two-order numbers, specifically $n = 0$ and $n = 1$. Three excitation states are considered: the normal pressure $P_o$, the longitudinal shear stress $P_x$, and the circumferential shear stress $P_\theta$.

The development proceeds using scalar and vector displacement potentials to describe the motion of the solid. The boundary conditions are specified in terms of the stresses and displacements, and thus must be written in terms of the displacement potentials. For the case of the two-layered cylinder, the problem is reduced to solving a 10-by-10 system matrix for the undetermined complex coefficients. This matrix requires inversion at each location in the wavenumber and frequency plane, allowing all dynamic quantities (stress, strain, and displacement) to be calculated from the coefficients. Even though the solution is closed form, a sizeable numerical computation is still necessary to extract information from the equations governing the solution.

An interesting application for the models derived here is in the field of fiber optics. The response of an optical fiber to external pressure loading has been the subject of much investigation in the literature. For example, in the early eighties Lagakos[3] developed static elasticity descriptions for the behavior of a coated optical fiber subject to external pressure loading. More recently, Hull[4] developed a model for the optical phase sensitivity of a bare

optical fiber subject to an axisymmetric pressure excitation at a definite wavenumber and frequency. What has been lacking in the field of fiber optics, however, is a dynamic model for the viscoelastic coated fiber subject to both axisymmetric and nonaxisymmetric forced vibration at definite wavenumber and frequency. This report describes such a model and presents results for a cylinder with material properties and dimensions consistent with those of an optical fiber. Numerical results for both the coated fiber (with an outer diameter of 8 mm) and bare fiber are presented.

## THE PHYSICAL MODEL

The physical model under analysis is shown in figure 1. A solid cylinder (cylinder 1) of radius $a$ is joined to a second cylinder (cylinder 2). Cylinder 2 is in intimate contact with cylinder 1 at radius $r = a$, extending to radius $r = b$. At radial distance $b$, cylinder 2 is in contact with the outer fluid. The outer fluid extends to infinity in radial coordinate $r$. The cylinders and fluid extend to plus and minus infinity in the longitudinal $x$-direction.

As stated earlier, the system is treated within the context of the linearized theory of elasticity. The assumption of linearity implies that both the cylinders and fluid obey linear constitutive equations. For the cylinders, this means that there is a linear relationship between stress and

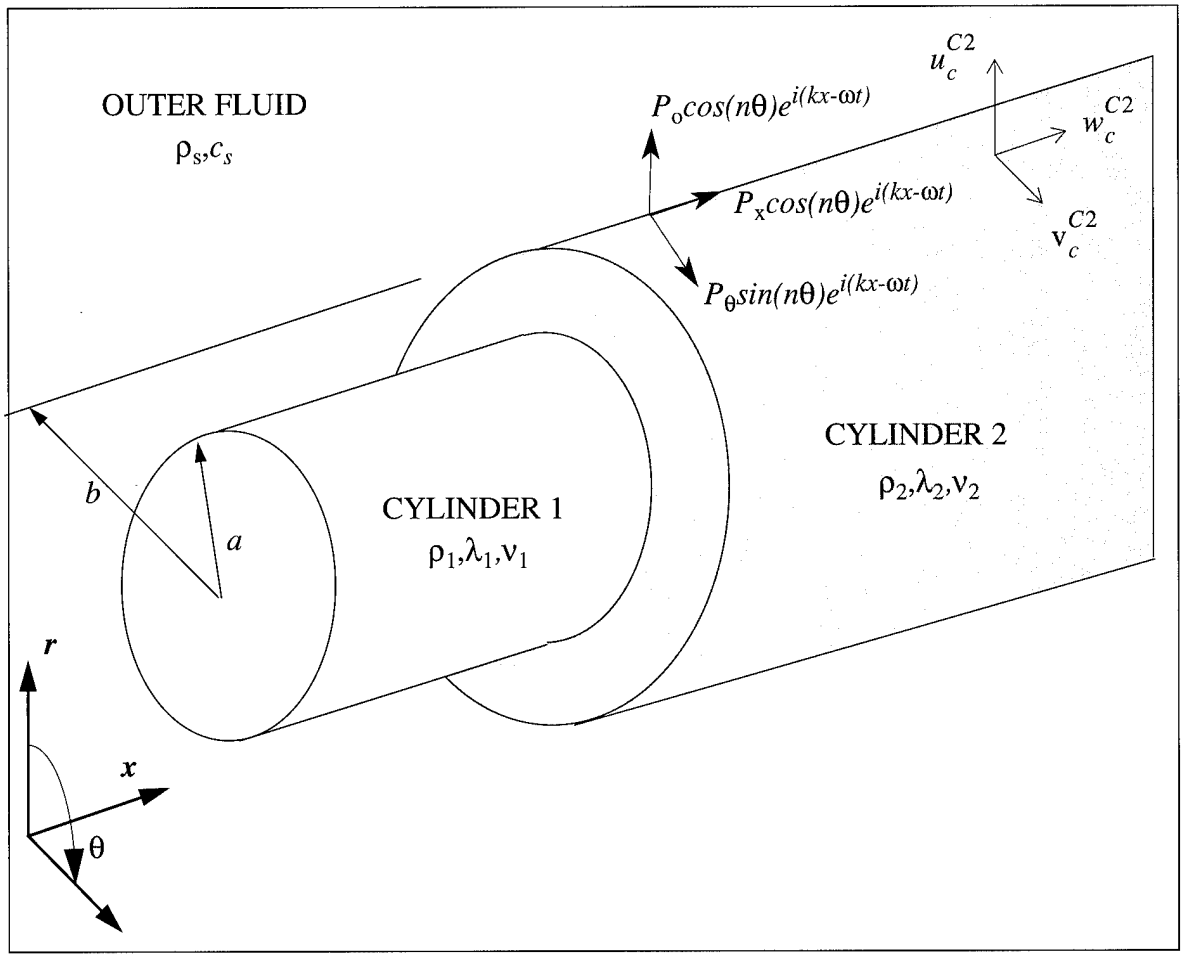


**Figure 1. Physical Model Diagram**

strain. For the fluid, deviations from the hydrostatic pressure are a linear function of the condensation (fractional density change) and similarly the dilatation (volume strain). Strains are assumed to be small compared to unity for both the cylinder and fluid; the response therefore is linearly related to the excitation. Both media are restricted to small signal analysis, i.e., excitation levels on the acoustic scale.

Damping is included by the use of a complex modulus of elasticity—the well-known structural damping form. Both cylinders are treated distinctly because each possesses different material properties. The outer fluid is modeled as inviscid for the purpose of fluid loading the moving structure. The radial velocity of the fluid and the second cylinder are identically equal at $r = b$. Under the inviscid assumption, the outer fluid interacts with only the radial motion of the cylinder and is uncoupled from the circumferential and longitudinal motions. A perfect slip condition is allowed between the cylinder and fluid for the longitudinal and circumferential directions. These assumptions avoid boundary layer physics within the context of this development.

Three harmonic excitations are applied by the outer fluid to cylinder 2 at $r = b$: a radial pressure $P_o$, shear stress $P_x$, and shear stress $P_\theta$. In practice, the shear stresses $P_x$ and $P_\theta$ would only be developed by the viscosity of a real outer fluid. Therefore, the amplitude distribution (at $r = b$) of the excitations in the wavenumber and frequency domain must be known *a priori*; otherwise a calculated quantity is normalized by an excitation stress magnitude. As shown in figure 1, the excitations are at a definite wavenumber ($k$) and frequency ($\omega$) and are of circumferential order number $n$. The response of the cylinder will therefore be a function of $k$, $\omega$, and $n$, as well as of the geometric and material properties of the composite system.

# EQUATIONS OF MOTION

## DISPLACEMENT POTENTIALS

The equations governing the motion of a homogeneous, isotropic, linearly elastic body are formulated with the strain-displacement relations (equation (1)), the constitutive relations (equation (2)), and the stress equations of motion (equation (3)) of reference 5:

$$\varepsilon_{ij} = \frac{1}{2}(u_{i,j} + u_{j,i}) \ , \tag{1}$$

$$\tau_{ij} = \lambda_c \varepsilon_{kk} \delta_{ij} + 2\mu_c \varepsilon_{ij} \ , \tag{2}$$

and

$$\tau_{ij,j} + \rho_c f_i = \rho_c \ddot{u}_i \ , \tag{3}$$

where $\varepsilon_{ij}$ are the components of the strain tensor, $\tau_{ij}$ are the components of the stress tensor, $u_i$ are the components of displacement, and $\rho_c$ is the density of the cylinder. The components of acceleration are indicated by $\ddot{u}_i$ and the body forces are indicated by $f_i$. The comma denotes partial differentiation in equations (1) and (3) as

$$u_{i,j} = \frac{\partial u_i}{\partial x_j} \ , \qquad \tau_{ij,j} = \frac{\partial \tau_{ij}}{\partial x_j} \ , \tag{4}$$

where the components of the vector of spatial coordinates $x_j$ are equal to $x_1 = r$, $x_2 = \theta$, and $x_3 = x$.

To obtain an equation only in terms of the displacements and their derivatives, equations (1) and (2) are substituted into equation (3), resulting in[6]

$$\mu_c u_{i,jj} + (\lambda_c + \mu_c) u_{j,ji} = \rho_c \ddot{u}_i . \tag{5}$$

Equation (5) is expressed in vector notation as

$$\mu_c \nabla^2 \boldsymbol{u} + (\lambda_c + \mu_c) \nabla \nabla \cdot \boldsymbol{u} = \rho_c \ddot{\boldsymbol{u}} . \tag{6}$$

The displacement vector is decomposed using the scalar and vector relationship

$$\boldsymbol{u} = \nabla\varphi + \nabla\times\psi \ , \tag{7}$$

where $\varphi = \varphi(r, \theta, x, t)$ is the scalar displacement potential and $\psi = \psi(r, \theta, x, t)$ is the vector displacement potential. Equations (6) and (7) reduce to

$$\nabla\left((\lambda_c + 2\mu_c)\nabla^2\varphi - \rho_c\ddot{\varphi}\right) + \nabla\times\left(\mu_c\nabla^2\psi - \rho_c\ddot{\psi}\right) = 0 . \tag{8}$$

From equation (8), we obtain the following scalar and vector displacement potentials:

$$\nabla^2\varphi = \frac{1}{c_l^2}\ddot{\varphi} \tag{9}$$

and

$$\nabla^2\psi = \frac{1}{c_t^2}\ddot{\psi} . \tag{10}$$

The dilatational and shear wave phase velocities are given by

$$c_l^2 = \frac{\lambda_c + 2\mu_c}{\rho_c} , \qquad c_t^2 = \frac{\mu_c}{\rho_c} , \tag{11}$$

where the Lame constants $\lambda_c$ and $\mu_c$ are equal to $\lambda_c = \dfrac{E_c\nu_c}{(1+\nu_c)(1-2\nu_c)}$ and the shear modulus of the material, respectively.[7]

For the present cylindrical geometry, we have the following scalar and uncoupled vector potentials:

$$\nabla^2\varphi = \frac{1}{c_l^2}\ddot{\varphi} \tag{12}$$

and

$$\nabla^2\psi_x = \frac{1}{c_t^2}\ddot{\psi}_x . \tag{13}$$

Two coupled vector potentials in $r$ and $\theta$ are

$$\nabla^2\psi_r - \frac{\psi_r}{r^2} - \frac{2}{r^2}\frac{\partial\psi_\theta}{\partial\theta} = \frac{1}{c_t^2}\frac{\partial^2\psi_r}{\partial t^2} \tag{14}$$

and

$$\nabla^2\psi_\theta - \frac{\psi_\theta}{r^2} + \frac{2}{r^2}\frac{\partial\psi_r}{\partial\theta} = \frac{1}{c_t^2}\frac{\partial^2\psi_\theta}{\partial t^2}. \tag{15}$$

The Laplacian is defined in cylindrical coordinates as

$$\nabla^2 = \frac{\partial^2}{\partial r^2} + \frac{1}{r}\frac{\partial}{\partial r} + \frac{1}{r^2}\frac{\partial^2}{\partial\theta^2} + \frac{\partial^2}{\partial x^2}. \tag{16}$$

Considering the scalar potential given by equation (12), we will assume a separation-of-variables-type solution in $r$ and $\theta$. The scalar potential $\varphi(r, \theta, x, t)$ is then of the form

$$\varphi = \Omega(r)\,\Theta(\theta)\,e^{i(kx-\omega t)}. \tag{17}$$

Equation (12) yields the following two equations:

$$\frac{d^2\Omega}{dr^2} + \frac{1}{r}\frac{d\Omega}{dr} + \left(\frac{\omega^2}{c_l^2} - k^2\right)\Omega - \frac{n^2}{r^2}\Omega = 0 \tag{18}$$

and

$$\frac{d^2\Theta}{d\theta^2} + n^2\Theta = 0. \tag{19}$$

The solution of equation (18) is in terms of Bessel functions. For a solid cylinder, such as cylinder 1, the field quantities must be finite at the center ($r = 0$); therefore we retain only Bessel functions of the first kind, $J_n$. However, for a hollow cylinder, such as cylinder 2, Bessel functions of both the first and second kind are retained. The solution to equation (19) is in terms

of the sine and cosine of argument $n\theta$. The total solution is therefore

$$\varphi = [A_1 \cos(n\theta) + A_2 \sin(n\theta)] J_n(pr)\, e^{i(kx-\omega t)}, \tag{20}$$

with $p$ defined as

$$p^2 = \frac{\omega^2}{c_l^2} - k^2. \tag{21}$$

A similar solution for the $x$-component of the vector potential, $\psi_x$, is

$$\psi_x = [B_1 \cos(n\theta) + B_2 \sin(n\theta)] J_n(qr)\, e^{i(kx-\omega t)}, \tag{22}$$

with $q$ defined as

$$q^2 = \frac{\omega^2}{c_t^2} - k^2. \tag{23}$$

The potentials for $\psi_r$ and $\psi_\theta$ can be uncoupled by noting that $\psi_r$ and $\psi_\theta$ contain trigonometric functions of $\theta$ and that a sine dependence on $\theta$ in $\psi_r$ is equivalent with a cosine dependence on $\theta$ in $\psi_\theta$, and vice versa.[8] With the use of the condition $\nabla \cdot \psi = 0$ to eliminate an extra constant, $\psi_r$ and $\psi_\theta$ become

$$\psi_r = [C_1 J_{n+1}(qr)] \sin(n\theta)\, e^{i(kx-\omega t)} \tag{24}$$

and

$$\psi_\theta = [-C_1 J_{n+1}(qr)] \cos(n\theta)\, e^{i(kx-\omega t)}. \tag{25}$$

### *Displacement Potential Summary for Cylinder 1*

In summary, the displacement potentials for the solid cylinder are given in terms of Bessel functions of the first kind,[9] with argument $p$ being based on the dilatational wave phase velocity and argument $q$ on the shear wave phase velocity as follows:

$$\varphi = A_1 J_n(pr)\cos(n\theta)\, e^{i(kx-\omega t)},$$

$$\psi_x = B_1 J_n(qr)\sin(n\theta)\, e^{i(kx-\omega t)},$$

$$\psi_r = C_1 J_{n+1}(qr)\sin(n\theta)\, e^{i(kx-\omega t)},$$

$$\psi_\theta = -C_1 J_{n+1}(qr)\cos(n\theta)\, e^{i(kx-\omega t)},$$

$$p^2 = \frac{\omega^2}{c_l^2} - k^2, \qquad q^2 = \frac{\omega^2}{c_t^2} - k^2 . \tag{26}$$

### *Displacement Potential Summary for Cylinder 2*

The outer cylinder requires Bessel functions of the first and second kind. The summary of the scalar and vector displacement potentials is

$$\varphi = [A_1 J_n(pr) + A_2 Y_n(pr)]\cos(n\theta)\, e^{i(kx-\omega t)},$$

$$\psi_x = [B_1 J_n(qr) + B_2 Y_n(qr)]\sin(n\theta)\, e^{i(kx-\omega t)},$$

$$\psi_r = [C_1 J_{n+1}(qr) + C_2 Y_{n+1}(qr)]\sin(n\theta)\, e^{i(kx-\omega t)},$$

$$\psi_\theta = [-C_1 J_{n+1}(qr) - C_2 Y_{n+1}(qr)]\cos(n\theta)\, e^{i(kx-\omega t)},$$

$$p^2 = \frac{\omega^2}{c_l^2} - k^2, \qquad q^2 = \frac{\omega^2}{c_t^2} - k^2 . \tag{27}$$

## PARTICLE DISPLACEMENT/DISPLACEMENT POTENTIAL

Intermediate relationships between the particle displacements and the displacement potentials are given by equations (28) through (30),[10] where $u_c$ is the displacement in the $r$-direction, $v_c$ is the displacement in the circumferential θ-direction, and $w_c$ is the displacement in the longitudinal $x$-direction:

$$u_c = \frac{\partial \varphi}{\partial r} + \frac{1}{r}\frac{\partial \psi_x}{\partial \theta} - \frac{\partial \psi_\theta}{\partial x}, \tag{28}$$

$$v_c = \frac{1}{r}\frac{\partial \varphi}{\partial \theta} + \frac{\partial \psi_r}{\partial x} - \frac{\partial \psi_x}{\partial r}, \tag{29}$$

and

$$w_c = \frac{\partial \varphi}{\partial x} + \frac{1}{r}\frac{\partial}{\partial r}(\psi_\theta r) - \frac{1}{r}\frac{\partial \psi_r}{\partial \theta}. \tag{30}$$

## STRESS/DISPLACEMENT EQUATIONS

In the problem posed, the boundary conditions are prescribed with the stresses and displacements. Equations (31) through (36) relate the stress components to the particle displacements. We now have a complete progression from displacement potentials to stresses, which will allow us to solve for the motion of the composite system:

$$\tau_{rr} = \lambda_c\left(\frac{\partial u_c}{\partial r} + \frac{u_c}{r} + \frac{1}{r}\frac{\partial v_c}{\partial \theta} + \frac{\partial w_c}{\partial x}\right) + 2\mu_c\frac{\partial u_c}{\partial r}, \tag{31}$$

$$\tau_{\theta\theta} = \lambda_c\left(\frac{\partial u_c}{\partial r} + \frac{u_c}{r} + \frac{1}{r}\frac{\partial v_c}{\partial \theta} + \frac{\partial w_c}{\partial x}\right) + 2\mu_c\left(\frac{u_c}{r} + \frac{1}{r}\frac{\partial v_c}{\partial \theta}\right), \tag{32}$$

$$\tau_{xx} = \lambda_c\left(\frac{\partial u_c}{\partial r} + \frac{u_c}{r} + \frac{1}{r}\frac{\partial v_c}{\partial \theta} + \frac{\partial w_c}{\partial x}\right) + 2\mu_c\frac{\partial w_c}{\partial x}, \tag{33}$$

$$\tau_{r\theta} = \mu_c\left(\frac{\partial v_c}{\partial r} - \frac{v_c}{r} + \frac{1}{r}\frac{\partial u_c}{\partial \theta}\right), \tag{34}$$

$$\tau_{\theta x} = \mu_c\left(\frac{1}{r}\frac{\partial w_c}{\partial \theta} + \frac{\partial v_c}{\partial x}\right), \tag{35}$$

and

$$\tau_{rx} = \mu_c\left(\frac{\partial u_c}{\partial x} + \frac{\partial w_c}{\partial r}\right). \tag{36}$$

The indicial notation is interpreted in the following manner. The first index refers to the plane normal to the coordinate identified by the first index. The second index refers to the direction in which the stress acts. Stresses $\tau_{rr}$, $\tau_{\theta\theta}$, and $\tau_{xx}$ are normal stresses, whereas $\tau_{rr}$ is a stress acting in the plane perdendicular to the radial coordinate in the radial direction. The remaining three stresses ($\tau_{r\theta}$, $\tau_{\theta x}$, and $\tau_{rx}$) are shear stresses. Shear stress $\tau_{r\theta}$ indicates a shear stress acting in the plane perpendicular to the radial coordinate in the circumferential $\theta$-direction.

## STRAIN/DISPLACEMENT EQUATIONS

These equations will be required for the particular output needed in the simulations that follow:

$$\varepsilon_{rr} = \frac{\partial u_c}{\partial r}, \tag{37}$$

$$\varepsilon_{\theta\theta} = \frac{u_c}{r} + \frac{1}{r}\frac{\partial v_c}{\partial \theta}, \tag{38}$$

and

$$\varepsilon_{zz} = \frac{\partial w_c}{\partial z}. \tag{39}$$

## STRESS, STRAIN, AND DISPLACEMENTS IN TERMS OF DISPLACEMENT POTENTIAL EQUATIONS

The stress equations needed to compose a suitable set for the application of the boundary conditions, together with the displacement equations, are written in terms of the displacement potentials by substituting equations (28) through (30) into equations (31), (34), and (36) to obtain equations (40), (41) and (42):

$$\tau_{rr} = \lambda_c\left(\frac{\partial^2\varphi_c}{\partial r^2} + \frac{1}{r}\frac{\partial\varphi_c}{\partial r} + \frac{1}{r^2}\frac{\partial^2\varphi_c}{\partial\theta^2} + \frac{\partial^2\varphi_c}{\partial x^2}\right) + 2\mu_c\left(\frac{\partial^2\varphi_c}{\partial r^2} - \frac{1}{r^2}\frac{\partial\psi_x}{\partial\theta} + \frac{1}{r}\frac{\partial^2\psi_x}{\partial\theta\partial r} - \frac{\partial^2\psi_\theta}{\partial x\partial r}\right), \quad (40)$$

$$\tau_{r\theta} = \mu_c\left(-\frac{2}{r^2}\frac{\partial\varphi_c}{\partial\theta} + \frac{2}{r}\frac{\partial^2\varphi_c}{\partial\theta\partial r} + \frac{\partial^2\psi_r}{\partial x\partial r} - \frac{1}{r}\frac{\partial\psi_r}{\partial x} - \frac{1}{r}\frac{\partial^2\psi_\theta}{\partial x\partial\theta} - \frac{\partial^2\psi_x}{\partial r^2} + \frac{1}{r}\frac{\partial\psi_x}{\partial r} + \frac{1}{r^2}\frac{\partial^2\psi_x}{\partial\theta^2}\right), \quad (41)$$

$$\tau_{rx} = \mu_c\left(2\frac{\partial^2\varphi_c}{\partial r\partial x} + \frac{1}{r^2}\frac{\partial\psi_r}{\partial\theta} - \frac{1}{r}\frac{\partial^2\psi_r}{\partial\theta\partial r} - \frac{\partial^2\psi_\theta}{\partial x^2} + \frac{\partial^2\psi_\theta}{\partial r^2} - \frac{1}{r^2}\psi_\theta + \frac{1}{r}\frac{\partial\psi_\theta}{\partial r} + \frac{1}{r}\frac{\partial^2\psi_x}{\partial\theta\partial x}\right). \quad (42)$$

This same substitution is performed on strain equations (37), (38), and (39) to obtain equations (43), (44), and (45):

$$\varepsilon_{rr} = \frac{\partial^2\varphi_c}{\partial r^2} - \frac{1}{r^2}\frac{\partial\psi_x}{\partial\theta} + \frac{1}{r}\frac{\partial^2\psi_x}{\partial\theta\partial r} - \frac{\partial^2\psi_\theta}{\partial x\partial r}, \quad (43)$$

$$\varepsilon_{\theta\theta} = \frac{1}{r}\frac{\partial\varphi_c}{\partial r} + \frac{1}{r^2}\frac{\partial\psi_x}{\partial\theta} - \frac{1}{r}\frac{\partial\psi_\theta}{\partial x} + \frac{1}{r^2}\frac{\partial^2\varphi_c}{\partial\theta^2} + \frac{1}{r}\frac{\partial^2\psi_r}{\partial x\partial\theta} - \frac{1}{r}\frac{\partial^2\psi_x}{\partial\theta\partial r}, \quad (44)$$

$$\varepsilon_{xx} = \frac{\partial^2\varphi_c}{\partial x^2} + \frac{\partial^2\psi_\theta}{\partial x\partial r} + \frac{1}{r}\frac{\partial\psi_\theta}{\partial x} - \frac{1}{r}\frac{\partial^2\psi_r}{\partial x\partial\theta}. \quad (45)$$

Equations (46), (47), and (48) are repeated to aid the reader:

$$u_c = \frac{\partial \varphi_c}{\partial r} + \frac{1}{r}\frac{\partial \psi_x}{\partial \theta} - \frac{\partial \psi_\theta}{\partial x}, \tag{46}$$

$$v_c = \frac{1}{r}\frac{\partial \varphi_c}{\partial \theta} + \frac{\partial \psi_r}{\partial x} - \frac{\partial \psi_x}{\partial r}, \tag{47}$$

and

$$w_c = \frac{\partial \varphi_c}{\partial x} + \frac{\partial \psi_\theta}{\partial r} + \frac{1}{r}\psi_\theta - \frac{1}{r}\frac{\partial \psi_r}{\partial \theta}. \tag{48}$$

## OUTER FLUID

As the surface of the cylinder is set into motion by the excitation of a pressure wave of magnitude $P_o$, a pressure field, $p_s$, is generated in the outer fluid by the cylinder surface. When the longitudinal wavenumber associated with the vibration of the cylinder surface is smaller than $\omega/c_s$, the pressure radiated into the outer fluid is in the form of a propagating wave. If the longitudinal wavenumber of the cylinder vibration is greater than $\omega/c_s$, the pressure field decays exponentially from the surface of the cylinder in the positive radial direction. The fluid is modeled as an ideal (nonviscous) linearly elastic media that cannot sustain shear stress, even when it is in motion.[11] The equation of state is then

$$\sigma_{ij} = -p_f \delta_{ij}, \tag{49}$$

whose components are given by Hooke's law, $\sigma_{ij} = \lambda_f \varepsilon_{kk} \delta_{ij} + 2\mu_f \varepsilon_{ij}$, by setting $\mu_f = 0$:

$$\sigma_{11} = \sigma_{22} = \sigma_{33} = \lambda_f \varepsilon_{kk} = -p_f,$$

$$\sigma_{12} = \sigma_{13} = \sigma_{23} = 0. \tag{50}$$

The following scalar displacement potential describes the dynamic motion of the fluid in cylindrical coordinates:[12]

$$\nabla^2 \varphi_f = \frac{1}{c_f^2} \frac{\partial^2 \varphi_f}{\partial t^2}, \tag{51}$$

where

$$\nabla^2 = \frac{\partial^2}{\partial r^2} + \frac{1}{r}\frac{\partial}{\partial r} + \frac{1}{r^2}\frac{\partial^2}{\partial \theta^2} + \frac{\partial^2}{\partial z^2}. \tag{52}$$

In the case of fluids, $c_f = \sqrt{\frac{\lambda_f}{\rho_f}}$, which is equivalent to $c_f = \sqrt{\frac{\beta}{\rho_f}}$, where $\beta$ is the bulk modulus of the fluid. The particle displacement and the pressure in the fluid can be expressed in terms of the displacement potential as follows:

$$u_f = \nabla \varphi_f \tag{53}$$

and

$$p_f = -\rho_f \frac{d^2 \varphi_f}{dt^2} . \tag{54}$$

For propagating wavenumbers, the scalar displacement potential is given by[13]

$$\varphi_s = M H_n^{(1)} (g_2 r) \cos(n\theta) e^{i(kx - \omega t)}, \quad g_2^2 = \frac{\omega^2}{c_s^2} - k^2, \qquad \text{for} \qquad \frac{\omega^2}{c_s^2} > k^2 . \tag{55}$$

For an outgoing wave described by $e^{i(k_r r - \omega t)}$, the field in the outer fluid is physically a radiation from the surface of the moving cylinder. The radial dependence in equation (55) is a Hankel function of the first kind, indicated by superscript (1); i.e., $H_n^{(1)} (g_2 r) = J_n (g_2 r) + i Y_n (g_2 r)$ .

Differentiating equation (55) with respect to radius and time yields equations (56) through (58) for the fluid pressure, particle displacement, and particle acceleration, respectively:

$$p_s = \omega^2 \rho_s M H_n^{(1)} (g_2 r) \cos(n\theta) e^{i(kx - \omega t)}, \tag{56}$$

$$u_s = M \frac{\partial}{\partial r} H_n^{(1)} (g_2 r) \cos(n\theta) e^{i(kx - \omega t)}, \tag{57}$$

and

$$\frac{\partial^2 u_s}{\partial t^2} = \omega^2 M \frac{\partial}{\partial r} H_n^{(1)} (g_2 r) \cos(n\theta) e^{i(kx - \omega t)} . \tag{58}$$

For nonpropagating wavenumbers in the outer fluid, the evanescently decaying field is given by the following displacement potential, where the radial dependence is in the form of the modified Bessel function $K_n$:

$$\varphi_s = H K_n (f_2 r) \cos(n\theta) e^{i(kx - \omega t)}, \quad f_2^2 = k^2 - \frac{\omega^2}{c_s^2}, \quad \text{for} \quad k^2 > \frac{\omega^2}{c_s^2} . \tag{59}$$

Similar to the above discussion of the propagating case, the pressure, particle displacement, and particle acceleration are given by equations (60) through (62) as

$$p_s = \omega^2 \rho_s H K_n(f_2 r) \cos(n\theta)\, e^{i(kx-\omega t)}, \tag{60}$$

$$u_s = H \frac{\partial}{\partial r} K_n(f_2 r) \cos(n\theta)\, e^{i(kx-\omega t)}, \tag{61}$$

and

$$\frac{\partial^2 u_s}{\partial t^2} = H \frac{\partial}{\partial r} K_n(f_2 r) \cos(n\theta)\, e^{i(kx-\omega t)}. \tag{62}$$

Figure 2 connects the wavenumber-frequency plane with the time-space characteristics of the field properties in the outer fluid. The vertical axis represents wavenumber with respect to the longitudinal $x$-axis of the cylinder. The horizontal axis is the frequency axis. The positive wavenumber direction corresponds to propagation in the positive $x$-direction and the negative wavenumber direction corresponds to propagation in the negative $x$-direction. There are two distinct regions in the wavenumber-frequency plane corresponding to propagating and non-propagating fields in the outer fluid.

To review, variable $k$ refers to the wavenumber that exists on the surface of the cylinder. The vibrating cylinder surface will initiate a propagating field in the outer fluid when $\omega^2/c_s^2 > k^2$. When this condition exists, the radial displacement ($u_c$) of the cylinder surface must project ($u_c$') onto the propagation direction of the field in the outer fluid. For a given frequency, the wavelength of cylinder vibration must be greater than the corresponding wavelength of vibration that the fluid will propagate. The axisymmetric $n = 0$ vibration produces a symmetric field in the outer fluid as a function of $\theta$. The spatial representation of a point $k_1$ $\omega_1$, in the region of propagating wavenumber-frequency pairs given by $k_s > k_1 > 0$, is shown in figure 3, where $L_1$ is the wavelength and $c_1$ is the velocity of propagation. In the limit of $k_1 \rightarrow 0$, the radiated field is physically a series of cylindrical, radially spreading wavefronts, emanating outward from and parallel to the surface of the cylinder. The intermediate range shown in figure 3 results in the

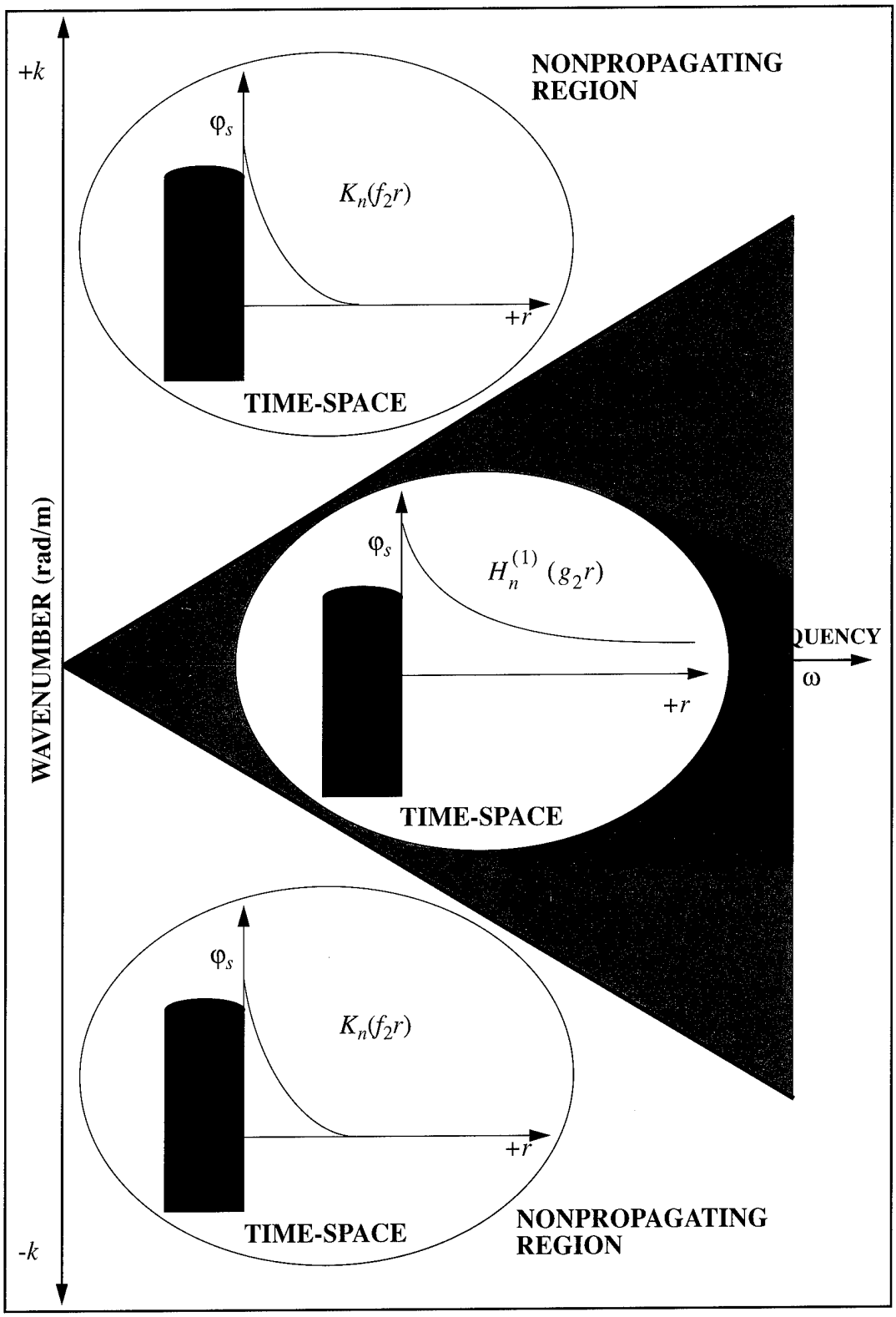


**Figure 2. Outer Fluid Propagating and Nonpropagating Regions of the Wavenumber-Frequency Plane**

wavefronts propagating out along conical planes forming an angle α with the longitudinal $x$-axis of the cylinder (figure 3). The direction, α, of the radiated field relative to the longitudinal $x$-axis of the cylinder will be given by equation (63):

$$\alpha = \text{acos}\frac{L_s}{L_1} = \text{acos}\frac{c_s}{c_1} = \text{acos}\frac{k_1}{k_s}. \tag{63}$$

Propagation ceases as $k_1 = k_s$. The fluid will only support propagation at $k_s$, remembering that

$$k_s = \frac{2\pi}{L_s} = \frac{\omega}{c_s}. \tag{64}$$

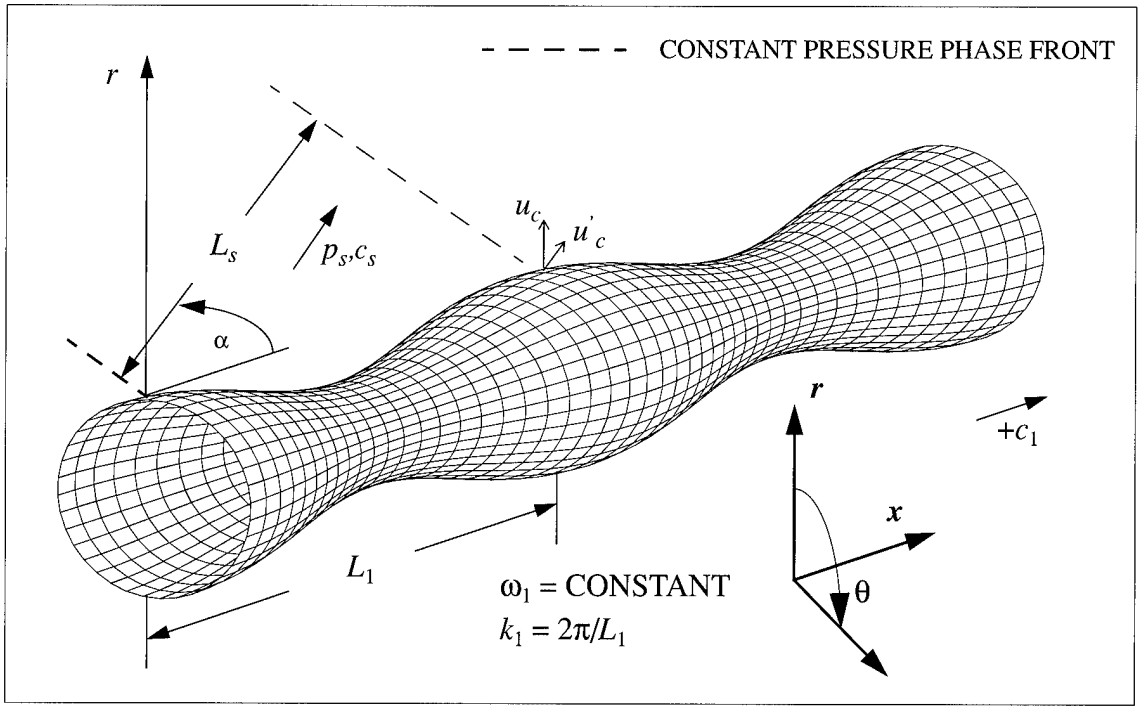


**Figure 3. Relationship Between Cylinder Vibration and Radiated Pressure $p_s$**

The condition $k_1 = k_s$ requires that $c_1 = c_s$; therefore the propagation in the fluid would be along the longitudinal $x$-direction. However, there is only coupling between the cylinder motion

and a propagating fluid pressure field when the radial displacement $u$ can be projected onto the propagation direction of the fluid. This is not possible when $k_1 = k_s$ since $u$ and $x$ are orthogonal to each other; this condition is the onset of the nonpropagating region shown in figure 2.

The Hankel function variation of the outer fluid displacement potential can be observed in the inset TIME-SPACE diagram in figure 2. This diagram depicts the radial spatial variation of the field quantities at a frozen instant of time.

As a line of constant frequency is traversed in the figure, the cylinder wavelength $L_1$ becomes shorter, ultimately reaching a length less than the length of the corresponding fluid wavelength that supports propagation. Under this condition, there is no longer a component of the radial displacement of the cylinder that can be projected onto the propagation direction of the field in the outer fluid; equation (63) is no longer valid; and the field in the outer fluid, $p_s$, induced by cylinder vibration ceases to propagate. The radial variation of the field quantities is, according to the modified Bessel function depicted in figure 2, for the nonpropagating regions. All field quantities, such as the displacement potential and all parameters related to it, undergo the same spatial variation.

## SOLID CYLINDER/FLUID INTERFACE

## BOUNDARY CONDITIONS

From this point on in the derivation that follows, subscript $c$ (Lame constants) will be replaced with 1 or 2 to indicate cylinder 1 or 2. Superscript $C1$ or $C2$ will be added to all other pertinent quantities to distinguish the first from the second cylinder. The solution to the solid cylinder in contact with an outer fluid is obtained by solving for the constants $A_1^{C1}, B_1^{C1}$, and $C_1^{C1}$ in equations (26) and (27) and for $M$ in equation (55) (or $H$ in equation (59)) for the pertinent boundary conditions by considering the state of stress and displacement at $r = a$ at the cylinder and fluid interface. The four boundary conditions are given by equations (65) through (68) as

Boundary condition 1

$$\tau_{rr}^{C1}\Big|_{r=a} = (-P_o - p_s)\Big|_{r=a}. \tag{65}$$

Boundary condition 2

$$\tau_{rx}^{C1}\Big|_{r=a} = -P_x\Big|_{r=a}. \tag{66}$$

Boundary condition 3

$$\tau_{r\theta}^{C1}\Big|_{r=a} = -P_\theta\Big|_{r=a}. \tag{67}$$

Boundary condition 4

$$u_c^{C1}\Big|_{r=a} = \frac{\partial \varphi_s}{\partial r}\Big|_{r=a}. \tag{68}$$

The first boundary condition for radial stress is assembled by substituting equation (56) and the appropriate derivatives of equation (26) into equation (40). The resulting expression is in terms of the unknown constants for the displacement potentials and is given as

$$\left[ (\lambda_1 + 2\mu_1) A_1^{C1} \frac{\partial^2}{\partial r^2} J_n(p_1 a) + \frac{\lambda_1}{a} A_1^{C1} \frac{\partial}{\partial r} J_n(p_1 a) - \frac{\lambda_1 n^2}{b^2} A_1^{C1} J_n(p_1 a) - B_1^{C1} \frac{2\mu_1 n}{a^2} J_n(q_1 a) \right.$$

$$\left. -\lambda_1 k^2 A_1^{C1} J_n(p_1 a) - B_1^{C1} \frac{2\mu_1 n}{a} \frac{\partial}{\partial r} J_n(q_1 a) + C_1^{C1} 2\mu_1 ik \frac{\partial}{\partial r} J_{n+1}(q_1 a) \right] \cos(n\theta)\, e^{i(kx - \omega t)}$$

$$= -P_o \cos(n\theta)\, e^{i(kx - \omega t)} - \omega^2 \rho_s M H_n^{(1)}(g_2 r) \cos(n\theta)\, e^{i(kx - \omega t)}. \tag{69}$$

The four boundary conditions at $r = a$ are represented diagrammatically in figure 4. All boundary conditions are in effect over the entire area of contact between the cylinder and the outer fluid.

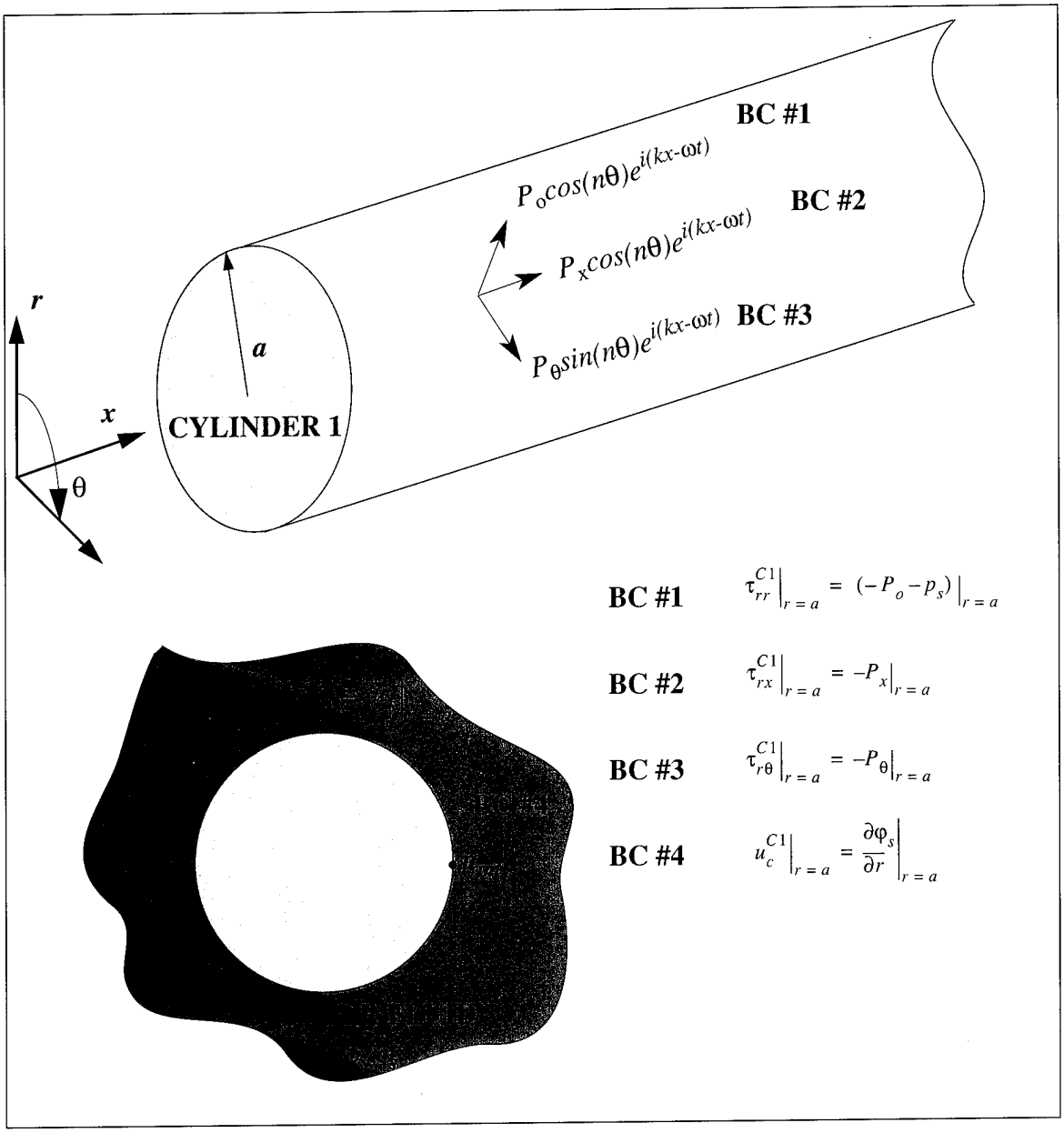


**Figure 4. Boundary Conditions for the Single Solid Infinite Cylinder and Fluid**

## SYSTEM MATRIX

The four boundary conditions in equations (65) through (68) are assembled in matrix form in equation (70):

$$\begin{bmatrix} SR(1,1) & SR(1,2) & SR(1,3) & SR(1,4) \\ SR(2,1) & SR(2,2) & SR(2,3) & 0 \\ SR(3,1) & SR(3,2) & SR(3,3) & 0 \\ SR(4,1) & SR(4,2) & SR(4,3) & SR(4,4) \end{bmatrix} \begin{bmatrix} A_1^{C1} \\ B_1^{C1} \\ C_1^{C1} \\ M \end{bmatrix} = \begin{bmatrix} -P_o \\ -P_x \\ -P_\theta \\ 0 \end{bmatrix}. \tag{70}$$

In numerical order, each boundary condition corresponds to the row number of system matrix *SR*. The elements of the *SR* matrix are shown in equations (71) through (86). Solution of equation (70) at each point in the wavenumber-frequency plane for the vector of unknown constants allows the displacement potentials of the system to be evaluated using equations (26), (55), and (59). Equation (70) will be evaluated for only one forcing function at a time. The coefficients will be normalized by the forcing function stress, which will cast the output in terms of a transfer function in the particular displacement, velocity, stress, or strain of the cylinder.

From boundary condition 1,

$$SR(1,1) = (\lambda_1 + 2\mu_1)\frac{\partial^2}{\partial r^2}J_n(p_1a) + \frac{\lambda_1}{a}\frac{\partial}{\partial r}J_n(p_1a) - \frac{\lambda_1 n^2}{a^2}J_n(p_1a) - k^2\lambda_1 J_n(p_1a), \tag{71}$$

$$SR(1,2) = -2\mu_1\left(\frac{n}{a^2}J_n(q_1a) - \frac{n}{a}\frac{\partial}{\partial r}J_n(q_1a)\right), \tag{72}$$

$$SR(1,3) = 2\mu_1 ik\frac{\partial}{\partial r}J_{n+1}(q_1a), \tag{73}$$

and

$$SR(1,4) = \omega^2\rho_s M H_n^{(1)}(g_2a). \tag{74}$$

From boundary condition 2,

$$SR(2,1) = i2\mu_1 k\frac{\partial}{\partial r}J_n(p_1a), \tag{75}$$

$$SR(2,2) = \frac{i\mu_1 kn}{a} J_n(q_1 a), \tag{76}$$

$$SR(2,3) = \mu_1\left(J_{n+1}(q_1 a)\left(\frac{n+1}{a^2} - k^2\right) - \frac{\partial}{\partial r}J_{n+1}(q_1 a)\left(\frac{n+1}{a}\right) - \frac{\partial^2}{\partial r^2}J_{n+1}(q_1 a)\right), \tag{77}$$

and

$$SR(2,4) = 0. \tag{78}$$

From boundary condition 3,

$$SR(3,1) = 2\mu_1\left(\frac{n}{a^2}J_n(p_1 a) - \frac{n}{a}\frac{\partial}{\partial r}J_n(p_1 a)\right), \tag{79}$$

$$SR(3,2) = \mu_1\left(-\frac{\partial^2}{\partial r^2}J_n(q_1 a) + \frac{1}{a}\frac{\partial}{\partial r}J_n(q_1 a) - \frac{n^2}{a^2}J_n(q_1 a)\right), \tag{80}$$

$$SR(3,3) = ik\mu_1\left(\frac{\partial}{\partial r}J_{n+1}(q_1 a) - J_{n+1}(q_1 a)\left(\frac{1+n}{a}\right)\right), \tag{81}$$

and

$$SR(3,4) = 0. \tag{82}$$

From boundary condition 4,

$$SR(4,1) = \frac{\partial}{\partial r}J_n(p_1 a), \tag{83}$$

$$SR(4,2) = \frac{n}{a}J_n(q_1 a), \tag{84}$$

$$SR(4,3) = ikJ_{n+1}(q_1 a), \tag{85}$$

and

$$SR(4,4) = \frac{\partial}{\partial r}H_n^{(1)}(g_2 a). \tag{86}$$

## DOUBLE SOLID CYLINDER/FLUID INTERFACES

## BOUNDARY CONDITIONS

In this section, we will formulate the boundary conditions for the two-cylinder problem shown in figure 1. At radius $r = b$, the second cylinder/fluid interface, the radial stress in cylinder 2 is set equal to the negative of the magnitude of the pressure in the fluid. Also at radius $r = b$, the radial displacement of the cylinder equals the radial displacement of the fluid. At radius $r = a$, there is continuity of displacements and stress components between each cylinder in the plane of contact perpendicular to the radial coordinate, $\tau_{rr}, \tau_{rx}, \tau_{r\theta}$. For the composite problem, the following description at the boundaries exists:

Boundary condition 1
$$\tau_{rr}^{C2}\Big|_{r=b} = (-P_o - p_s)\Big|_{r=b}. \tag{87}$$

Boundary condition 2
$$\tau_{rx}^{C2}\Big|_{r=b} = -P_x\Big|_{r=b}. \tag{88}$$

Boundary condition 3
$$\tau_{r\theta}^{C2}\Big|_{r=b} = -P_\theta\Big|_{r=b}. \tag{89}$$

Boundary condition 4
$$u_c^{C2}\Big|_{r=b} = u_s\Big|_{r=b}. \tag{90}$$

Boundary condition 5
$$\tau_{rr}^{C2}\Big|_{r=a} = \tau_{rr}^{C1}\Big|_{r=a}. \tag{91}$$

Boundary condition 6
$$\tau_{rx}^{C2}\Big|_{r=a} = \tau_{rx}^{C1}\Big|_{r=a}. \tag{92}$$

Boundary condition 7
$$\tau_{r\theta}^{C2}\Big|_{r=a} = \tau_{r\theta}^{C1}\Big|_{r=a}. \tag{93}$$

Boundary condition 8
$$u_c^{C2}\Big|_{r=a} = u_c^{C1}\Big|_{r=a}. \tag{94}$$

Boundary condition 9
$$v_c^{C2}\Big|_{r=a} = v_c^{C1}\Big|_{r=a}. \tag{95}$$

Boundary condition 10 $$w_c^{C2}\Big|_{r=a} = w_c^{C1}\Big|_{r=a}. \tag{96}$$

The 10 boundary conditions are represented diagrammatically in figure 5 for the double solid cylinder immersed in an outer fluid. All boundary conditions are in effect over the entire surface of contact at radii $r = a$ and $r = b$.

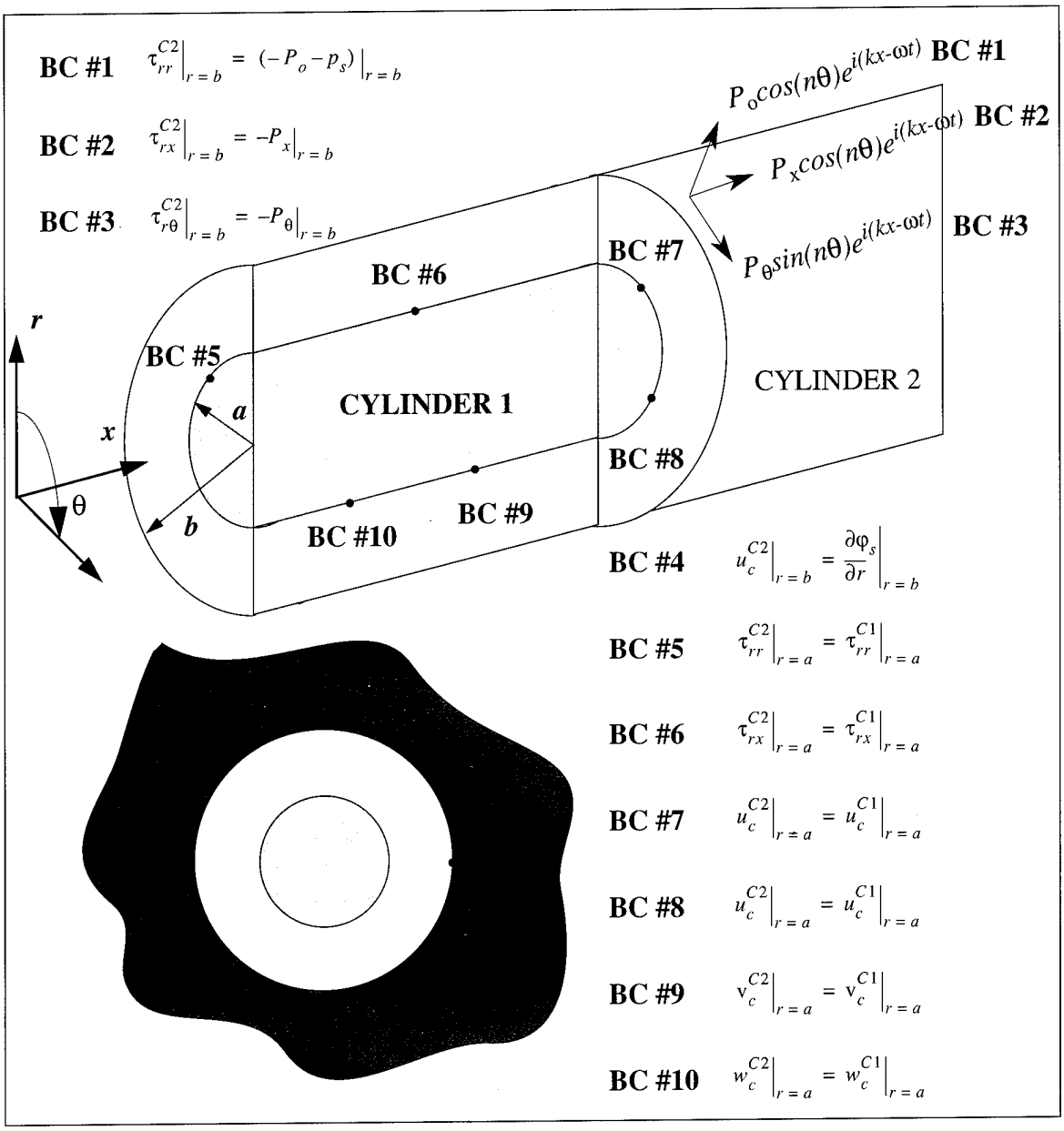


**Figure 5. Boundary Conditions for the Double Solid Cylinder and Fluid**

## SYSTEM MATRIX

The previous 10 boundary conditions are assembled into matrix form in the following expression:

$$\begin{bmatrix} S(1,1) & S(1,2) & S(1,3) & S(1,4) & S(1,5) & S(1,6) & 0 & 0 & 0 & S(1,10) \\ S(2,1) & S(2,2) & S(2,3) & S(2,4) & S(2,5) & S(2,6) & 0 & 0 & 0 & 0 \\ S(3,1) & S(3,2) & S(3,3) & S(3,4) & S(3,5) & S(3,6) & 0 & 0 & 0 & 0 \\ S(4,1) & S(4,2) & S(4,3) & S(4,4) & S(4,5) & S(4,6) & 0 & 0 & 0 & S(4,10) \\ S(5,1) & S(5,2) & S(5,3) & S(5,4) & S(5,5) & S(5,6) & S(5,7) & S(5,8) & S(5,9) & 0 \\ S(6,1) & S(6,2) & S(6,3) & S(6,4) & S(6,5) & S(6,6) & S(6,7) & S(6,8) & S(6,9) & 0 \\ S(7,1) & S(7,2) & S(7,3) & S(7,4) & S(7,5) & S(7,6) & S(7,7) & S(7,8) & S(7,9) & 0 \\ S(8,1) & S(8,2) & S(8,3) & S(8,4) & S(8,5) & S(8,6) & S(8,7) & S(8,8) & S(8,9) & 0 \\ S(9,1) & S(9,2) & S(9,3) & S(9,4) & S(9,5) & S(9,6) & S(9,7) & S(9,8) & S(9,9) & 0 \\ S(10,1) & S(10,2) & 0 & 0 & S(10,5) & S(10,6) & S(10,7) & 0 & S(10,9) & 0 \end{bmatrix} \begin{bmatrix} A_1^{C2} \\ A_2^{C2} \\ B_1^{C2} \\ B_2^{C2} \\ C_1^{C2} \\ C_2^{C2} \\ A_1^{C1} \\ B_1^{C1} \\ C_1^{C1} \\ M \end{bmatrix} = \begin{bmatrix} -P_o \\ -P_x \\ -P_\theta \\ 0 \\ 0 \\ 0 \\ 0 \\ 0 \\ 0 \\ 0 \end{bmatrix}. \quad (97)$$

The elements of equation (97) are given by equations (98) through (197). From boundary condition 1, the first row yields

$$S(1,1) = (\lambda_2 + 2\mu_2)\frac{\partial^2}{\partial r^2}J_n(p_2 b) + \frac{\lambda_2}{b}\frac{\partial}{\partial r}J_n(p_2 b) - \lambda_2 J_n(p_2 b)\left(\frac{n^2}{b^2} + k^2\right), \quad (98)$$

$$S(1,2) = (\lambda_2 + 2\mu_2)\frac{\partial^2}{\partial r^2}Y_n(p_2 b) + \frac{\lambda_2}{b}\frac{\partial}{\partial r}Y_n(p_2 b) - \lambda_2 Y_n(p_2 b)\left(\frac{n^2}{b^2} + k^2\right), \quad (99)$$

$$S(1,3) = -2\mu_2\frac{n}{b^2}\left(J_n(q_2 b) - b\frac{\partial}{\partial r}J_n(q_2 b)\right), \quad (100)$$

$$S(1,4) = -2\mu_2\frac{n}{b^2}\left(Y_n(q_2 b) - b\frac{\partial}{\partial r}Y_n(q_2 b)\right), \quad (101)$$

$$S(1,5) = i2\mu_2 k\frac{\partial}{\partial r}J_{n+1}(q_2 b), \quad (102)$$

$$S(1,6) = i2\mu_2 k\frac{\partial}{\partial r}Y_{n+1}(q_2 b), \quad (103)$$

$$S(1,7) = 0, \tag{104}$$

$$S(1,8) = 0, \tag{105}$$

$$S(1,9) = 0, \tag{106}$$

and

$$S(1,10) = \omega^2 \rho_s M H_n^{(1)}(g_2 b) . \tag{107}$$

From boundary condition 2,

$$S(2,1) = i2\mu_2 k\frac{\partial}{\partial r}J_n(p_2 b), \tag{108}$$

$$S(2,2) = i2\mu_2 k\frac{\partial}{\partial r}Y_n(p_2 b), \tag{109}$$

$$S(2,3) = \frac{i\mu_2 kn}{b}J_n(q_2 b), \tag{110}$$

$$S(2,4) = \frac{i\mu_2 kn}{b}Y_n(q_2 b), \tag{111}$$

$$S(2,5) = \mu_2\left(J_{n+1}(q_2 b)\left(\frac{n+1}{b^2}-k^2\right)-\frac{\partial}{\partial r}J_{n+1}(q_2 b)\left(\frac{n+1}{b}\right)-\frac{\partial^2}{\partial r^2}J_{n+1}(q_2 b)\right), \tag{112}$$

$$S(2,6) = \mu_2\left(Y_{n+1}(q_2 b)\left(\frac{n+1}{b^2}-k^2\right)-\frac{\partial}{\partial r}Y_{n+1}(q_2 b)\left(\frac{n+1}{b}\right)-\frac{\partial^2}{\partial r^2}Y_{n+1}(q_2 b)\right), \tag{113}$$

$$S(2,7) = 0, \tag{114}$$

$$S(2,8) = 0, \tag{115}$$

$$S(2,9) = 0, \tag{116}$$

and

$$S(2,10) = 0. \tag{117}$$

From boundary condition 3,

$$S(3,1) = \frac{2\mu_2 n}{b}\left(\frac{1}{b}J_n(p_2 b) - \frac{\partial}{\partial r}J_n(p_2 b)\right), \tag{118}$$

$$S(3,2) = \frac{2\mu_2 n}{b}\left(\frac{1}{b}Y_n(p_2 b) - \frac{\partial}{\partial r}Y_n(p_2 b)\right), \tag{119}$$

$$S(3,3) = \mu_2\left(-\frac{\partial^2}{\partial r^2}J_n(q_2 b) + \frac{1}{b}\frac{\partial}{\partial r}J_n(q_2 b) - \frac{n^2}{b^2}J_n(q_2 b)\right), \tag{120}$$

$$S(3,4) = \mu_2\left(-\frac{\partial^2}{\partial r^2}Y_n(q_2 b) + \frac{1}{b}\frac{\partial}{\partial r}Y_n(q_2 b) - \frac{n^2}{b^2}Y_n(q_2 b)\right), \tag{121}$$

$$S(3,5) = ik\mu_2\left(\frac{\partial}{\partial r}J_{n+1}(q_2 b) - J_{n+1}(q_2 b)\left(\frac{1+n}{b}\right)\right), \tag{122}$$

$$S(3,6) = ik\mu_2\left(\frac{\partial}{\partial r}Y_{n+1}(q_2 b) - Y_{n+1}(q_2 b)\left(\frac{1+n}{b}\right)\right), \tag{123}$$

$$S(3,7) = 0, \tag{124}$$

$$S(3,8) = 0, \tag{125}$$

$$S(3,9) = 0, \tag{126}$$

and

$$S(3,10) = 0. \tag{127}$$

From boundary condition 4,

$$S(4, 1) = \frac{\partial}{\partial r} J_n(p_2 b), \tag{128}$$

$$S(4, 2) = \frac{\partial}{\partial r} Y_n(p_2 b), \tag{129}$$

$$S(4, 3) = \frac{n}{b} J_n(q_2 b), \tag{130}$$

$$S(4, 4) = \frac{n}{b} Y_n(q_2 b), \tag{131}$$

$$S(4, 5) = ikJ_{n+1}(q_2 b), \tag{132}$$

$$S(4, 6) = ikY_{n+1}(q_2 b), \tag{133}$$

$$S(4, 7) = 0, \tag{134}$$

$$S(4, 8) = 0, \tag{135}$$

$$S(4, 9) = 0, \tag{136}$$

and

$$S(4, 10) = -\frac{\partial}{\partial r} H_n^{(1)}(g_2 b). \tag{137}$$

From boundary condition 5,

$$S(5,1) = (\lambda_2 + 2\mu_2)\frac{\partial^2}{\partial r^2}J_n(p_2a) + \frac{\lambda_2}{a}\frac{\partial}{\partial r}J_n(p_2a) - \lambda_2 J_n(p_2a)\left(\frac{n^2}{a^2} + k^2\right), \tag{138}$$

$$S(5,2) = (\lambda_2 + 2\mu_2)\frac{\partial^2}{\partial r^2}Y_n(p_2a) + \frac{\lambda_2}{a}\frac{\partial}{\partial r}Y_n(p_2a) - \lambda_2 Y_n(p_2a)\left(\frac{n^2}{a^2} + k^2\right), \tag{139}$$

$$S(5,3) = -2\mu_2\frac{n}{a^2}\left(J_n(q_2a) - a\frac{\partial}{\partial r}J_n(q_2a)\right), \tag{140}$$

$$S(5,4) = -2\mu_2\frac{n}{a^2}\left(Y_n(q_2a) - a\frac{\partial}{\partial r}Y_n(q_2a)\right), \tag{141}$$

$$S(5,5) = i2\mu_2 k\frac{\partial}{\partial r}J_{n+1}(q_2a), \tag{142}$$

$$S(5,6) = i2\mu_2 k\frac{\partial}{\partial r}Y_{n+1}(q_2a), \tag{143}$$

$$S(5,7) = (\lambda_1 + 2\mu_1)\frac{\partial^2}{\partial r^2}J_n(p_1a) + \frac{\lambda_1}{a}\frac{\partial}{\partial r}J_n(p_1a) - \lambda_1 J_n(p_1a)\left(\frac{n^2}{a^2} + k^2\right), \tag{144}$$

$$S(5,8) = \frac{-2\mu_1 n}{a}\left(\frac{\partial}{\partial r}J_n(q_1a) - \frac{1}{a}J_n(q_1a)\right), \tag{145}$$

$$S(5,9) = -2\mu_1 ik\frac{\partial}{\partial r}J_{n+1}(q_1a), \tag{146}$$

and

$$S(5,10) = 0. \tag{147}$$

From boundary condition 6,

$$S(6,1) = i2\mu_2 k\frac{\partial}{\partial r}J_n(p_2a), \tag{148}$$

$$S(6,2) = i2\mu_2 k\frac{\partial}{\partial r}Y_n(p_2a), \tag{149}$$

$$S(6,3) = \frac{i\mu_2 kn}{a}J_n(q_2a), \tag{150}$$

$$S(6,4) = \frac{i\mu_2 kn}{a}Y_n(q_2a), \tag{151}$$

$$S(6,5) = \mu_2\left(J_{n+1}(q_2a)\left(\frac{n+1}{a^2}-k^2\right)-\frac{\partial}{\partial r}J_{n+1}(q_2a)\left(\frac{n+1}{a}\right)-\frac{\partial^2}{\partial r^2}J_{n+1}(q_2a)\right), \tag{152}$$

$$S(6,6) = \mu_2\left(Y_{n+1}(q_2a)\left(\frac{n+1}{a^2}-k^2\right)-\frac{\partial}{\partial r}Y_{n+1}(q_2a)\left(\frac{n+1}{a}\right)-\frac{\partial^2}{\partial r^2}Y_{n+1}(q_2a)\right), \tag{153}$$

$$S(6,7) = -i2\mu_1 k\frac{\partial}{\partial r}J_n(p_1a), \tag{154}$$

$$S(6,8) = -\frac{i\mu_1 kn}{a}J_n(q_1a), \tag{155}$$

$$S(6,9) = -\mu_1\left(J_{n+1}(q_1a)\left(\frac{n+1}{a^2}-k^2\right)-\frac{\partial}{\partial r}J_{n+1}(q_1a)\left(\frac{n+1}{a}\right)-\frac{\partial^2}{\partial r^2}J_{n+1}(q_1a)\right), \tag{156}$$

and

$$S(6,10) = 0. \tag{157}$$

From boundary condition 7,

$$S(7,1) = \frac{2\mu_2 n}{a}\left(\frac{1}{a}J_n(p_2a) - \frac{\partial}{\partial r}J_n(p_2a)\right), \tag{158}$$

$$S(7,2) = \frac{2\mu_2 n}{a}\left(\frac{1}{a}Y_n(p_2a) - \frac{\partial}{\partial r}Y_n(p_2a)\right), \tag{159}$$

$$S(7,3) = \mu_2\left(-\frac{\partial^2}{\partial r^2}J_n(q_2a) + \frac{1}{a}\frac{\partial}{\partial r}J_n(q_2a) - \frac{n^2}{a^2}J_n(q_2a)\right), \tag{160}$$

$$S(7,4) = \mu_2\left(-\frac{\partial^2}{\partial r^2}Y_n(q_2a) + \frac{1}{a}\frac{\partial}{\partial r}Y_n(q_2a) - \frac{n^2}{a^2}Y_n(q_2a)\right), \tag{161}$$

$$S(7,5) = ik\mu_2\left(\frac{\partial}{\partial r}J_{n+1}(q_2a) - J_{n+1}(q_2a)\left(\frac{1+n}{a}\right)\right), \tag{162}$$

$$S(7,6) = ik\mu_2\left(\frac{\partial}{\partial r}Y_{n+1}(q_2a) - Y_{n+1}(q_2a)\left(\frac{1+n}{a}\right)\right), \tag{163}$$

$$S(7,7) = -\frac{2\mu_1 n}{a^2}\left(J_n(p_1a) - a\frac{\partial}{\partial r}J_n(p_1a)\right), \tag{164}$$

$$S(7,8) = -\mu_1\left(-\frac{\partial^2}{\partial r^2}J_n(q_1a) + \frac{1}{a}\frac{\partial}{\partial r}J_n(q_1a) - \frac{n^2}{a^2}J_n(q_1a)\right), \tag{165}$$

$$S(7,9) = -ik\mu_1\left(\frac{\partial}{\partial r}J_{n+1}(q_1a) - J_{n+1}(q_1a)\left(\frac{1+n}{a}\right)\right), \tag{166}$$

and

$$S(7,10) = 0. \tag{167}$$

From boundary condition 8,

$$S(8,1) = \frac{\partial}{\partial r} J_n(p_2 a), \tag{168}$$

$$S(8,2) = \frac{\partial}{\partial r} Y_n(p_2 a), \tag{169}$$

$$S(8,3) = \frac{n}{a} J_n(q_2 a), \tag{170}$$

$$S(8,4) = \frac{n}{a} Y_n(q_2 a), \tag{171}$$

$$S(8,5) = ikJ_{n+1}(q_2 a), \tag{172}$$

$$S(8,6) = ikY_{n+1}(q_2 a), \tag{173}$$

$$S(8,7) = -\frac{\partial}{\partial r} J_n(p_1 a), \tag{174}$$

$$S(8,8) = -\frac{n}{a} J_n(q_1 a), \tag{175}$$

$$S(8,9) = -ikJ_{n+1}(q_1 a), \tag{176}$$

and

$$S(8,10) = 0. \tag{177}$$

From boundary condition 9,

$$S(9,1) = -\frac{n}{a}J_n(p_2a), \tag{178}$$

$$S(9,2) = -\frac{n}{a}Y_n(p_2a), \tag{179}$$

$$S(9,3) = -\frac{\partial}{\partial r}J_n(q_2a), \tag{180}$$

$$S(9,4) = -\frac{\partial}{\partial r}Y_n(q_2a), \tag{181}$$

$$S(9,5) = ikJ_{n+1}(q_2a), \tag{182}$$

$$S(9,6) = ikY_{n+1}(q_2a), \tag{183}$$

$$S(9,7) = \frac{n}{a}J_n(p_1a), \tag{184}$$

$$S(9,8) = \frac{\partial}{\partial r}J_n(q_1a), \tag{185}$$

$$S(9,9) = -ikJ_{n+1}(q_1a), \tag{186}$$

and

$$S(9,10) = 0. \tag{187}$$

From boundary condition 10,

$$S(10,1) = ikJ_n(p_2a), \tag{188}$$

$$S(10,2) = ikY_n(p_2a), \tag{189}$$

$$S(10,3) = 0, \tag{190}$$

$$S(10,4) = 0, \tag{191}$$

$$S(10,5) = -\frac{\partial}{\partial r}J_{n+1}(q_2a) - \frac{n+1}{a}J_{n+1}(q_2a), \tag{192}$$

$$S(10,6) = -\frac{\partial}{\partial r}Y_{n+1}(q_2a) - \frac{n+1}{a}Y_{n+1}(q_2a), \tag{193}$$

$$S(10,7) = -ikJ_n(p_1a), \tag{194}$$

$$S(10,8) = 0, \tag{195}$$

$$S(10,9) = \frac{\partial}{\partial r}J_{n+1}(q_1a) + \frac{n+1}{a}J_{n+1}(q_1a), \tag{196}$$

and

$$S(10,10) = 0. \tag{197}$$

# RESULTS

## BARE OPTICAL FIBER

### *Optical Phase Sensitivity*

The first numerical example will be a calculation using the solid cylinder model with properties of a bare optical glass fiber immersed in water (tables 1 and 2). The optical phase sensitivity $\frac{\Delta\phi}{\phi p}$ will be computed using the following expression,[14] where $p = P_o$, $P_x$, or $P_\theta$:

$$\frac{\Delta\phi}{\phi p} = \varepsilon_{xx} - \frac{n_o^2}{2}(\varepsilon_{rr}(P_{11} + P_{12}) + \varepsilon_{xx}P_{12}) . \tag{198}$$

**Table 1. Optical Fiber Properties**

| Property | Definition |
|---|---|
| $E_1 = 7.2\times10^{10}\frac{\mathrm{N}}{\mathrm{m}^2}$ | Young's Modulus |
| $\zeta_1 = 0.005$ | Structural Loss Factor |
| $\rho_1 = 2600\frac{\mathrm{kg}}{\mathrm{m}^3}$ | Density |
| $\nu_1 = 0.17$ | Poisson's Ratio |
| $a = 62.5\times10^{-6}\mathrm{m}$ | Cladding Outer Radius |
| $r_c = 4.5\times10^{-6}\mathrm{m}$ | Core Radius |
| $r_1 = 1.0\times10^{-6}\mathrm{m}$ | Calculation Radius |
| $n_o = 1.46$ | Refractive Index |
| $P_{11} = 0.126$ | Pockel Coefficient |
| $P_{12} = 0.27$ | Pockel Coefficient |

**Table 2. Outer Fluid Properties**

| Property | Definition |
|---|---|
| $\rho_s = 1000.0 \frac{kg}{m^3}$ | Density |
| $c_s = 1500.0 \frac{m}{sec}$ | Speed of Sound |

As was previously discussed, the system matrix, equation (70), is evaluated for the optical fiber properties listed above. The calculation radius is near to the center of the optical fiber core at $r_1 = 1.0 \times 10^{-6}$ m. The coefficients obtained from the matrix inversion normalized by the forcing function stress are substituted into equation (26) for the displacement potentials, and next into equations (43) and (45) for the strains. The strains are then used to obtain the optical phase sensitivity via equation (198).

### *Numerical Considerations*

The procedure just described is repeated over the domain of wavenumber and frequency at regular intervals. For the $n = 0$ case, the frequency range is 1.0 to 500.0 Hz at intervals of 2.5 Hz, and the wavenumber range is -2.0 to 2.0 rad/m at intervals of 0.02 rad/m. These ranges provide an image size of 200-by-200 points before interpolation for display. For the $n = 1$ case, the frequency range remains the same; however, the wavenumber range is increased to -200.0 to 200.0 rad/m. The wavenumber interval is increased so that the final calculated image size is consistent with that of the $n = 0$ case. A numerical artifact is apparent in the simulations due to the finite wavenumber and frequency interval when sharp resonances are present. This is most evident in the $n = 0$ simulations described later in the report. The extensional wave resonance is not continuously resolved, but appears as a series of dots in both the magnitude and phase surfaces. Small asymmetries with respect to wavenumber are also evident in the magnitude cuts as well. The first problem is a function of the graphics software used to display the wire frame surfaces, and the second problem results when, for a given frequency, slightly different wavenumber locations are being calculated in the minus and plus wavenumber half-planes. These problems could be eliminated by decreasing both the frequency and wavenumber

interval by several orders of magnitude. A corresponding increase in calculation time would result. The 200-by-200 point image (40,000 points) was selected as an appropriate compromise between calculation time and the requirement to convey the physics embodied in the simulations.

Evaluation of the equations required the use of the quad precision complex data type. The language of choice is FORTRAN (version 3.0) running on a Sun Microsystems SPARC Station model 10SX-512, Operating System Solaris 2.3. In the course of this research, the author discovered a "bug" in the Fortran complier when using quad precision complex functions. Therefore, calculations were limited to double precision complex. However, even with the accuracy afforded with the double precision data type, numerical accuracy problems are encountered with the bare fiber parameters and the $n = 1$ excitation. As shown later in the report, numerical accuracy problems will manifest themselves as random spots concentrated at low frequency (below 50 Hz) for all wavenumbers and at all frequencies for wavenumbers below approximately $\pm 50$ rad/m. In this case, the occurrence of such problems is due to the choice of optical fiber material properties and dimensions. Several other cases (not shown) were evaluated, one being a urethane rod (approximating a solid garden hose), which did not display any of the numerical accuracy problems evident in the optical fiber simulations presented.

The FORTRAN algorithms developed to produce the simulations contained here are published in a separate document,[15] which will be available (for one year only from the date of publication of this technical report) via e-mail at *peloquin@cascade.nl.nuwc.navy.mil*.

## CIRCUMFERENTIAL ORDER SHAPES

For the simulations that follow in the remainder of this report, the motion of the cylinder will take the form depicted in one of the two circumferential order shapes shown in figures 6 and 7. Figure 6 depicts the longitudinal $x$-displacement that occurs in the cylinder as energy is propagating in the first branch of wave propagation corresponding to circumferential order number $n = 0$. This first branch of wave propagation is commonly referred to as an extensional wave.

The displacement shape depicted in figure 7 causes the cylinder to undergo bending in the *rx*-plane. The nonaxisymmetric excitations considered here ($n \neq 0$) excite this mode of wave propagation. As energy is propagating in the branches of the $n = 1$ simulations shown, the cylinder is undergoing a vibration principally depicted by the deformation shape of figure 7.

The cylinder displacements in figures 6 through 8 have been magnified for the purpose of visualizing the deformation. It should be remembered that this is a small strain analysis, suitable for analyzing problems undergoing loading on an acoustic scale.

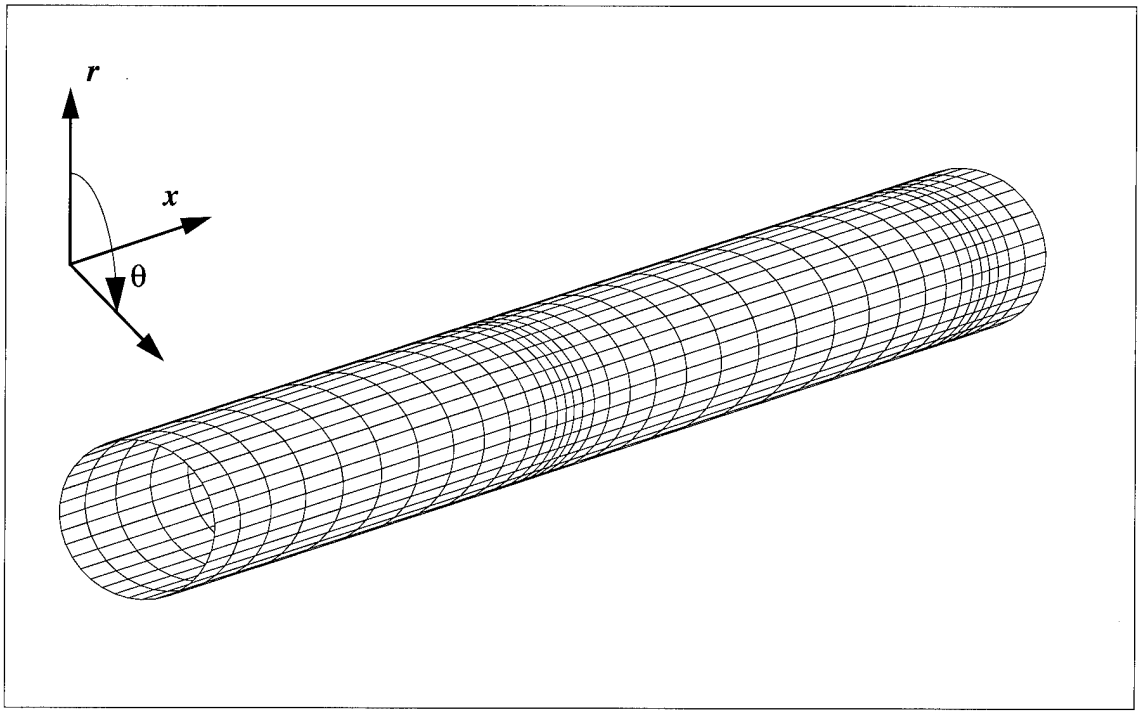


**Figure 6. Circumferential Order Number $n$ = 0, First Branch**

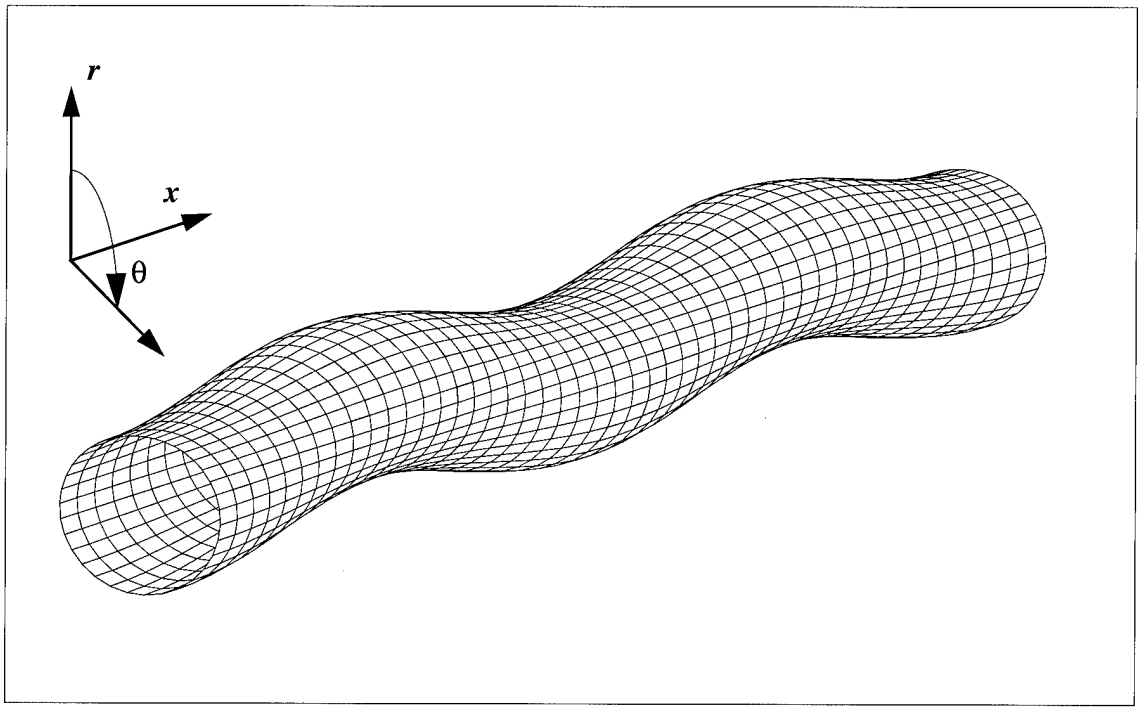


**Figure 7. Circumferential Order Number $n$ = 1, First Branch**

### *Transfer Surfaces*

The simulation for axisymmetric radial pressure excitation results in transfer surfaces for each strain component and the optical phase sensitivity, as displayed in figures 9 through 16. The cuts through the magnitude surfaces show the character of the field quantities as functions of wavenumber. The wavenumber axis is marked with major tick marks at the limits of the range for acoustic plane wave propagation in water. These points correspond to minus and plus endfire. The predominant motion of the cylinder is in the longitudinal $x$-direction, as depicted in figure 6. The major feature in this simulation is the supersonic extensional wave at 5571 m/sec.

Since the extensional wave phase velocity is supersonic, it generates a radial component of cylinder displacement that can be projected onto the fluid propagation direction; energy will thus be radiated into the outer fluid at the fluid dilatational wave speed. Note that a projection of the extensional wavelength of the cylinder, $L_e$, onto the corresponding fluid wavelength, $L_s$, exists. Constant pressure phase fronts in the fluid will leave the cylinder at $\alpha = 74$ degrees relative to the

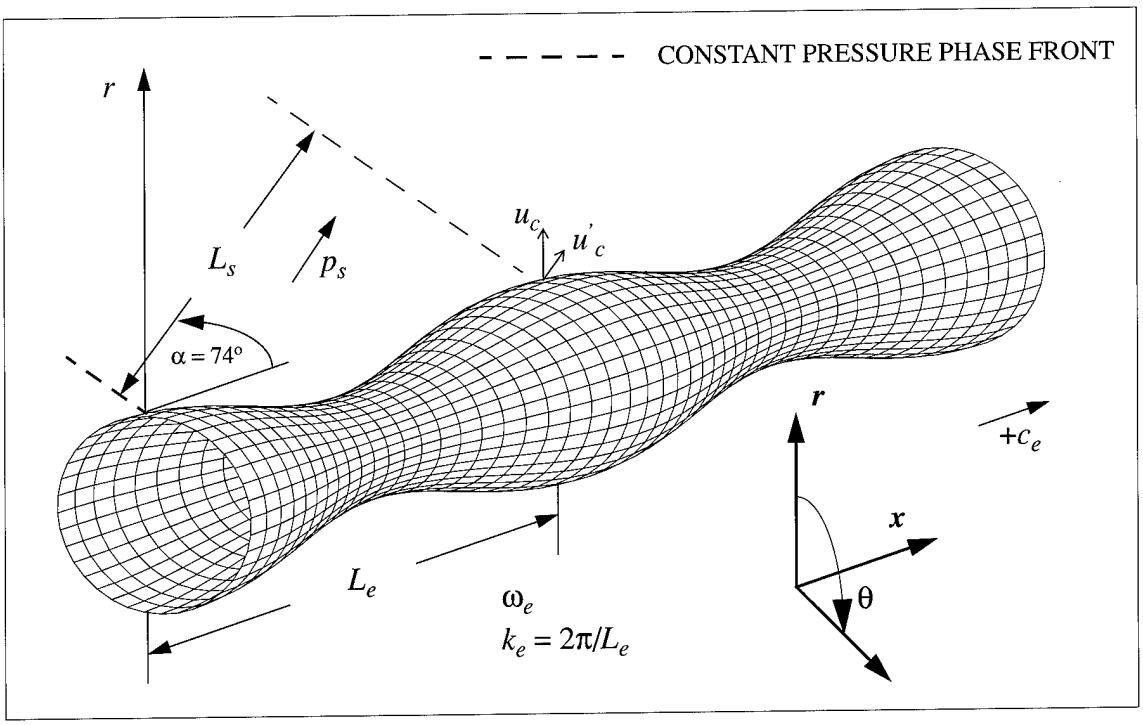


**Figure 8. Radiation of Pressure From the Cylinder Surface at 105 Degrees**

longitudinal $x$-axis (figure 8), the fluid medium being water with $c_s$ = 1500 m/sec, as given in the list of outer fluid properties. Figure 8 represents the qualitative relationship that exists between the wavelengths for every location in the wavenumber-frequency plane along the branch representing extensional wave propagation.

Conversely, a pressure wave in the outer fluid incident upon the cylinder at 74 degrees, as shown in figure 8, would excite an extensional wave response in the cylinder. Remembering that $k_e = 2\pi/L_e$ and $k_e = \omega/c_e$, the relationship between the incident/radiated angle, wavelength, phase velocity, and wavenumber is

$$\alpha = \operatorname{acos}\frac{L_s}{L_e} = \operatorname{acos}\frac{c_s}{c_e} = \operatorname{acos}\frac{k_e}{k_s}. \tag{199}$$

To review, in an infinite isotropic elastic media, the dilatational wave phase velocity is given by equation (200) as

$$c_l = \sqrt{\frac{E_c(1-\nu_c)}{\rho_c(1+\nu_c)(1-2\nu_c)}}. \tag{200}$$

For a dilatational wave, the particle velocity and the wave propagation vector are coincident. For the wavenumber and frequency range shown in the simulations, the manifestation of this wave in the cylinder produces a modified phase velocity known as the bar velocity or extensional wave phase velocity, given by equation (201) as

$$c_e = \sqrt{\frac{E_c}{\rho_c}}. \tag{201}$$

The simulation for axisymmetric longitudinal shear stress results in figures 17 through 24. Note again the prominent extensional wave resonant peak. The strain and optical phase sensitivity (in the fiber) to longitudinal shear stress is some 30 to 110 dB greater than it is for sensitivity to radial pressure excitation. This is evident by comparing the difference in levels between figures 10 and 18, figures 12 and 20, figures 14 and 22, and figures 16 and 24. At the

extensional wave resonance peak, the excess is 110 dB. At the edge of the acoustic cone, the excess is 70 dB, and at broadside ($k$ = 0), the excess is 30 dB. Thus, it is quite clear that sensitivity to longitudinal shear stress exceeds sensitivity to radial pressure excitation by over 5 orders of magnitude.

Two nonaxisymmetric simulations have been performed for circumferential order number $n$ = 1, $P_o$, and $P_x$. The nonaxisymmetric radial pressure simulation is contained in figures 25 through 32. This excitation imparts a bending excitation to the fiber whose motion exists primarily in the $rx$-plane. This excitation results in dispersive wave propagation, which produces the nonstraight-line characteristic of the branches in figure 25. Energy propagates at a much slower rate in the $n$ = 1 branches than in the $n$ = 0 branches seen in the earlier figures. The phase velocity ranges from 12 to 20 m/sec over the frequency range from 1 to 500 Hz, as shown in figure 25.

An $n$ = 1 longitudinal shear stress excitation produces a deformation, principally in the $rx$-plane of the cylinder. The strains and optical phase sensitivities for this simulation are shown in figures 33 through 40. For the $n$ = 1 case, the magnitude of the strains produced by the longitudinal shear stress excitation is 20 to 100 dB smaller than the magnitude of the strains produced by the radial pressure excitation (compare figure 34 with 26). Both of the $n$ = 1 simulations suffer from the numerical accuracy problem described earlier, which is the reason for the spottiness in the $n$ = 1 figures. All of the $n$ = 1 simulations are performed at a calculation radius of $3.936 \times 10^{-5}$ meters, which is outside of the fiber core but within the fiber outer diameter.

Mechanical damping in the cylinder is incorporated by the use of the structural loss factor. This structural loss factor is the imaginary component of the complex modulus of elasticity:

$$E^*_j = E_j(1 + i\zeta_j) , \tag{202}$$

where $j$ equals 1 or 2, corresponding to the first and second layer, respectively. It is therefore possible, within the formulation presented here, to have different structural loss factors for each

cylinder. This is, in fact, how the double layer simulations were performed.

When phase is used as a label for the lower of the two images in the figures that follow, it is the phase between the applied excitation stress and the particular variable under consideration. This is the phase between the applied stress and response of the cylinder. It should not be confused with the optical phase sensitivity defined by equation (198).

*Axisymmetric Radial Pressure Excitation (n = 0)*

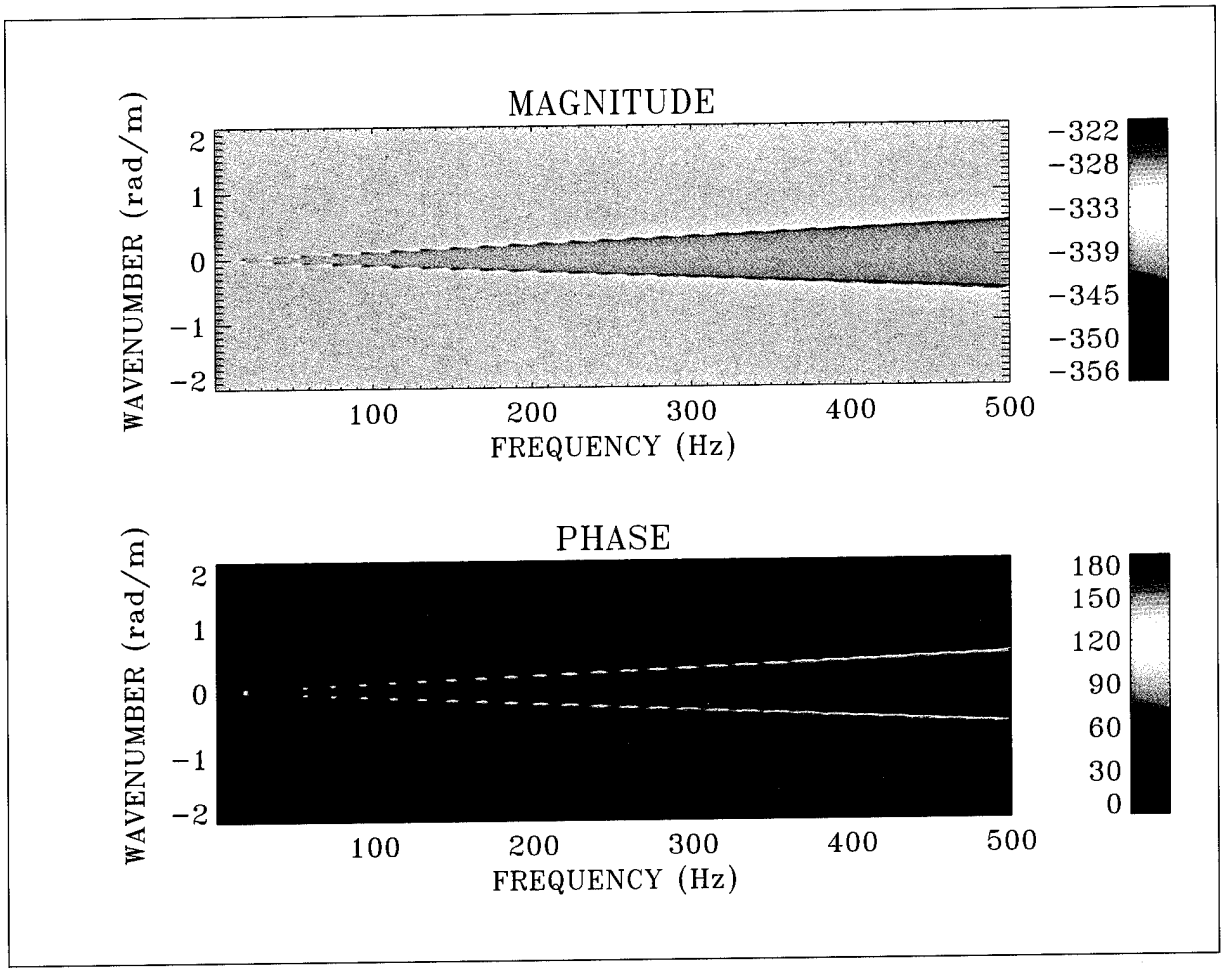


**Figure 9. Radial Strain Transfer Surface: Magnitude = 10Log($\varepsilon_{rr}/P_o$)$^2$ and Phase in Degrees (One Layer, $n$ = 0)**

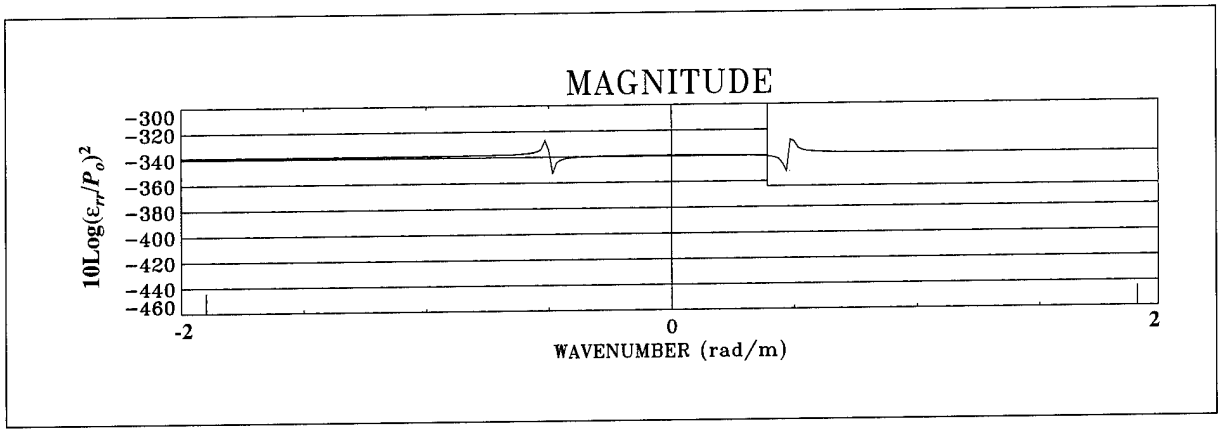


**Figure 10. Frequency Cut at 453.19 Hz Through the Magnitude Surface of Figure 9**

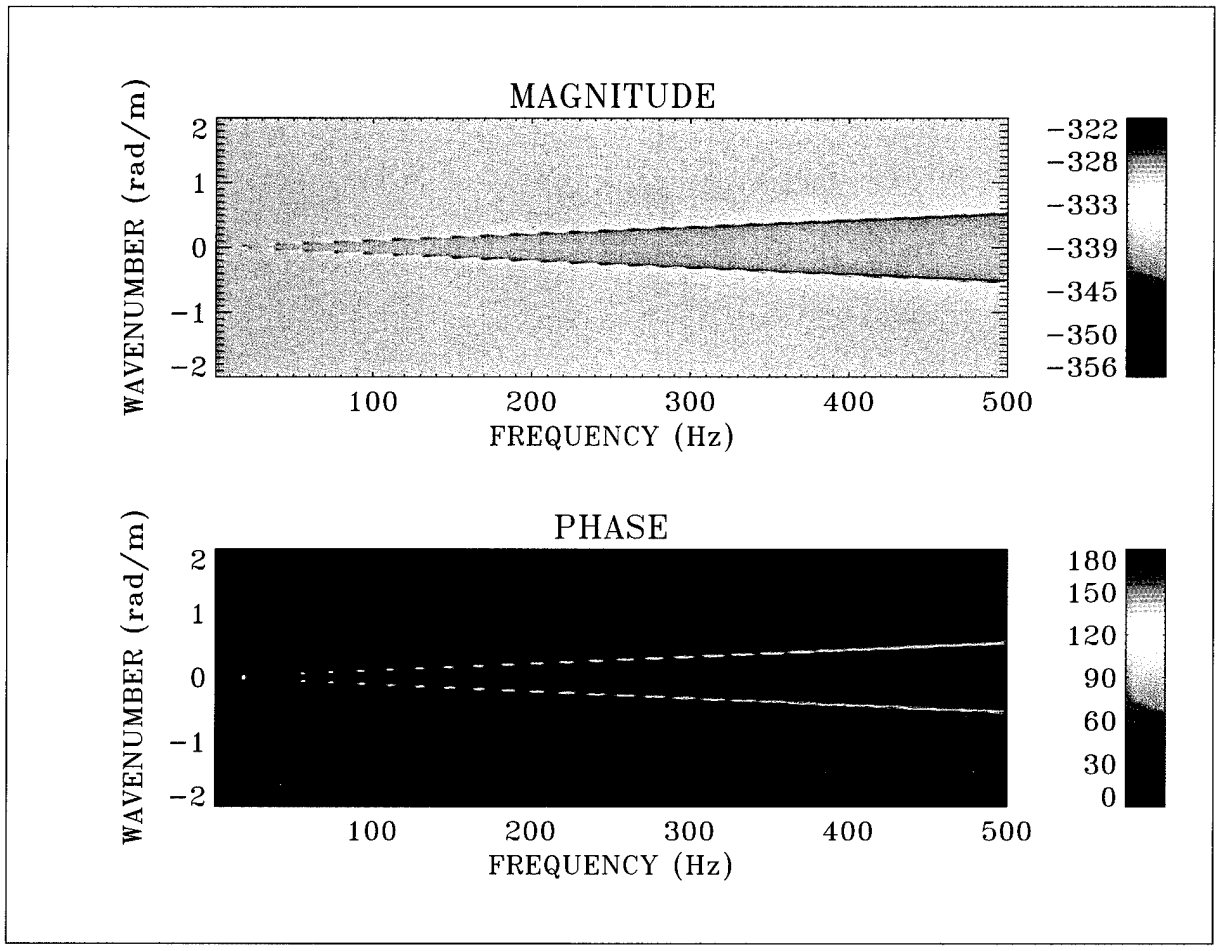


**Figure 11. Circumferential Strain Transfer Surface: Magnitude = $10\text{Log}(\varepsilon_{\theta\theta}/P_o)^2$ and Phase in Degrees (One Layer, $n = 0$)**

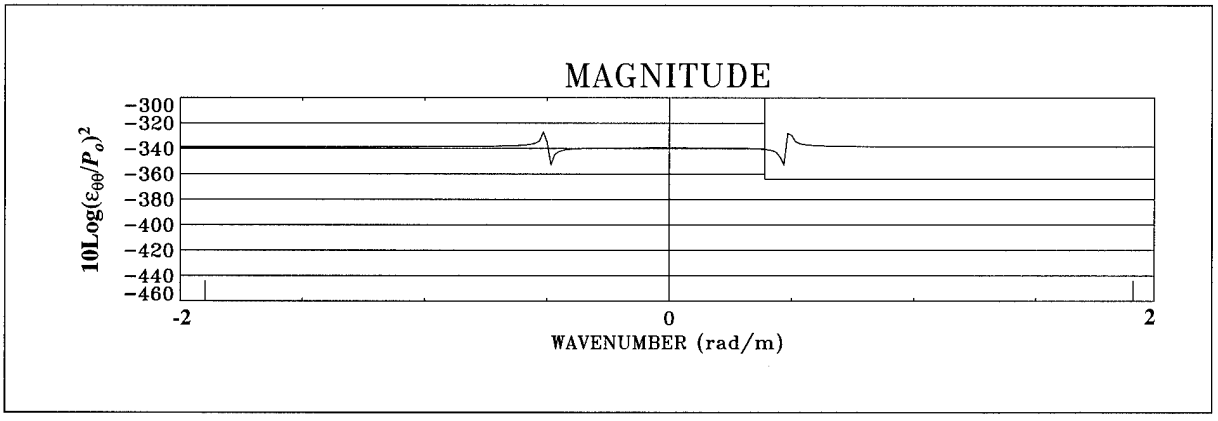


**Figure 12. Frequency Cut at 453.19 Hz Through the Magnitude Surface of Figure 11**

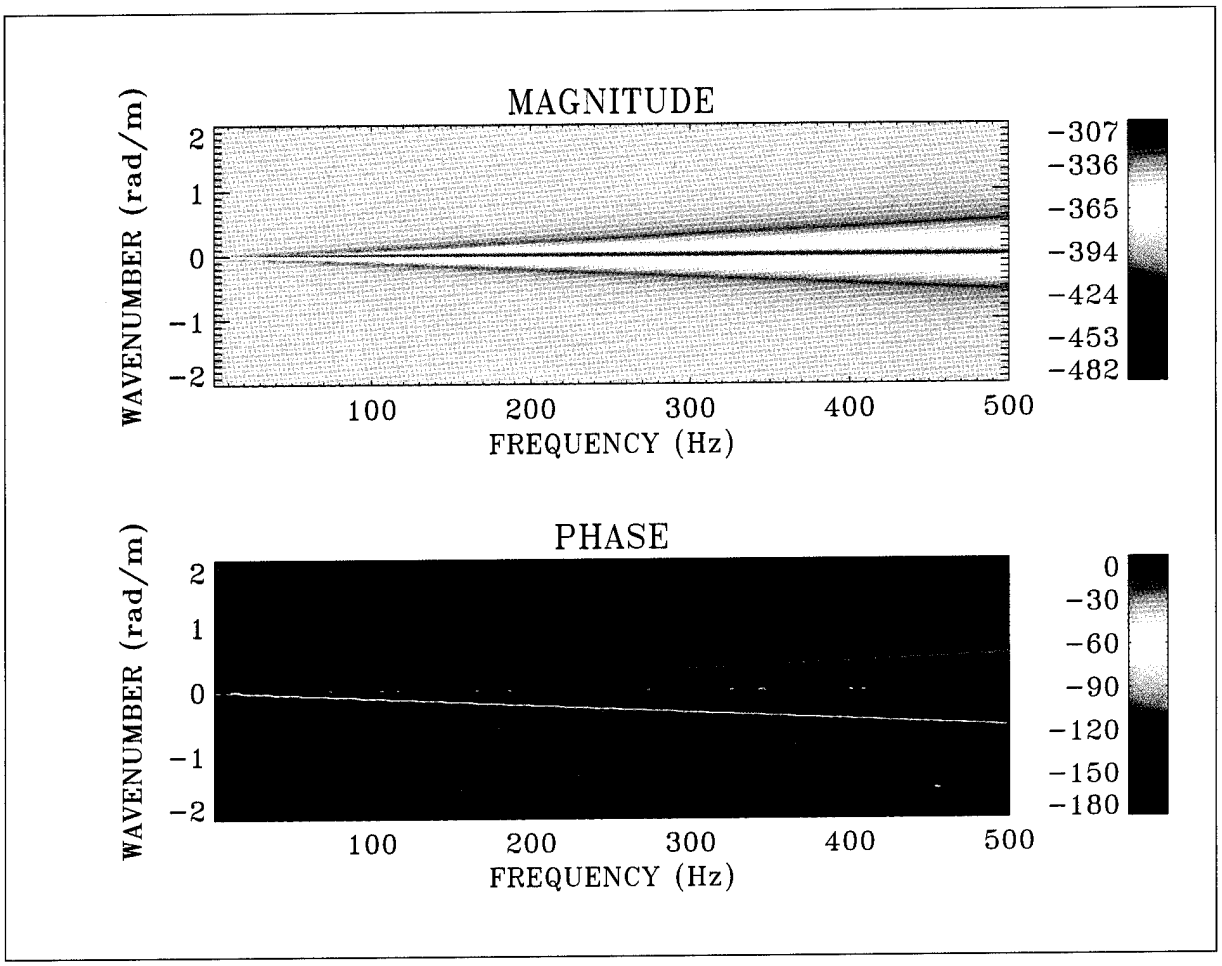


**Figure 13. Longitudinal Strain Transfer Surface: Magnitude = $10\text{Log}(\varepsilon_{xx}/P_o)^2$ and Phase in Degrees (One Layer, $n = 0$)**

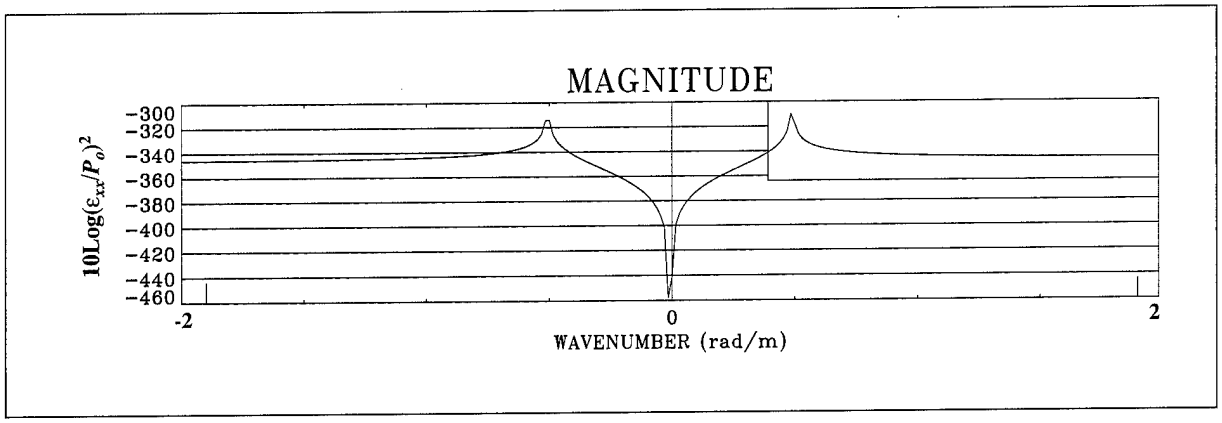


**Figure 14. Frequency Cut at 453.19 Hz Through the Magnitude Surface of Figure 13**

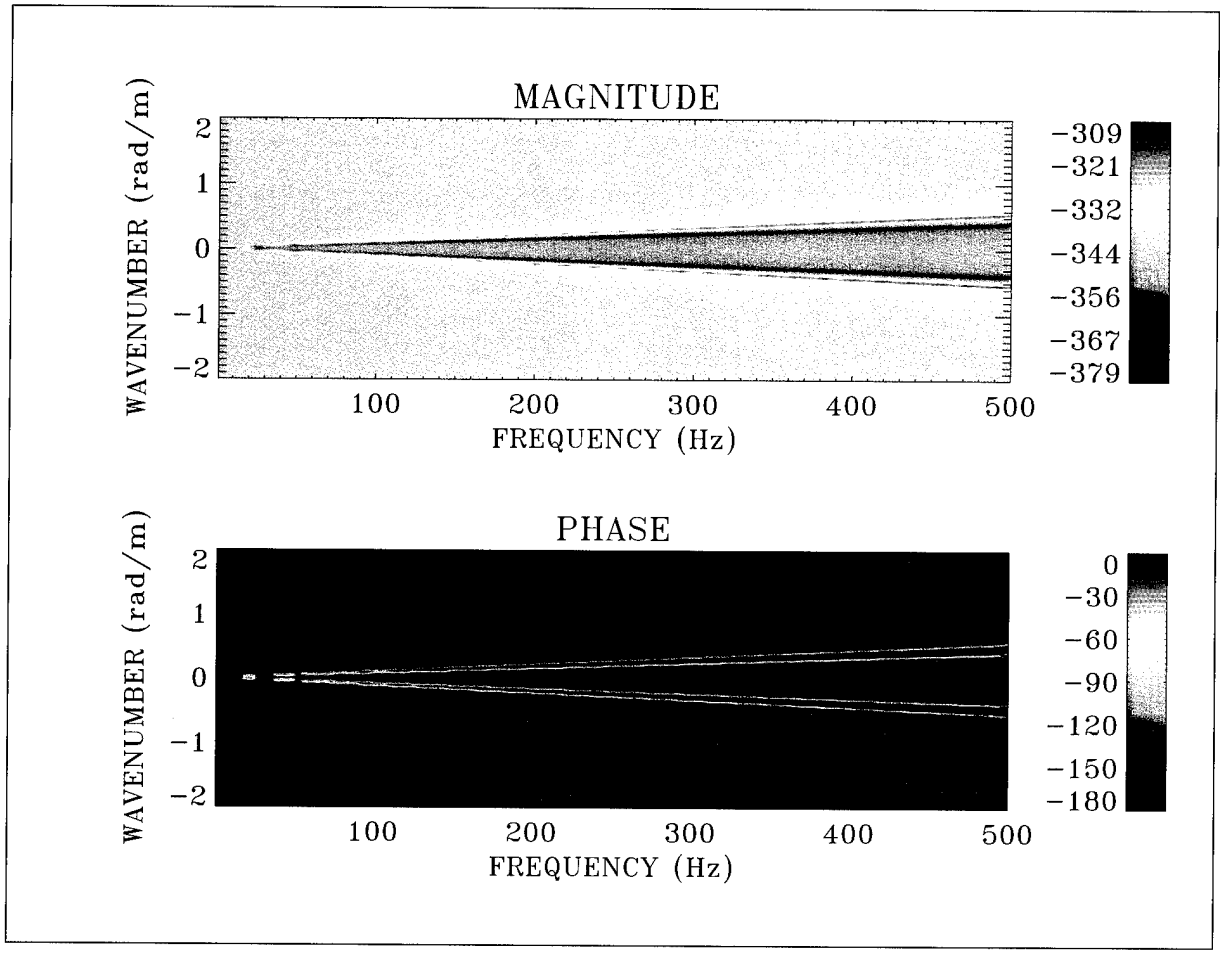


**Figure 15. Optical Phase Sensitivity Strain Transfer Surface: Magnitude = 10Log($\Delta\phi/\phi/P_o$)$^2$ and Phase in Degrees (One Layer, $n$ = 0)**

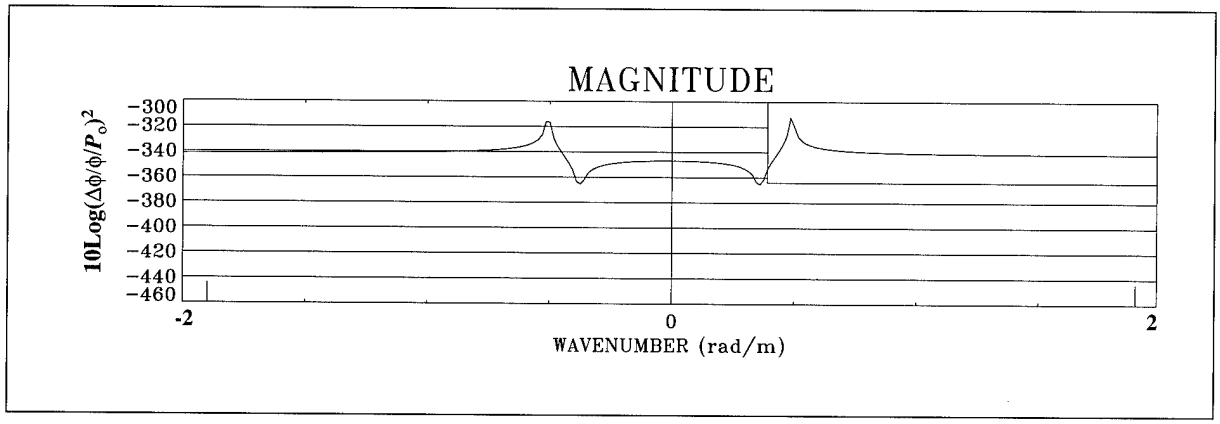


**Figure 16. Frequency Cut at 453.19 Hz Through the Magnitude Surface of Figure 15**

*Axisymmetric Longitudinal Shear Stress Excitation (n = 0)*

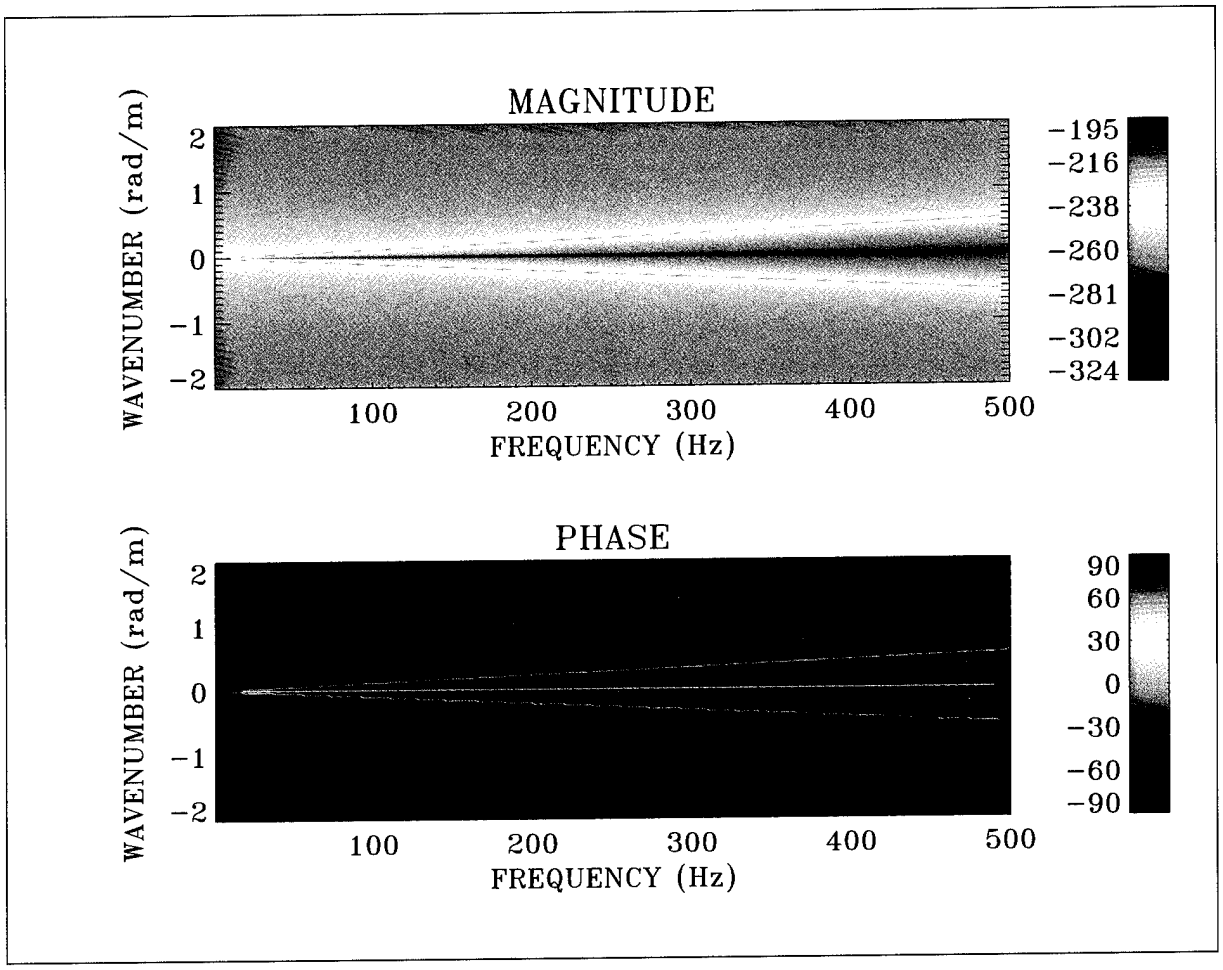


**Figure 17. Radial Strain Transfer Surface: Magnitude = 10Log($\varepsilon_{rr}/P_x$)$^2$ and Phase in Degrees (One Layer, $n$ = 0)**

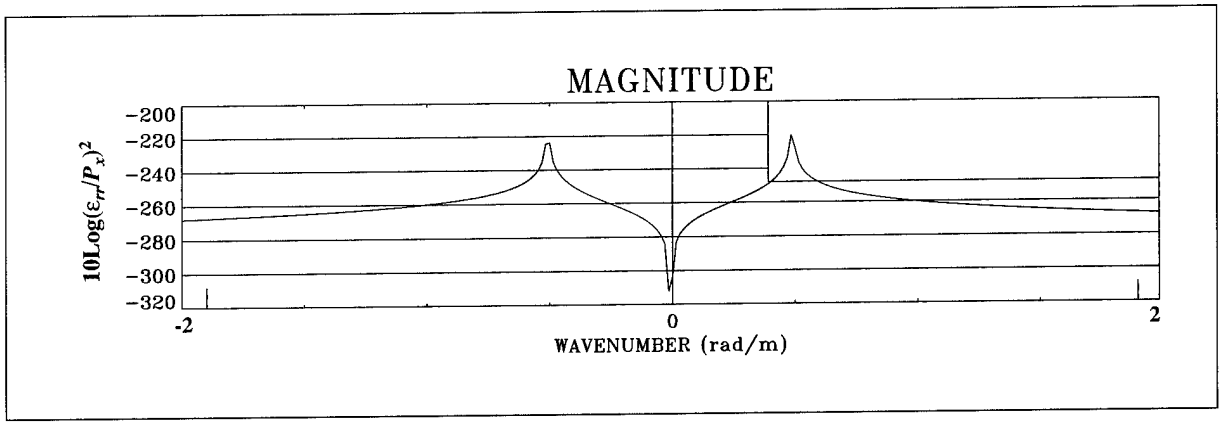


**Figure 18. Frequency Cut at 453.19 Hz Through the Magnitude Surface of Figure 17**

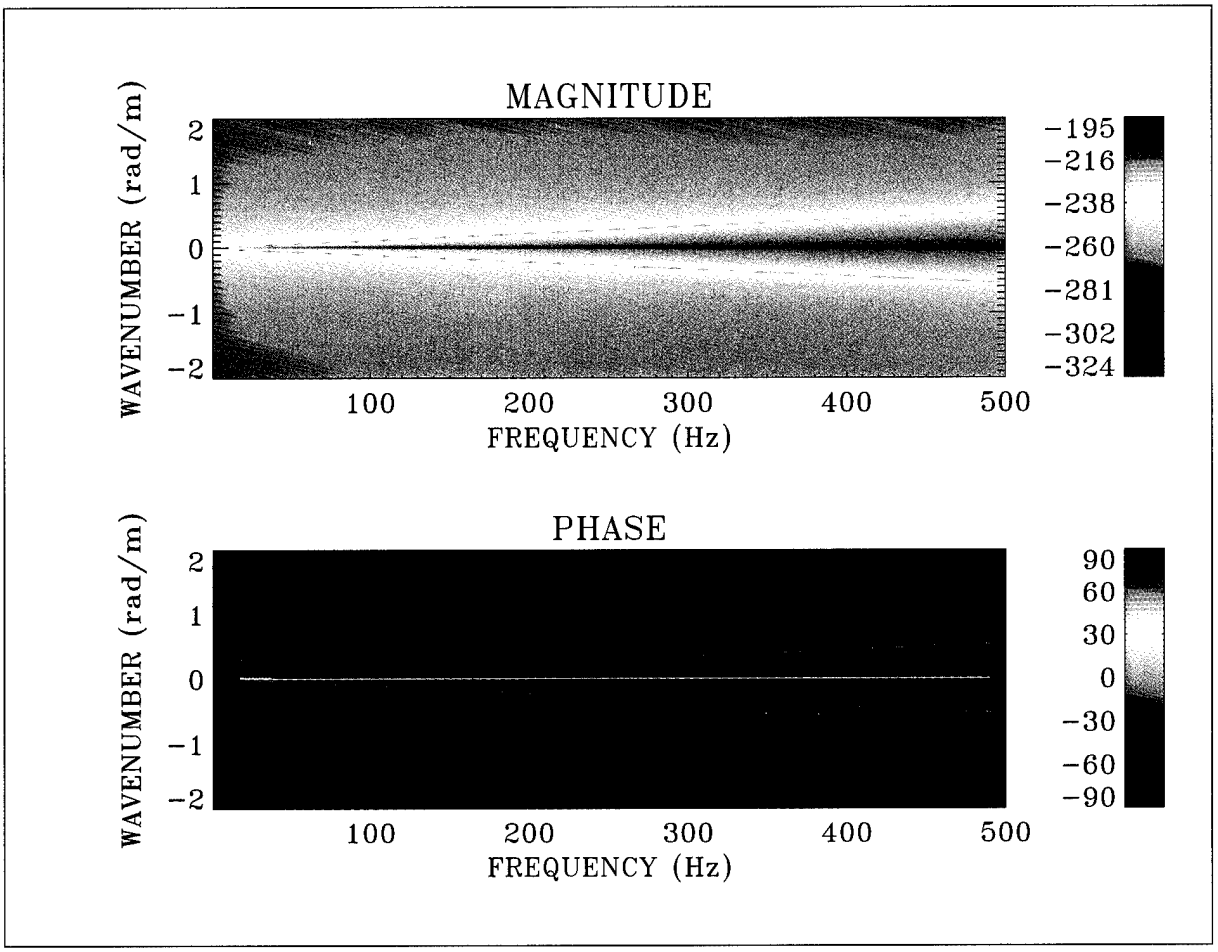


**Figure 19. Circumferential Strain Transfer Surface: Magnitude = 10Log($\varepsilon_{\theta\theta}/P_x$)$^2$ and Phase in Degrees (One Layer, $n$ = 0)**

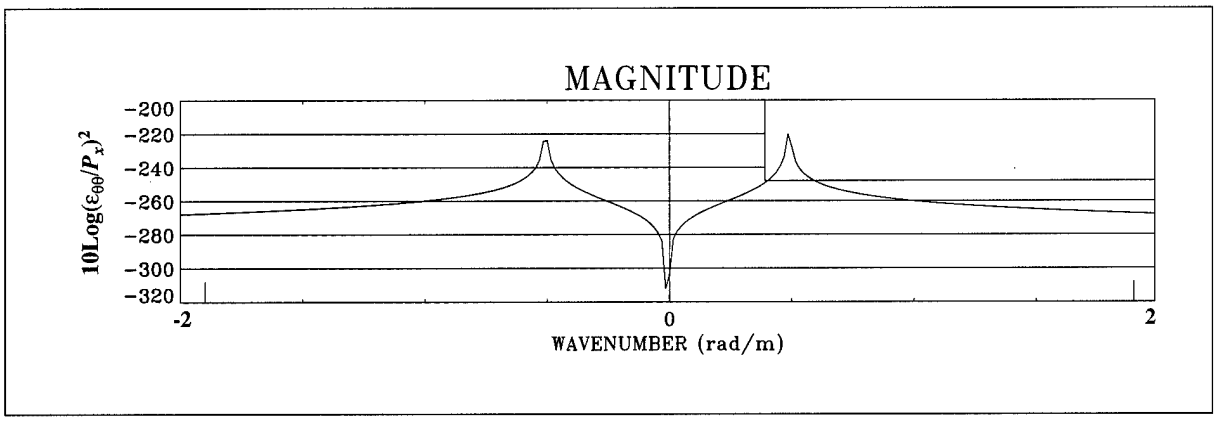


**Figure 20. Frequency Cut at 453.19 Hz Through the Magnitude Surface of Figure 19**

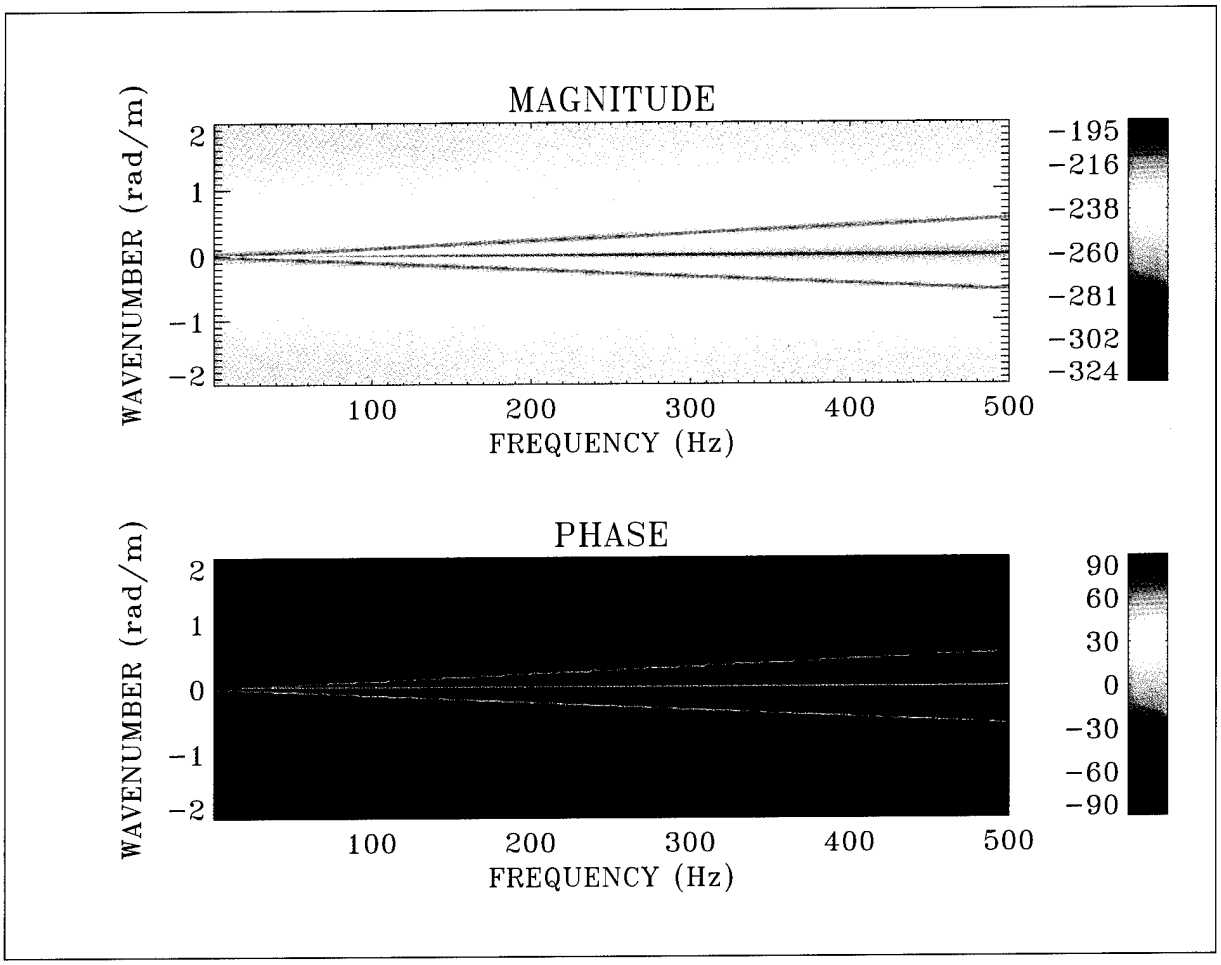


**Figure 21. Longitudinal Strain Transfer Surface: Magnitude = 10Log($\varepsilon_{xx}/P_x$)$^2$ and Phase in Degrees (One Layer, $n$ = 0)**

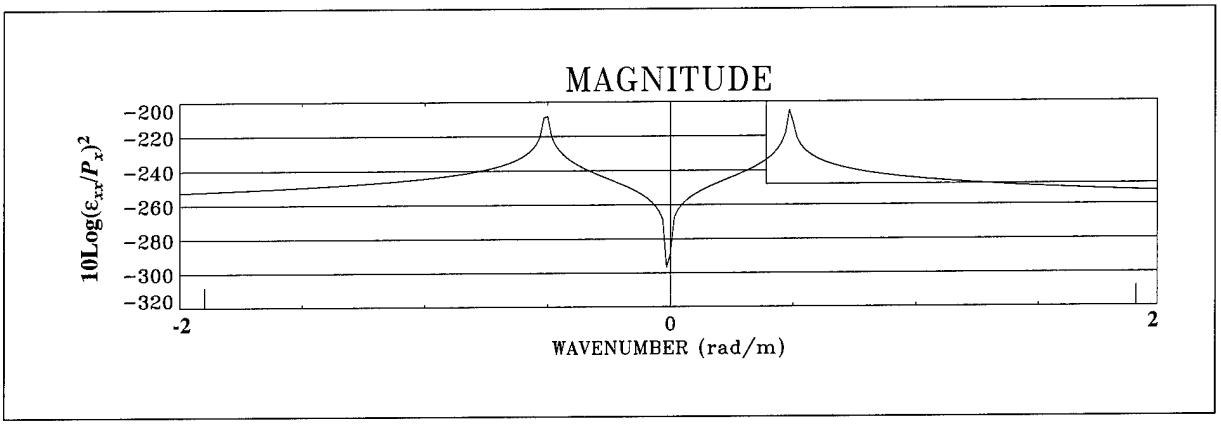


**Figure 22. Frequency Cut at 453.19 Hz Through the Magnitude Surface of Figure 21**

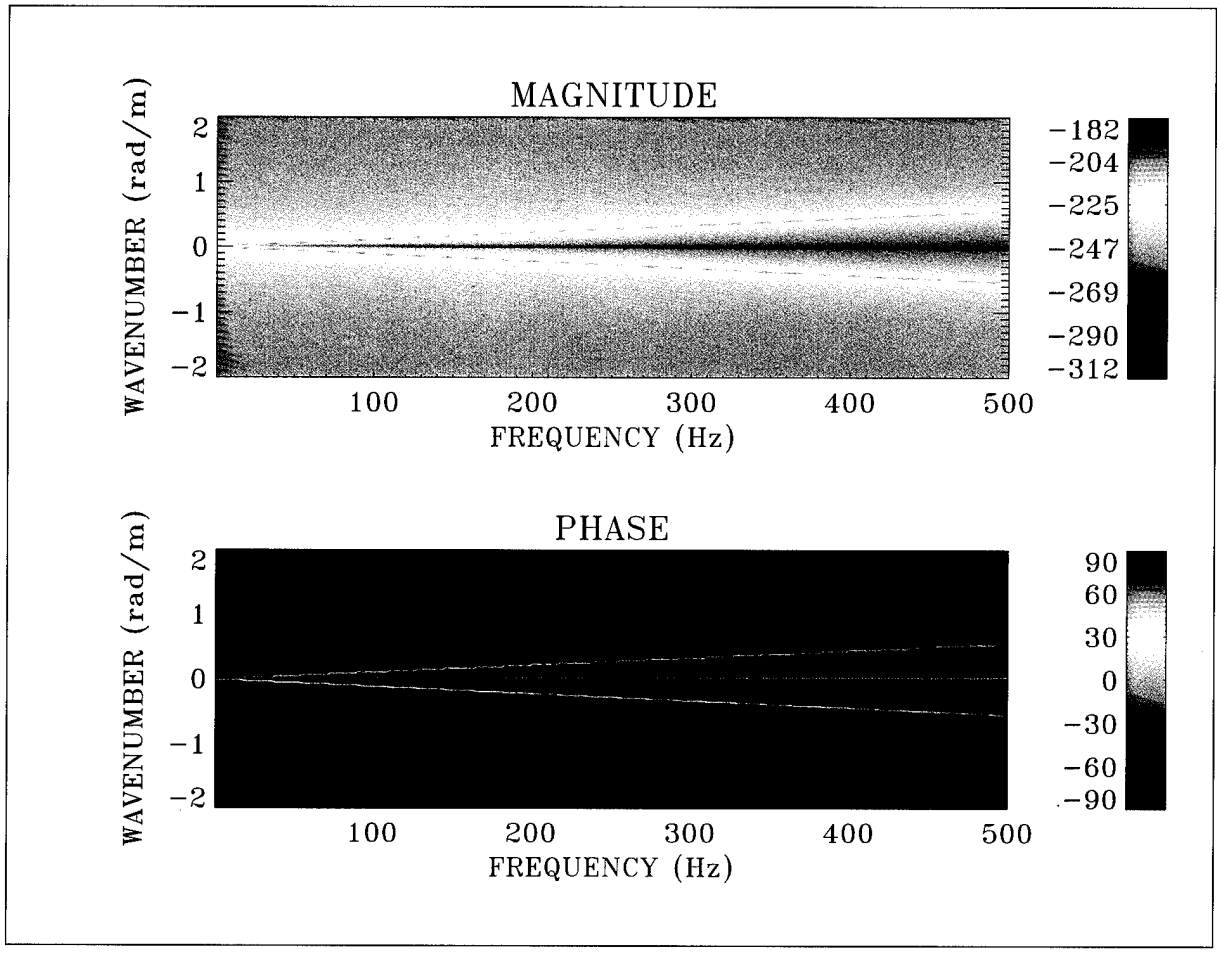


**Figure 23. Optical Phase Sensitivity Strain Transfer Surface: Magnitude = 10Log($\Delta\phi/\phi/P_x$)$^2$ and Phase in Degrees (One Layer, $n$ = 0)**

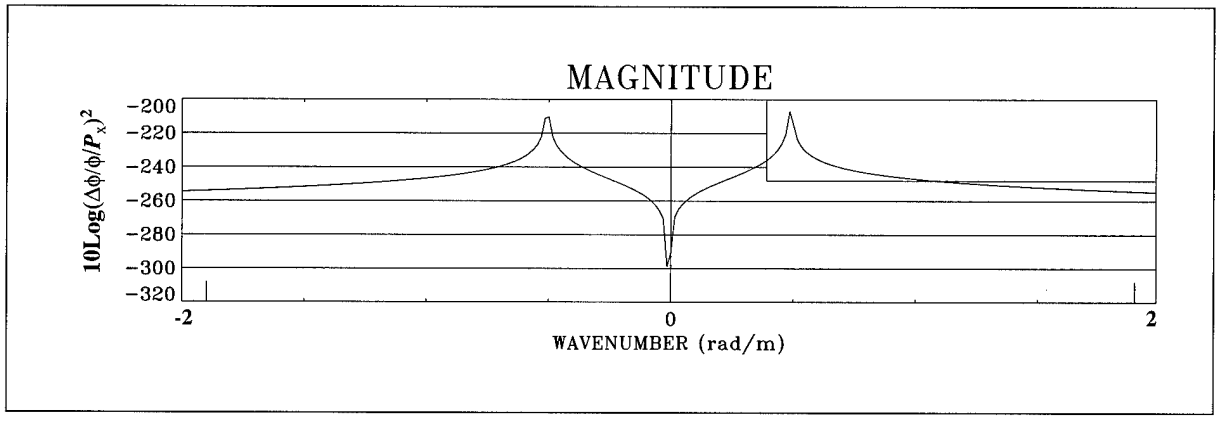


**Figure 24. Frequency Cut at 453.19 Hz Through the Magnitude Surface of Figure 23**

*Nonaxisymmetric Radial Pressure Excitation (n = 1)*

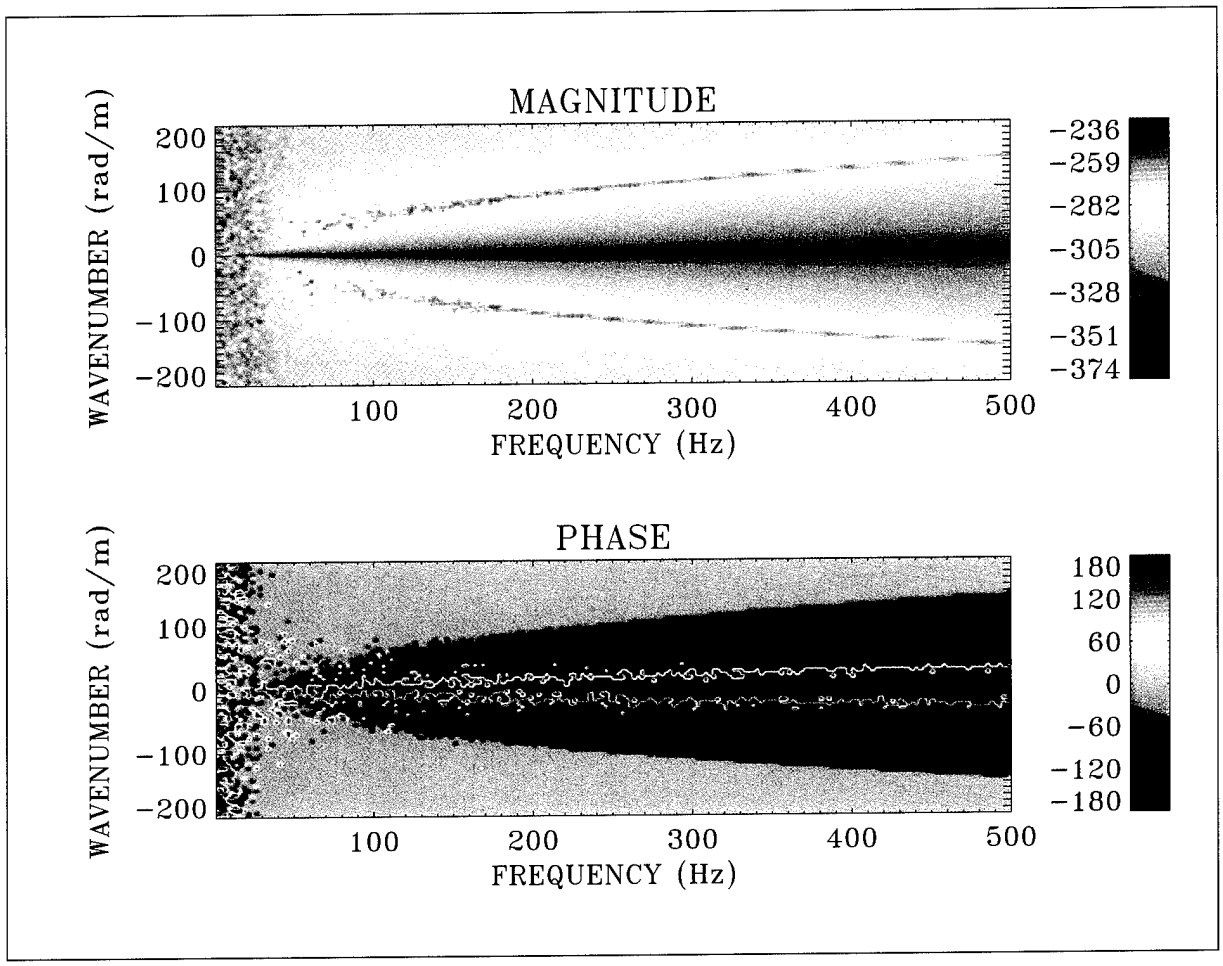


**Figure 25. Radial Strain Transfer Surface: Magnitude = 10Log($\varepsilon_{rr}/P_o$)$^2$ and Phase in Degrees (One Layer, $n$ = 1)**

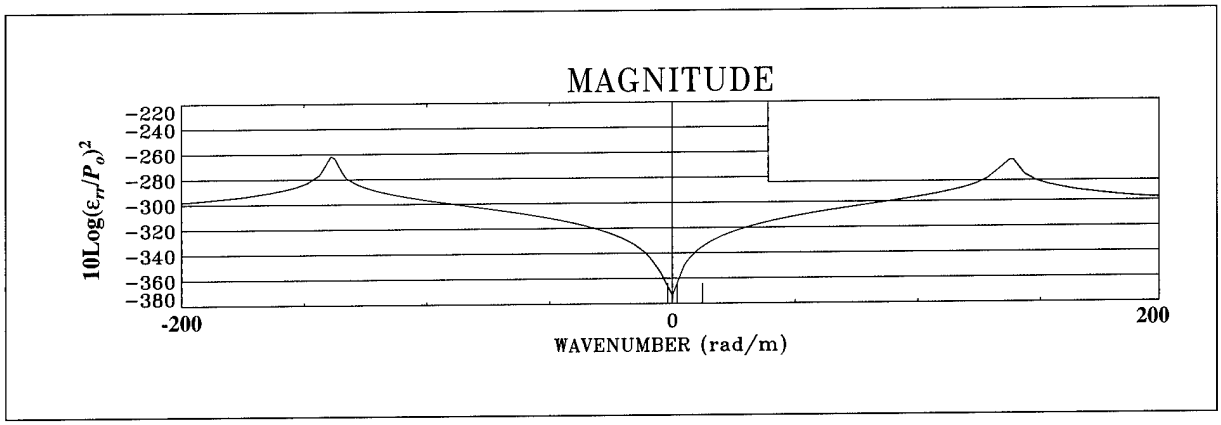


**Figure 26. Frequency Cut at 453.19 Hz Through the Magnitude Surface of Figure 25**

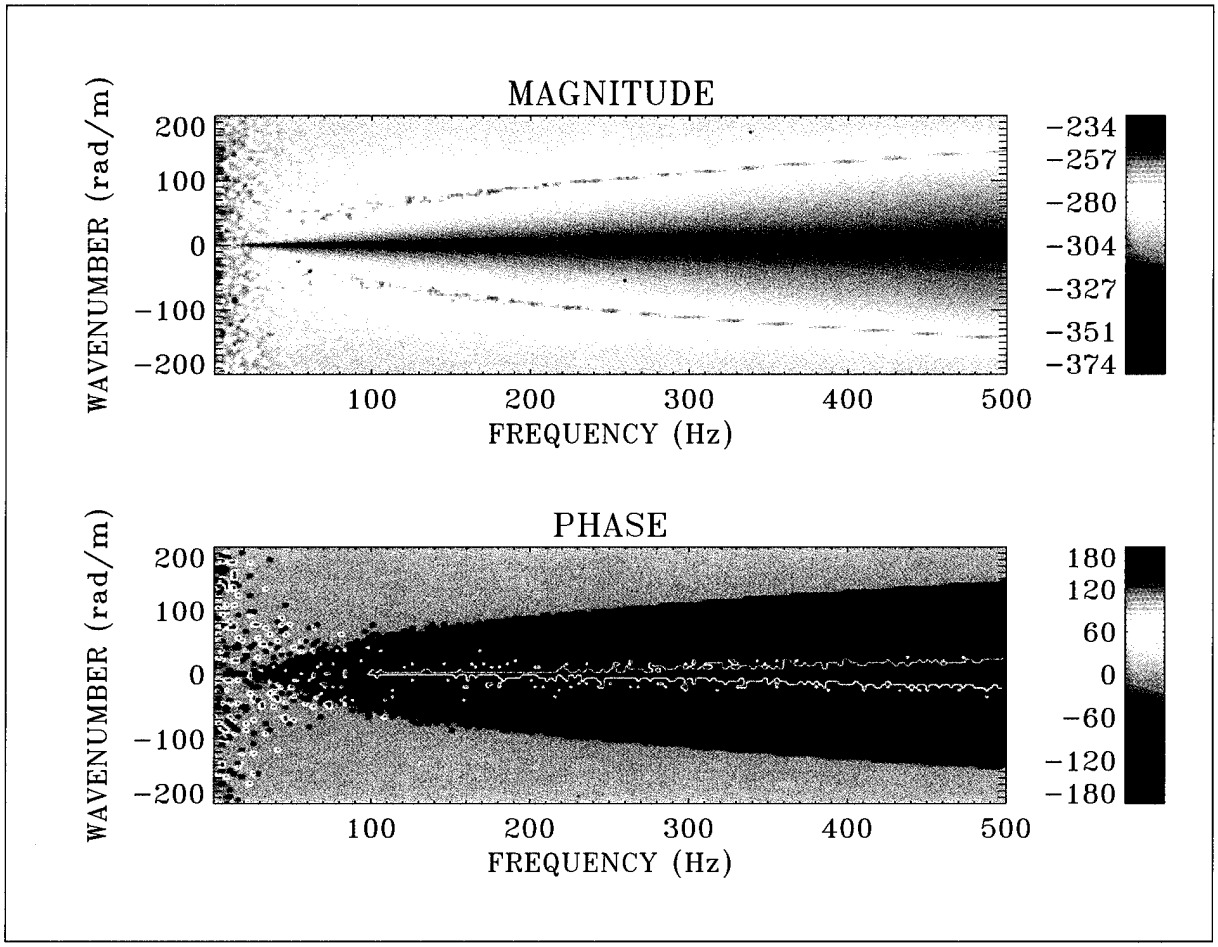


**Figure 27. Circumferential Strain Transfer Surface: Magnitude = 10Log($\varepsilon_{\theta\theta}/P_o$)$^2$ and Phase in Degrees (One Layer, $n$ = 1)**

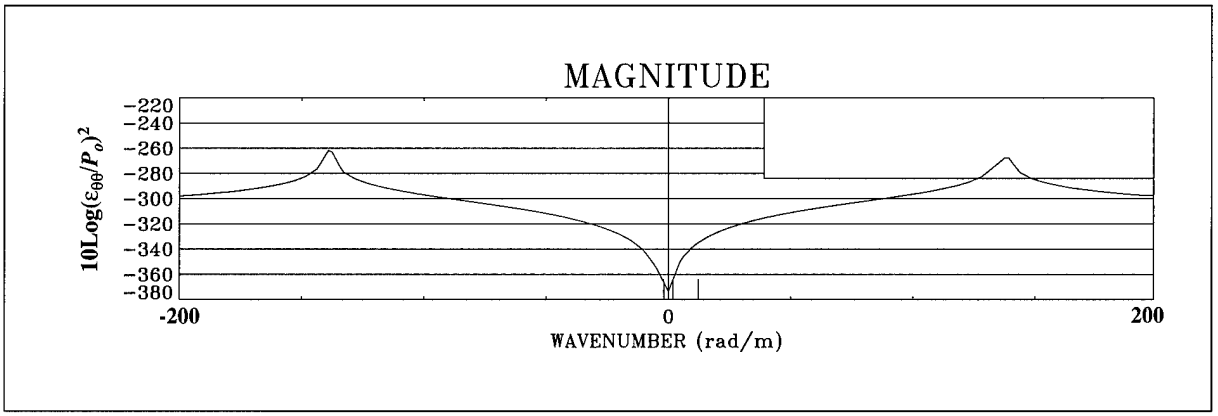


**Figure 28. Frequency Cut at 453.19 Hz Through the Magnitude Surface of Figure 27**

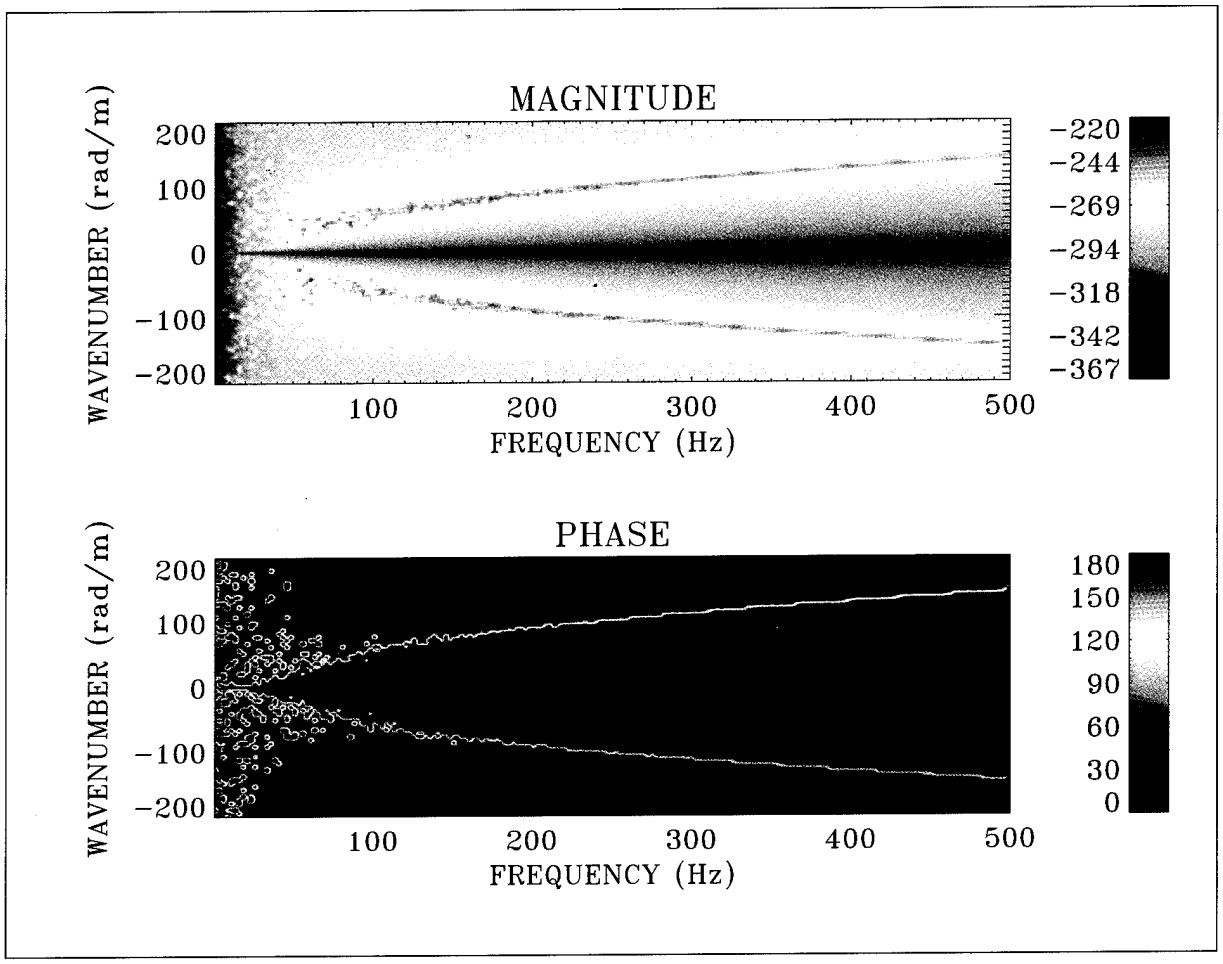


**Figure 29. Longitudinal Strain Transfer Surface: Magnitude = 10Log($\varepsilon_{xx}/P_o$)$^2$ and Phase in Degrees (One Layer, $n$ = 1)**

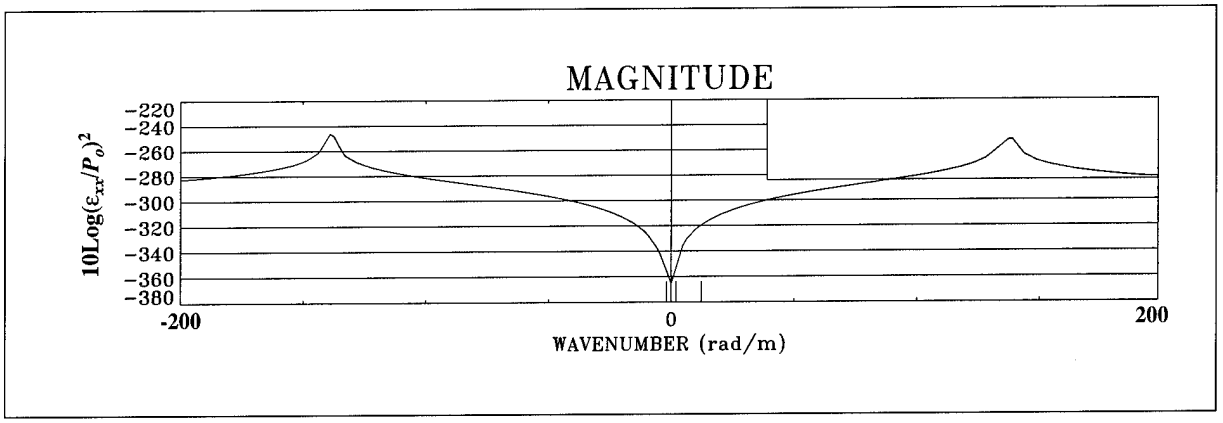


**Figure 30. Frequency Cut at 453.19 Hz Through the Magnitude Surface of Figure 29**

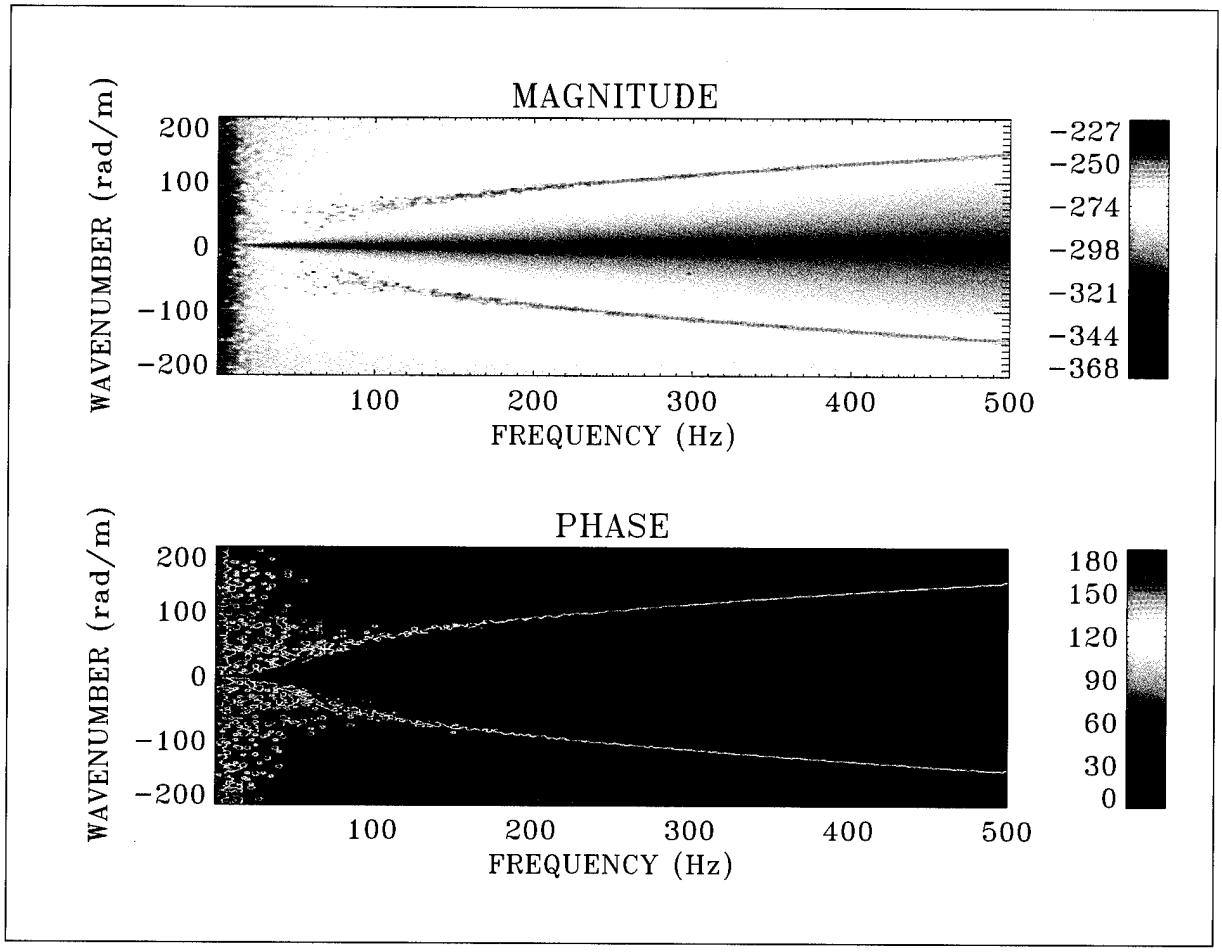


**Figure 31. Optical Phase Sensitivity Strain Transfer Surface: Magnitude = 10Log($\Delta\phi/\phi/P_o$)$^2$ and Phase in Degrees (One Layer, $n$ = 1)**

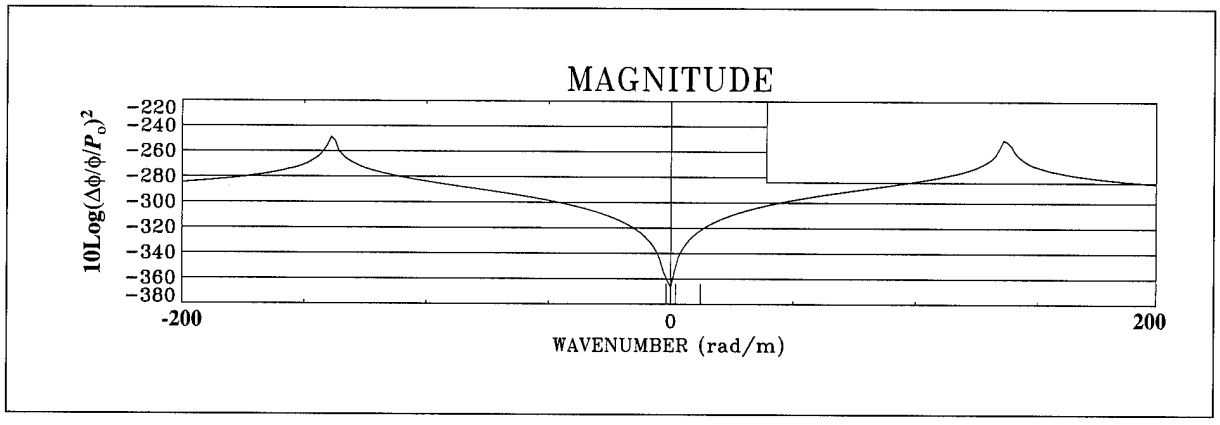


**Figure 32. Frequency Cut at 453.19 Hz Through the Magnitude Surface of Figure 31**

*Nonaxisymmetric Longitudinal Shear Stress Excitation (n = 1)*

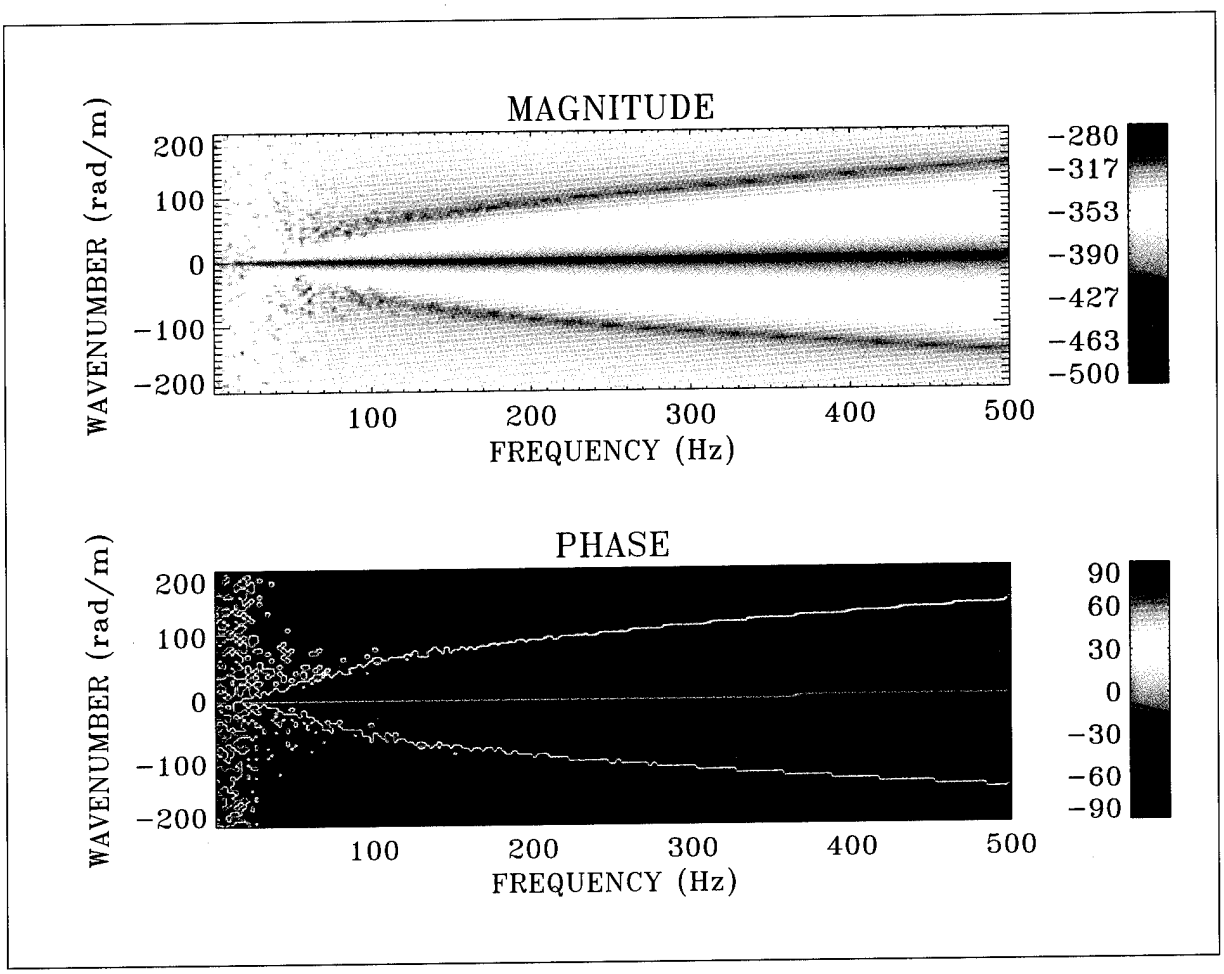


**Figure 33. Radial Strain Transfer Surface: Magnitude = 10Log($\varepsilon_{rr}/P_x$)$^2$ and Phase in Degrees (One Layer, $n$ = 1)**

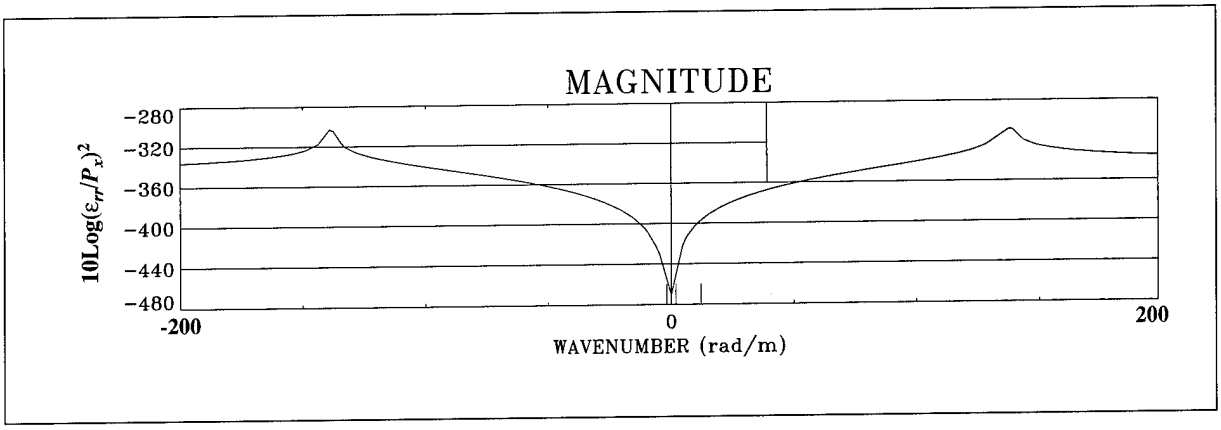


**Figure 34. Frequency Cut at 453.19 Hz Through the Magnitude Surface of Figure 33**

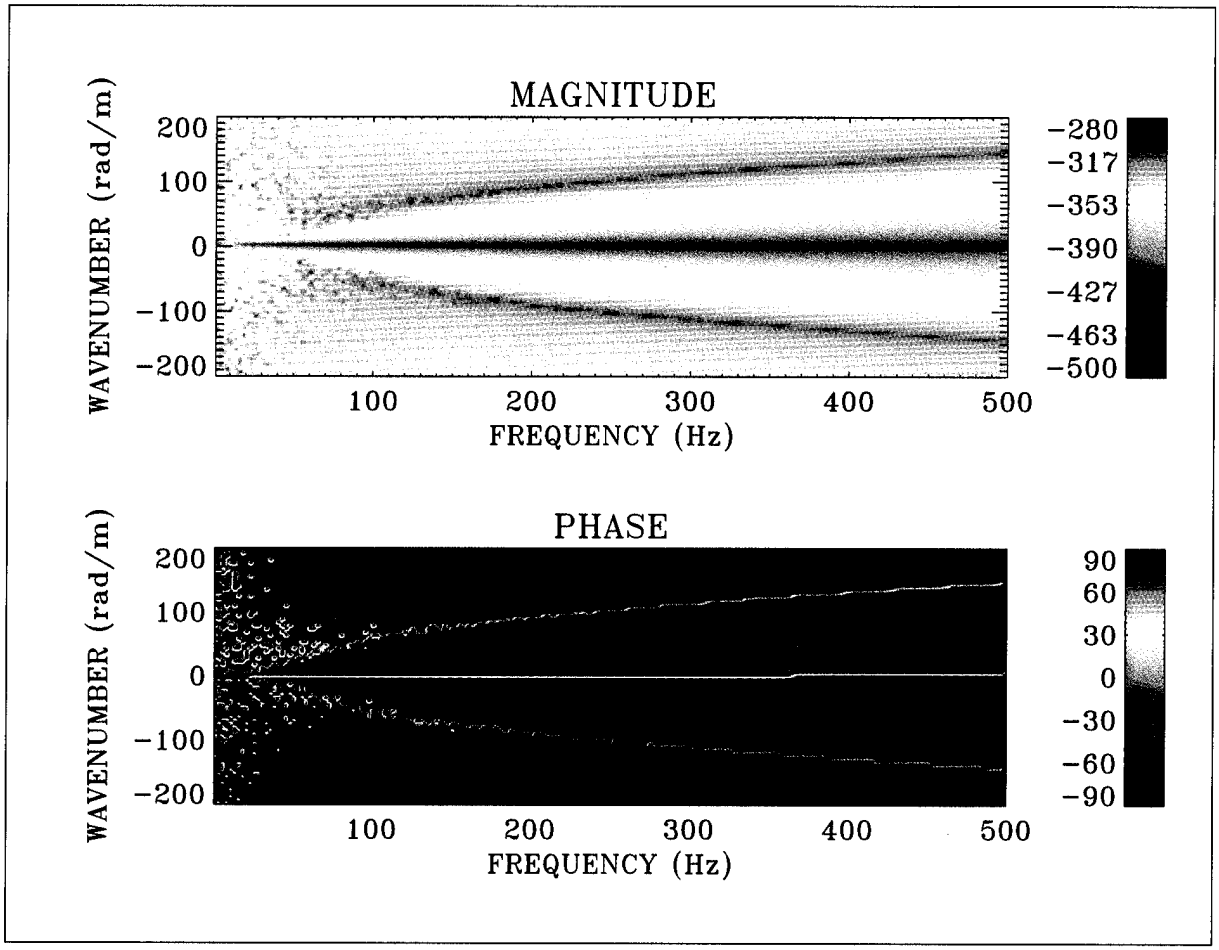


**Figure 35. Circumferential Strain Transfer Surface: Magnitude = 10Log($\varepsilon_{\theta\theta}/P_x$)$^2$ and Phase in Degrees (One Layer, $n$ = 1)**

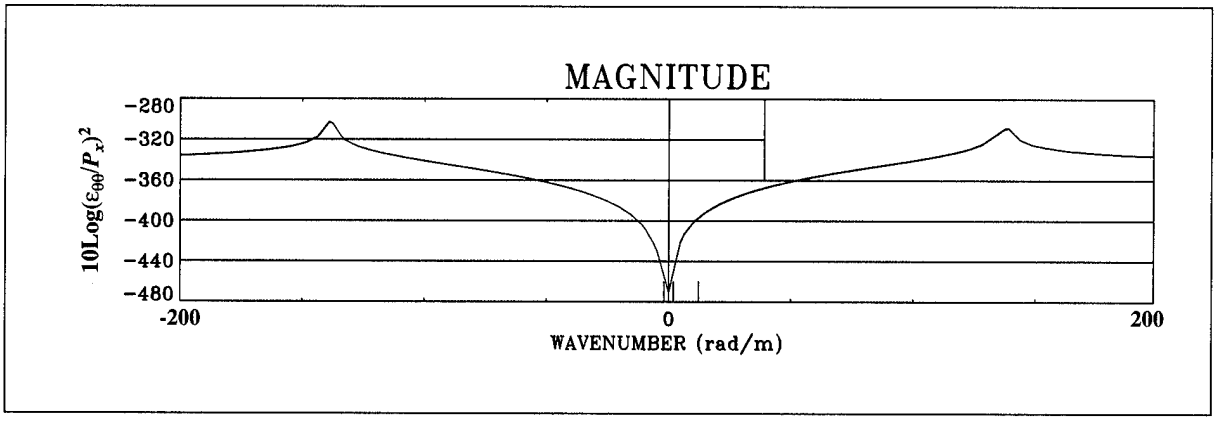


**Figure 36. Frequency Cut at 453.19 Hz Through the Magnitude Surface of Figure 35**

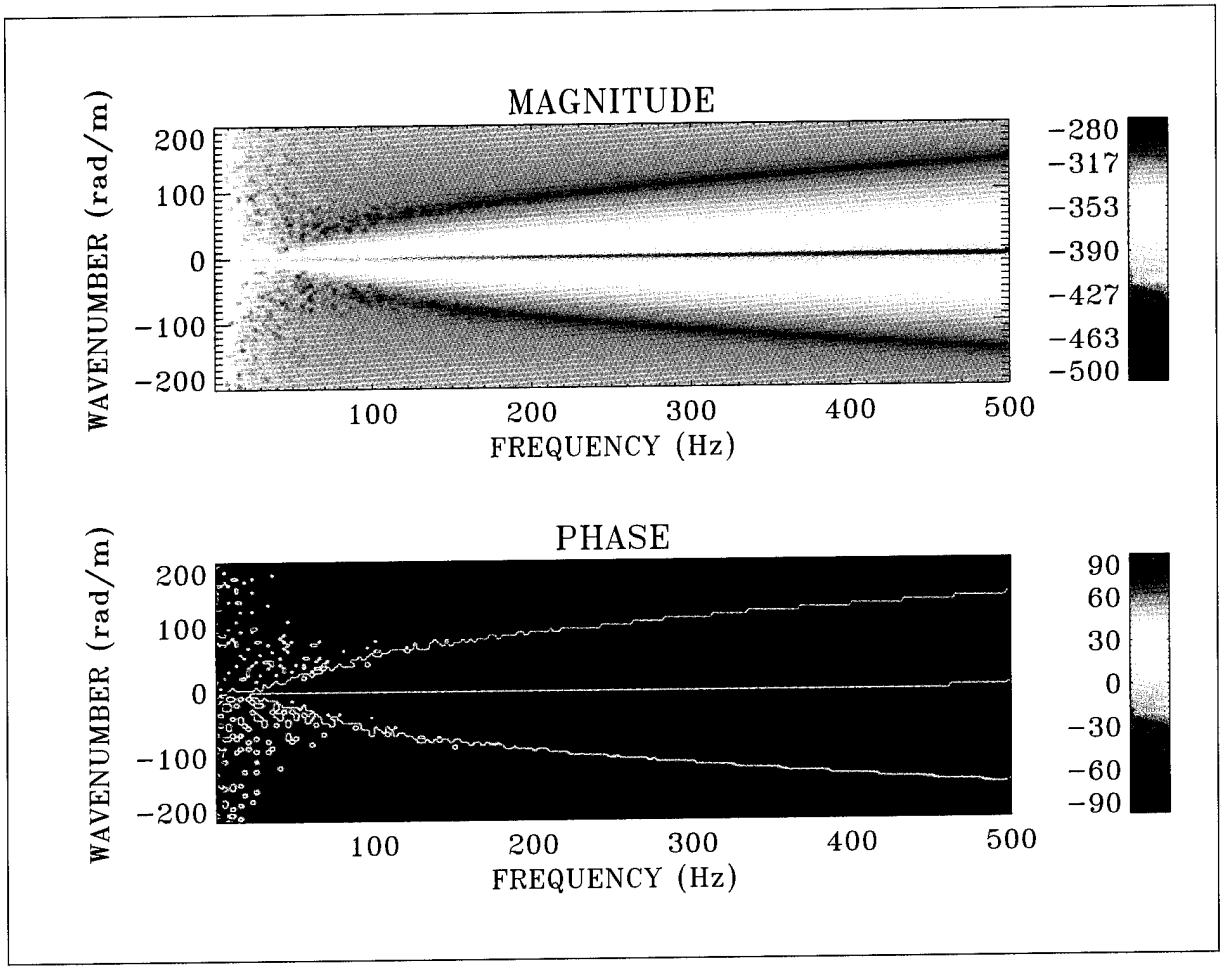


**Figure 37. Longitudinal Strain Transfer Surface: Magnitude = 10Log($\varepsilon_{xx}/P_x$)$^2$ and Phase in Degrees (One Layer, $n$ = 1)**

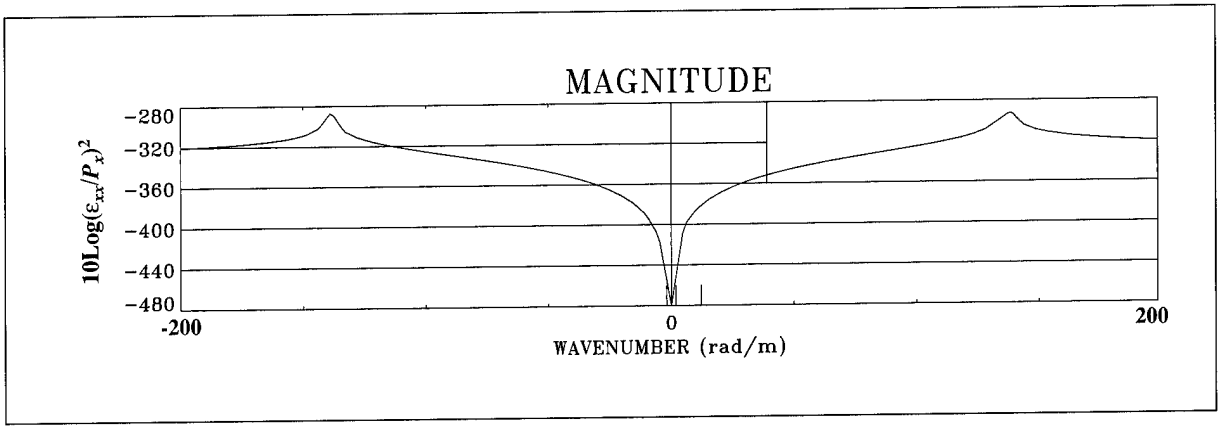


**Figure 38. Frequency Cut at 453.19 Hz Through the Magnitude Surface of Figure 37**

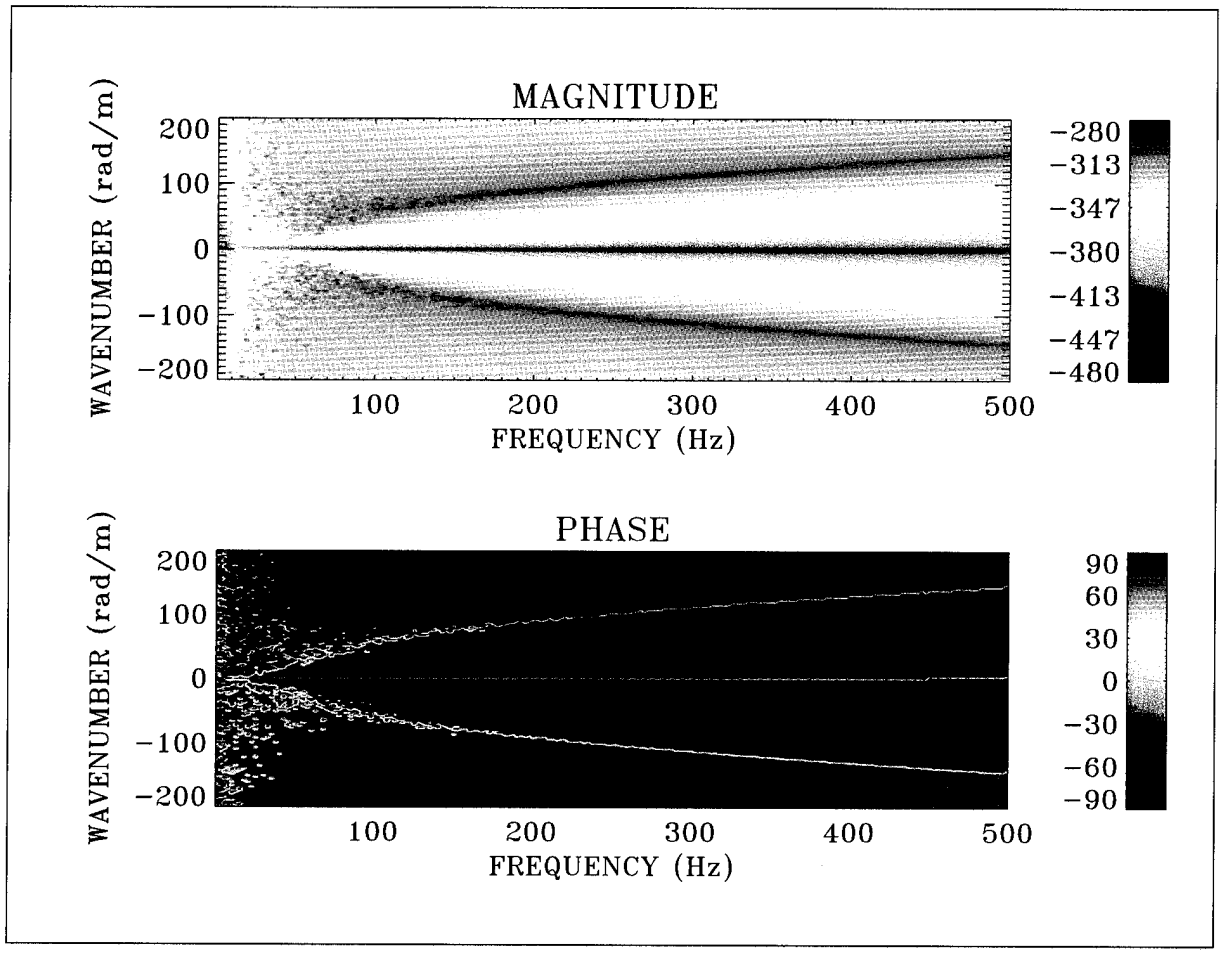


**Figure 39. Optical Phase Sensitivity Strain Transfer Surface: Magnitude = 10Log($\Delta\phi/\phi/P_x$)$^2$ and Phase in Degrees (One Layer, $n$ = 1)**

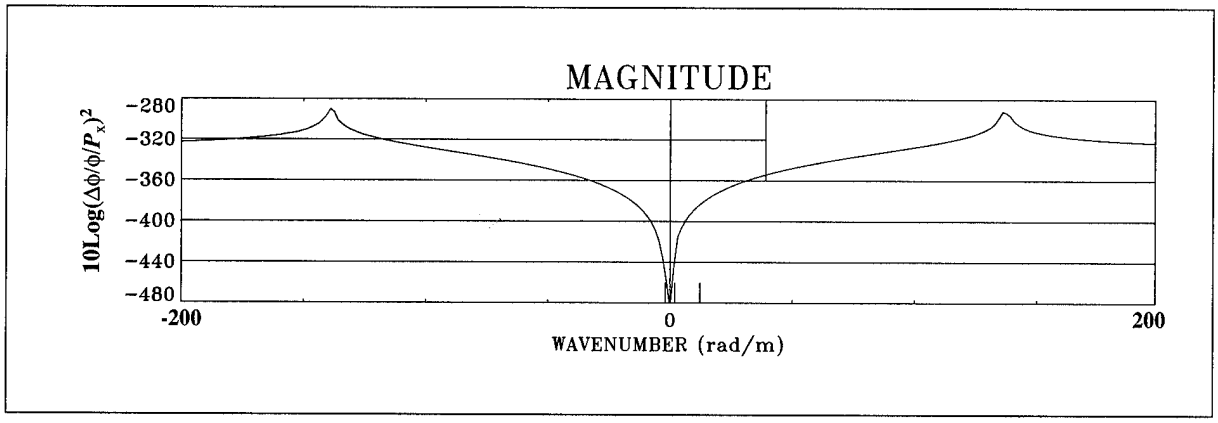


**Figure 40. Frequency Cut at 453.19 Hz Through the Magnitude Surface of Figure 39**

### *Effects of Poisson Ratio*

The Poisson ratio influences the shape of the dynamic response as a function of wavenumber. Figure 41 compares $10\text{Log}(\varepsilon_{rr}/P_o)^2$ for three different values of Poisson ratio. The case of $\nu_c = 0$ results in the flat response indicated by the solid line; the extensional wave is not excited for this case. When $\nu_c = 0$, the three strains are decoupled from each other. Since the excitation, $P_o$, is in the radial direction there is no way to perturb the longitudinal direction, hence the lack of extensional wave response. The Poisson ratio increasing from 0.17 to 0.45 results in an increasingly large extensional wave resonance amplitude. As the value of the Poisson ratio increases, the relative difference between the $k = 0$ value of $10\text{Log}(\varepsilon_{rr}/P_o)^2$ and the value of $10\text{Log}(\varepsilon_{rr}/P_o)^2$ above the extensional wave resonance (flat plateau) increases. This increase of

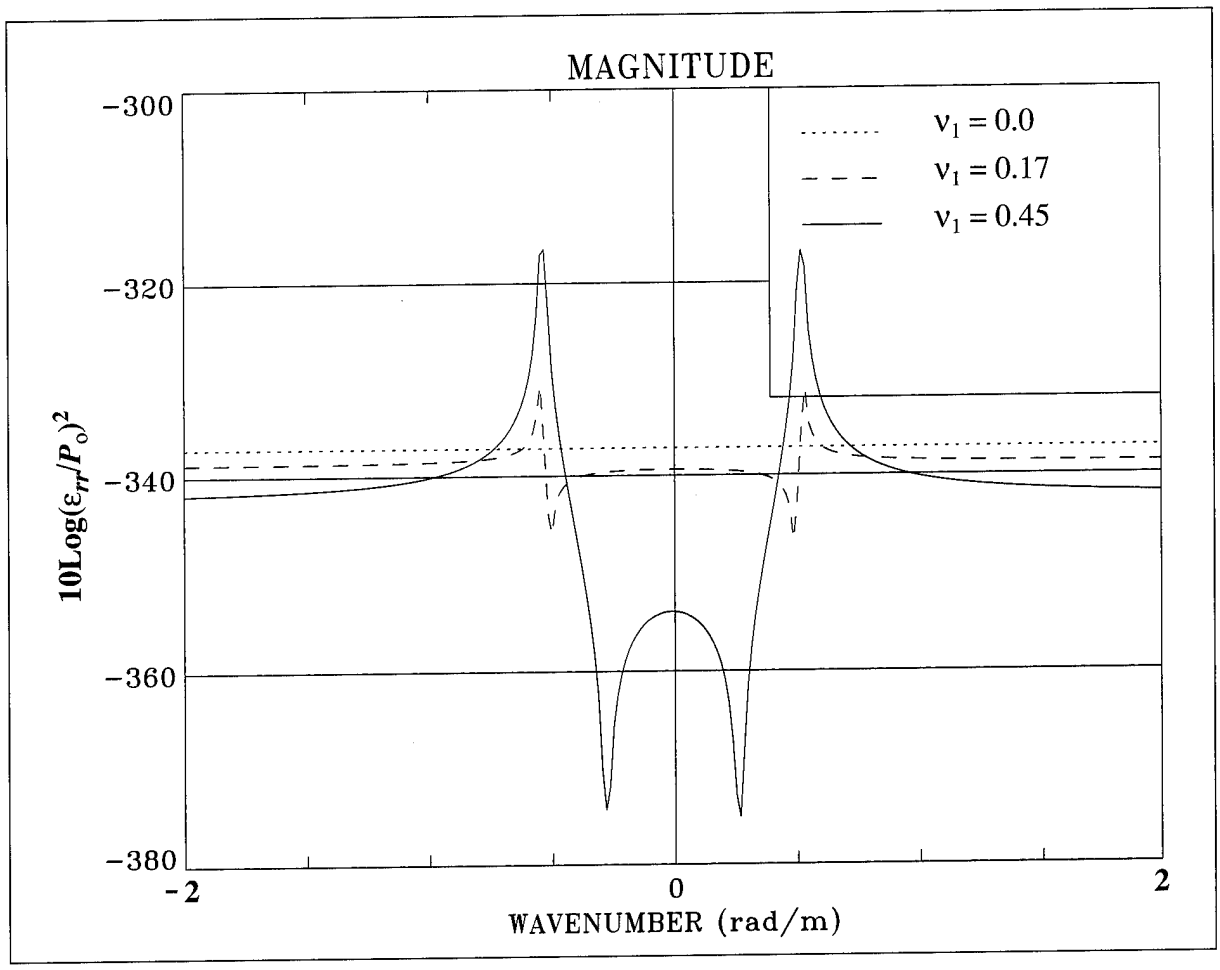


**Figure 41. Effects of Poisson Ratio on the Radial Strain at 480 Hz**

the difference in relative levels above and below extensional wave resonance is also evident when a coating is applied to the fiber, which will be seen in the next section.

## COATED OPTICAL FIBER

The bare optical fiber of the previous section is coated with an ALCRYN layer. ALCRYN is a viscoelastic rubber whose properties are listed in table 3. The dynamic material properties of

**Table 3. Optical Fiber and ALCRYN Properties**

| Optical Fiber Property | ALCRYN Property | Definition |
|---|---|---|
| $E_1 = 7.2\times10^{10}\frac{N}{m^2}$ | $E_2 = 1.64\times10^{7}\frac{N}{m^2}$ | Young's Modulus |
| $\zeta_1 = 0.005$ | $\zeta_2 = 0.47$ | Structural Loss Factor |
| $\rho_1 = 2600\frac{kg}{m^3}$ | $\rho_2 = 1000\frac{kg}{m^3}$ | Density |
| $\nu_1 = 0.17$ | $\nu_2 = 0.45$ | Poisson's Ratio |
| $a = 62.5\times10^{-6}$m | | Cladding Outer Radius |
| $r_c = 4.5\times10^{-6}$m | | Core Radius |
| $r_1 = 1.0\times10^{-6}$m | | Calculation Radius |
| | $a = 62.5\times10^{-6}$m | Coating Inner Radius |
| | $b = 4.0\times10^{-3}$m | Coating Outer Radius |
| $n_o = 1.46$ | | Refractive Index |
| $P_{11} = 0.126$ | | Pockel Coefficient |
| $P_{12} = 0.27$ | | Pockel Coefficient |

ALCRYN were measured with a Metravib dynamic mechanical analyzer at the Naval Undersea Warfare Center Detachment in New London, Connecticut. The cladding outer radius is always equal to the inner radius of the coating (see table 3), consistent with boundary condition 8.

### *Transfer Surfaces, Two Layers*

Similar to the previous section for the bare optical fiber, the response of the coated fiber will be simulated using the two-layer infinite cylinder model for two different circumferential order numbers and three different excitation types.

The response to the first excitation, $P_o$, is covered in figures 42 through 49. Each strain component is displayed individually along with the corresponding optical phase sensitivity image (figure 48) and the corresponding cuts through the image (figure 49). The most dramatic effect of the coating is to slow the extensional wave to 190 m/sec, down from 5,571 m/sec for the bare fiber of figure 9. In the radial strain simulation at 40 Hz (figure 43), the extensional wave resonance peak is greater than 60 dB above the $k = 0$ level. The difference grows to over 80 dB in the optical phase sensitivity cuts shown in figure 49. The effects of material properties (first observed in the case of the bare fiber), which create a relative difference in strain response between $k = 0$ and the wavenumber region at and above extensional wave resonance, are much greater for the coated fiber case. Additionally, since the coating is much softer than the fiber, it contributes mass to the composite, adding very little stiffness. This is why the extensional wave phase velocity slowed so dramatically.

The simulations for the response to longitudinal shear stress excitation are shown in figures 50 through 57. Similar to the $P_o$ excitation (figure 42), the extensional wave phase velocity has slowed to 190 m/sec. Comparison is made between the optical phase response to $P_o$ and to $P_x$ in figure 58. Notice the tremendous increase in sensitivity to shear stress $P_x$ over the sensitivity to normal pressure $P_o$—on the order of 50 to 70 dB.

All of the nonaxisymmetric excitations, $P_o$, $P_x$, and $P_\theta$, produce dispersive branches of wave

propagation, as seen in figures 59 through 82. The motion of the cylinder follows the deformation shape depicted in figure 7. Excitations $P_o$ and $P_\theta$ produce strains of approximately equivalent magnitude. Excitation $P_x$ produces strains some 10 dB lower than $P_o$ and $P_\theta$, as can be observed by inspection of these figures.

*Axisymmetric Radial Pressure Excitation (n = 0), Two Layers*

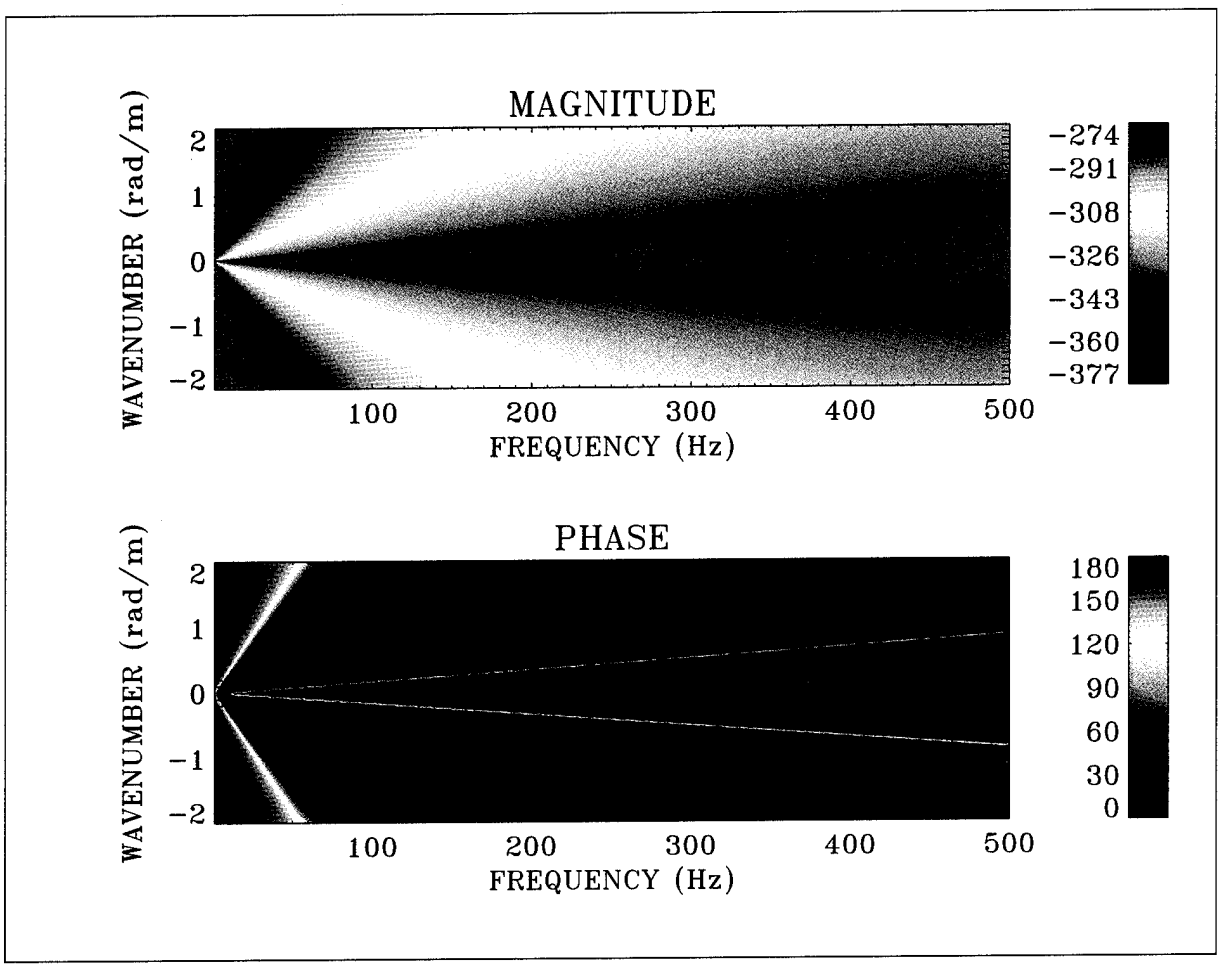


**Figure 42. Radial Strain Transfer Surface: Magnitude = 10Log($\varepsilon_{rr}/P_o$)$^2$ and Phase in Degrees (Two Layers, $n$ = 0)**

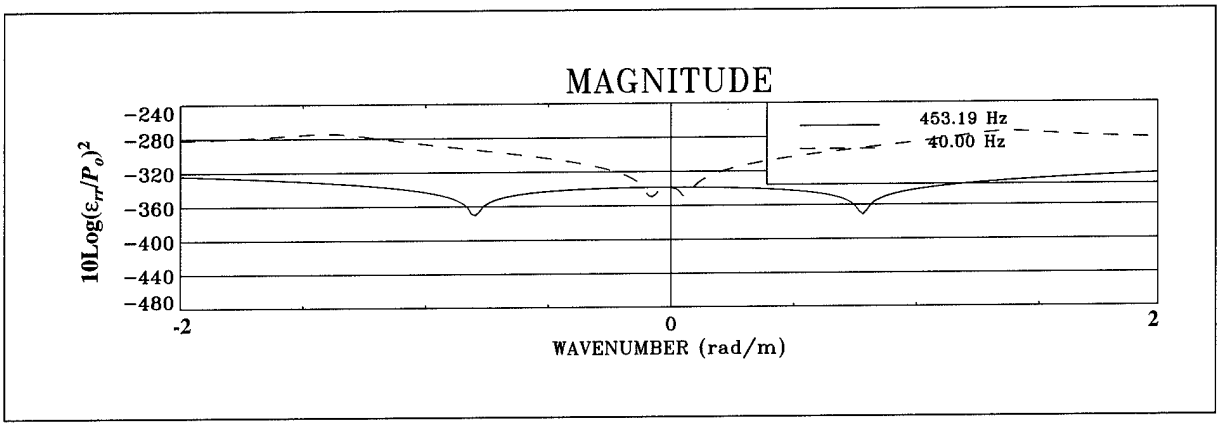


**Figure 43. Frequency Cut at 453.19 Hz Through the Magnitude Surface of Figure 42**

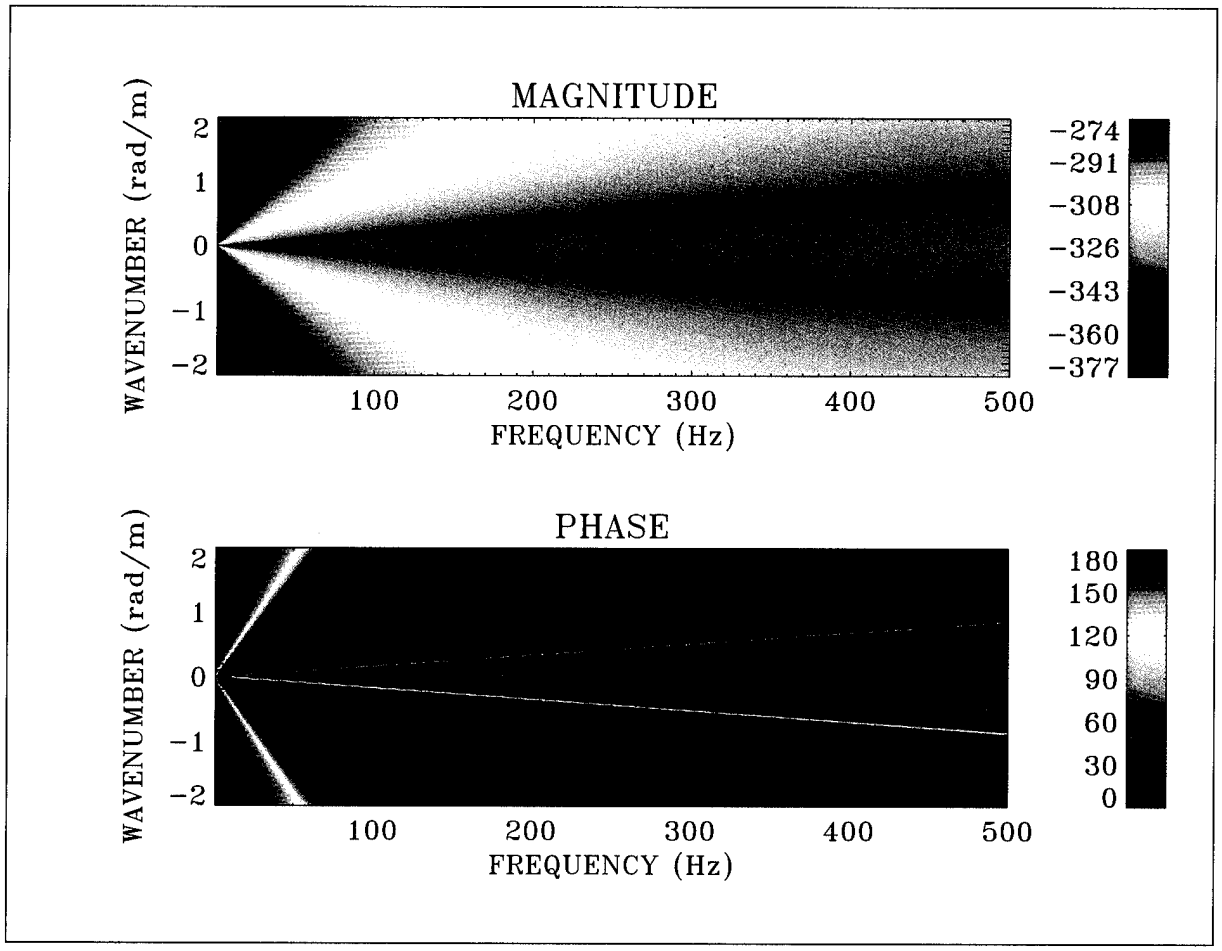


**Figure 44. Circumferential Strain Transfer Surface: Magnitude = 10Log($\varepsilon_{\theta\theta}/P_o$)$^2$ and Phase in Degrees (Two Layers, $n$ = 0)**

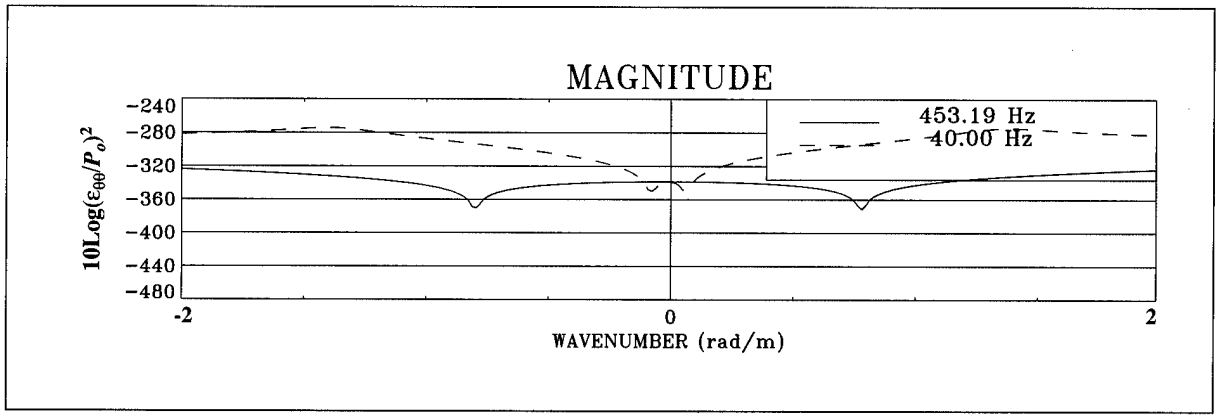


**Figure 45. Frequency Cut at 453.19 Hz Through the Magnitude Surface of Figure 44**

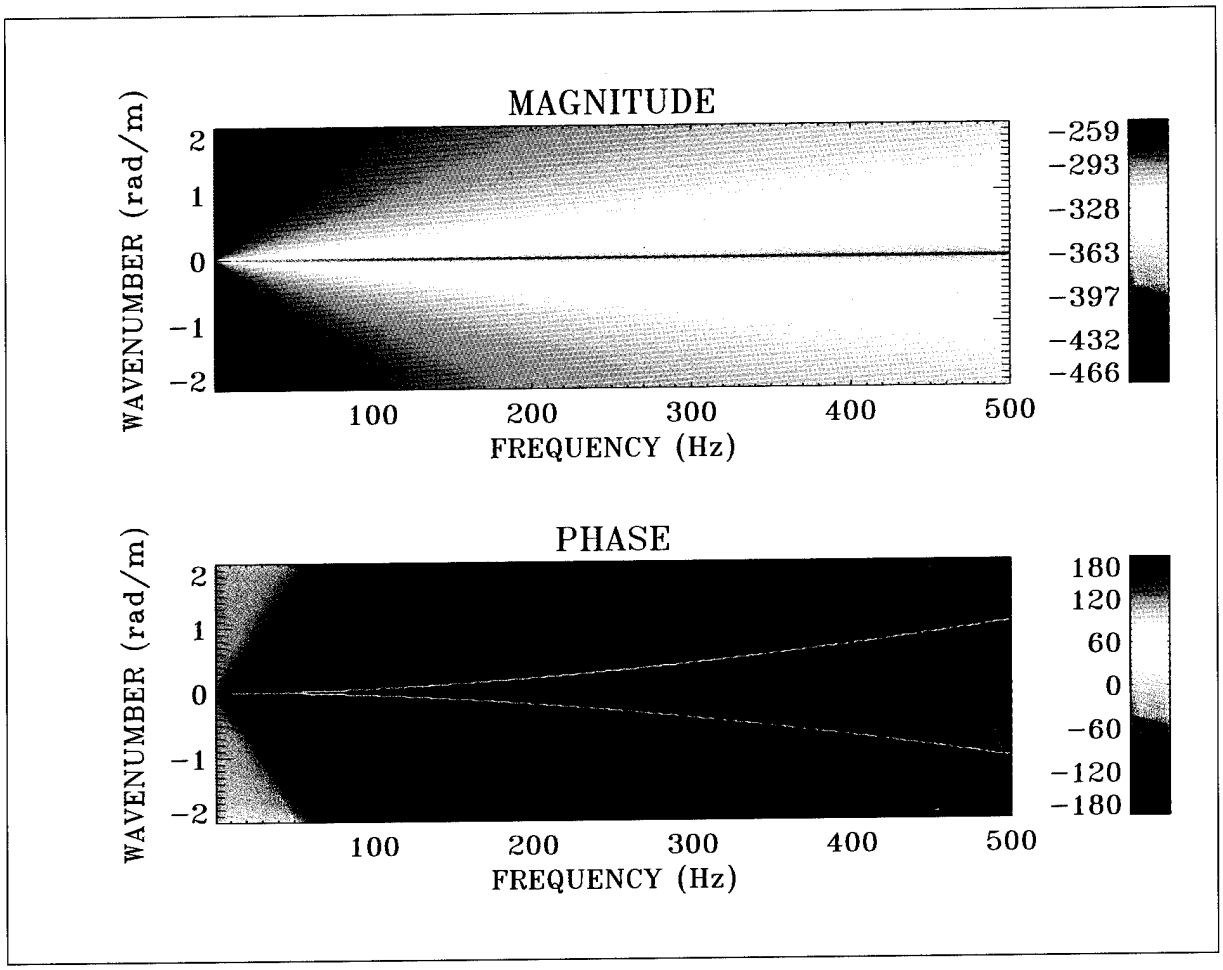


**Figure 46. Longitudinal Strain Transfer Surface: Magnitude = 10Log($\varepsilon_{xx}/P_o$)$^2$ and Phase in Degrees (Two Layers, $n$ = 0)**

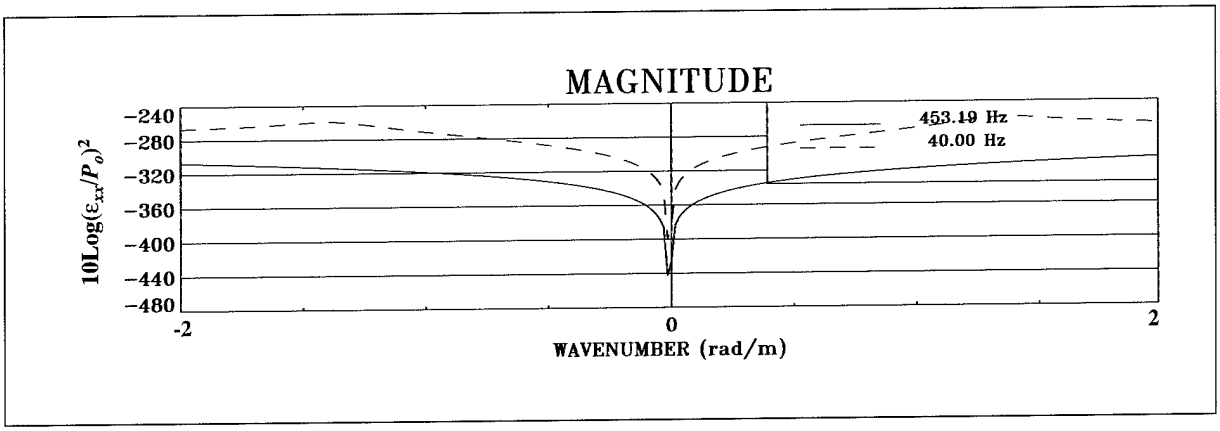


**Figure 47. Frequency Cut at 453.19 Hz Through the Magnitude Surface of Figure 46**

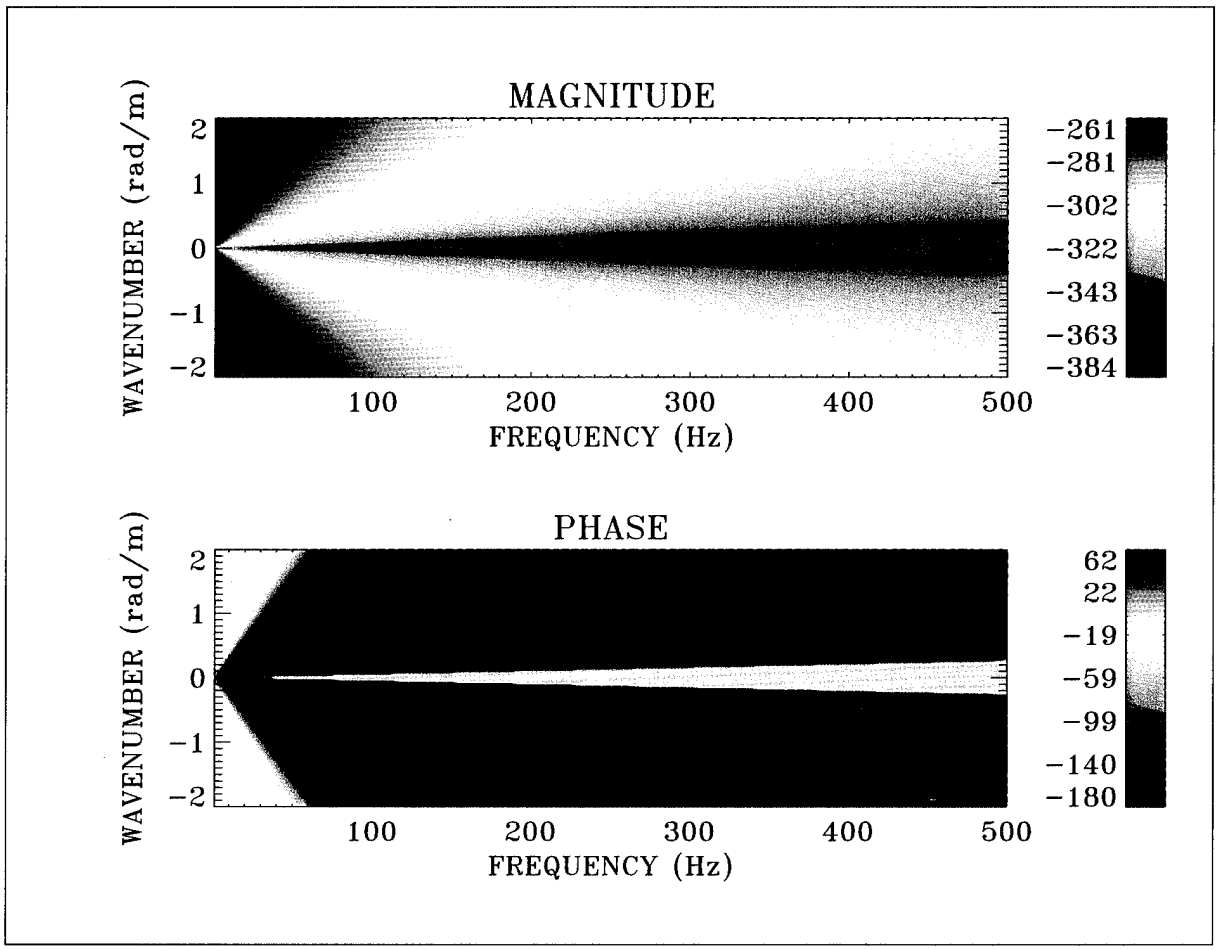


**Figure 48. Optical Phase Sensitivity Strain Transfer Surface: Magnitude = 10Log$(\Delta\phi/\phi/P_o)^2$ and Phase in Degrees (Two Layers, $n$ = 0)**

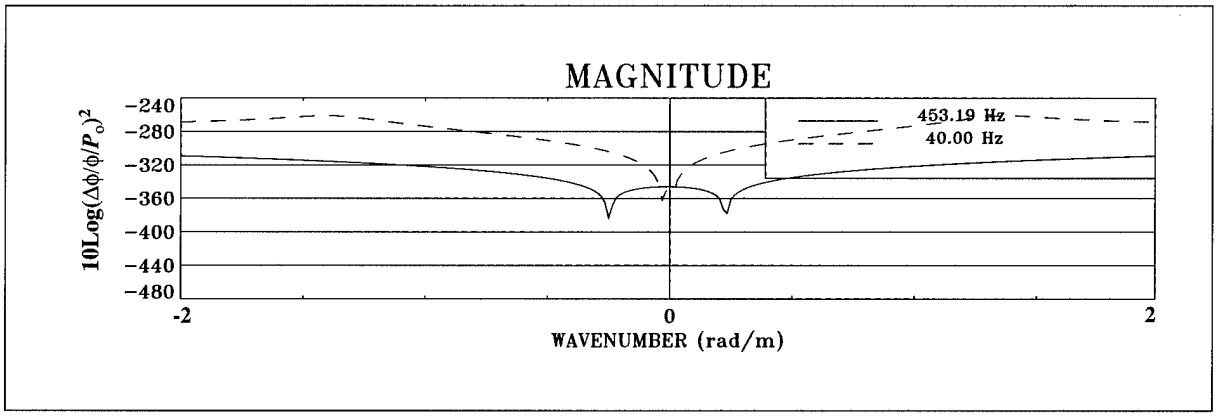


**Figure 49. Frequency Cut at 453.19 Hz Through the Magnitude Surface of Figure 48**

*Axisymmetric Longitudinal Shear Stress Excitation (n = 0), Two Layers*

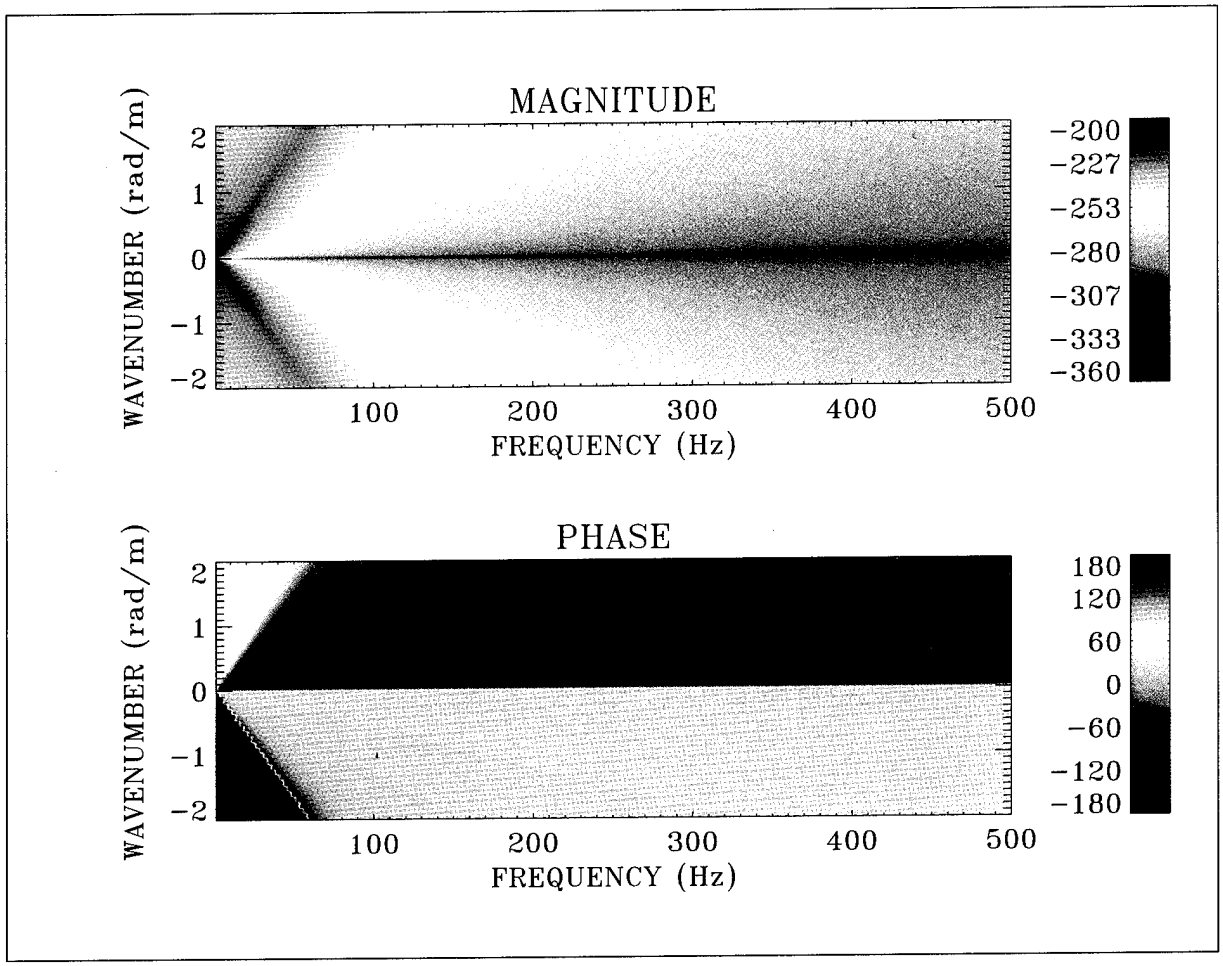


**Figure 50. Radial Strain Transfer Surface: Magnitude = 10Log($\varepsilon_{rr}/P_x$)$^2$ and Phase in Degrees (Two Layers, $n$ = 0)**

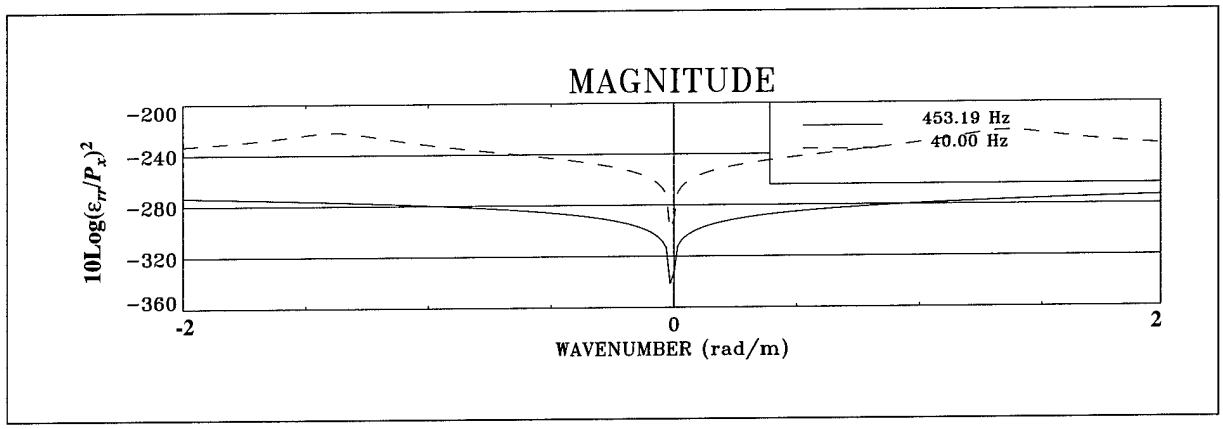


**Figure 51. Frequency Cut at 453.19 Hz Through the Magnitude Surface of Figure 50**

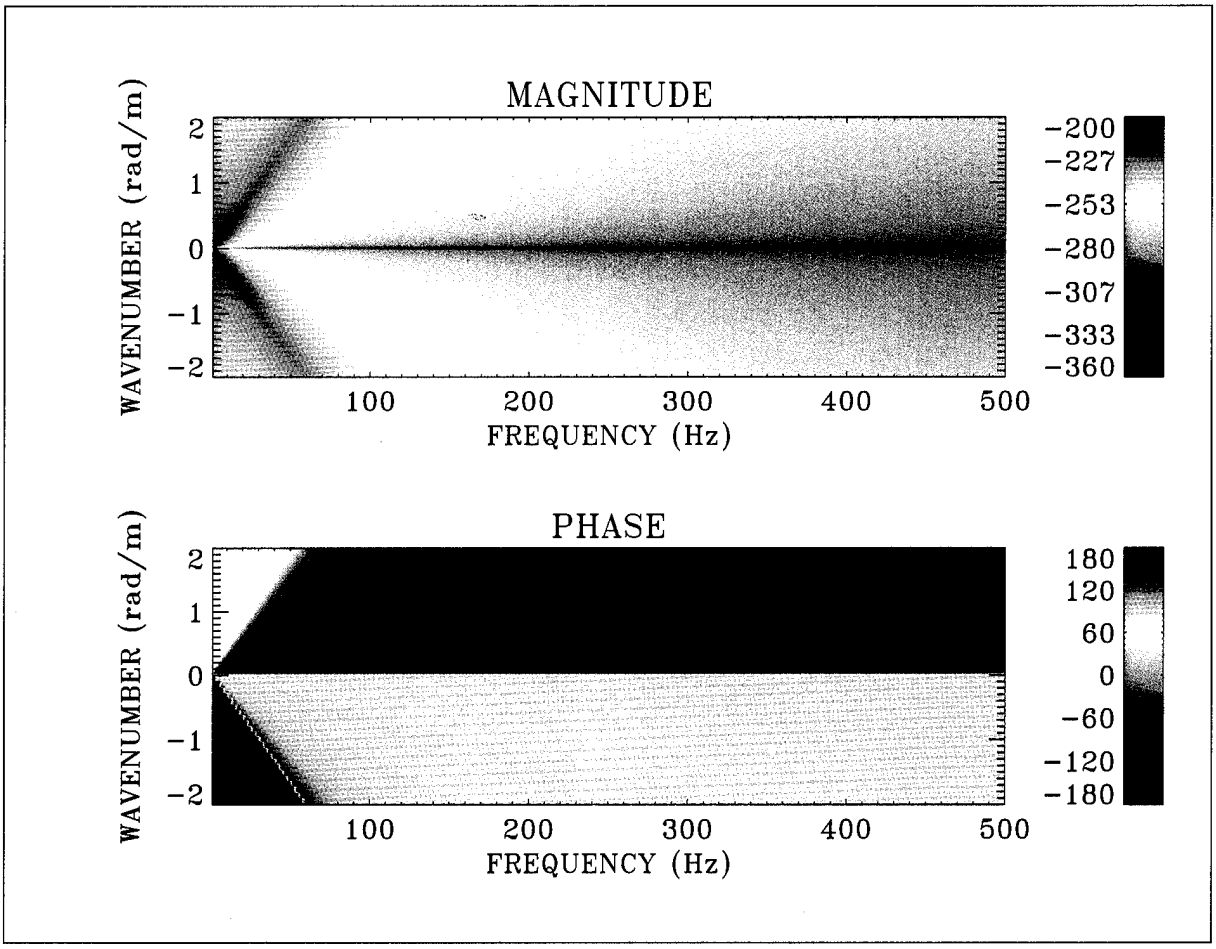


**Figure 52. Circumferential Strain Transfer Surface: Magnitude = 10Log($\varepsilon_{\theta\theta}/P_x$)$^2$ and Phase in Degrees (Two Layers, $n$ = 0)**

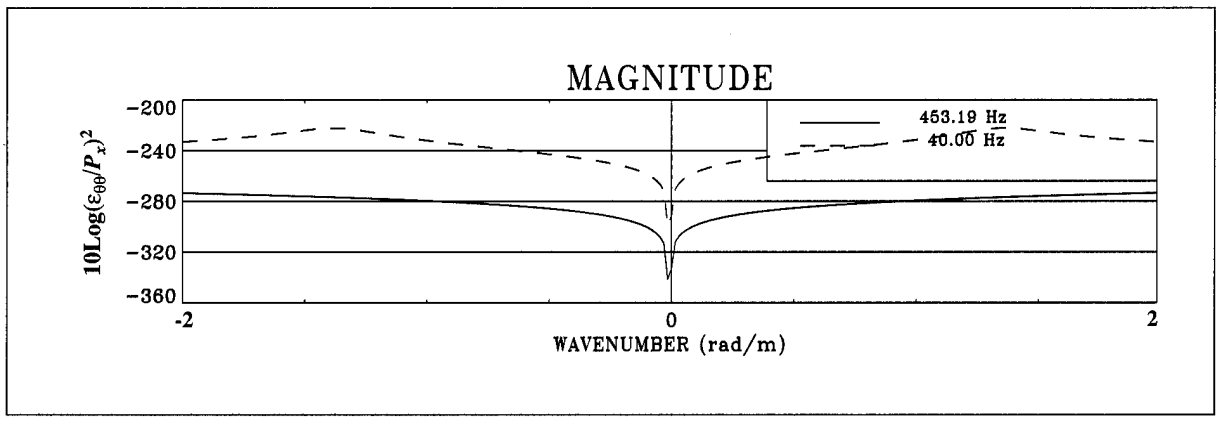


**Figure 53. Frequency Cut at 453.19 Hz Through the Magnitude Surface of Figure 52**

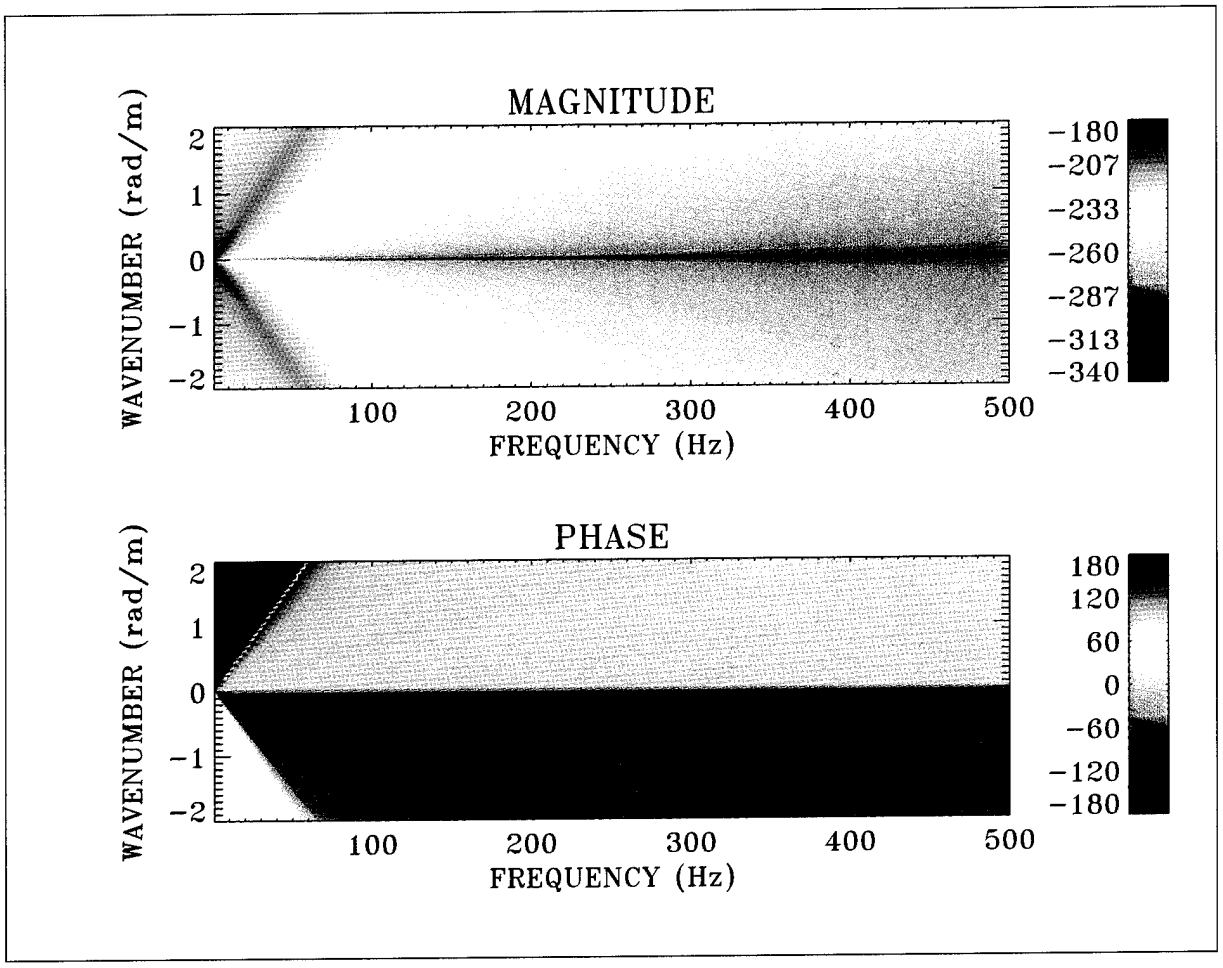


**Figure 54. Longitudinal Strain Transfer Surface: Magnitude = 10Log($\varepsilon_{xx}/P_x$)$^2$ and Phase in Degrees (Two Layers, $n$ = 0)**

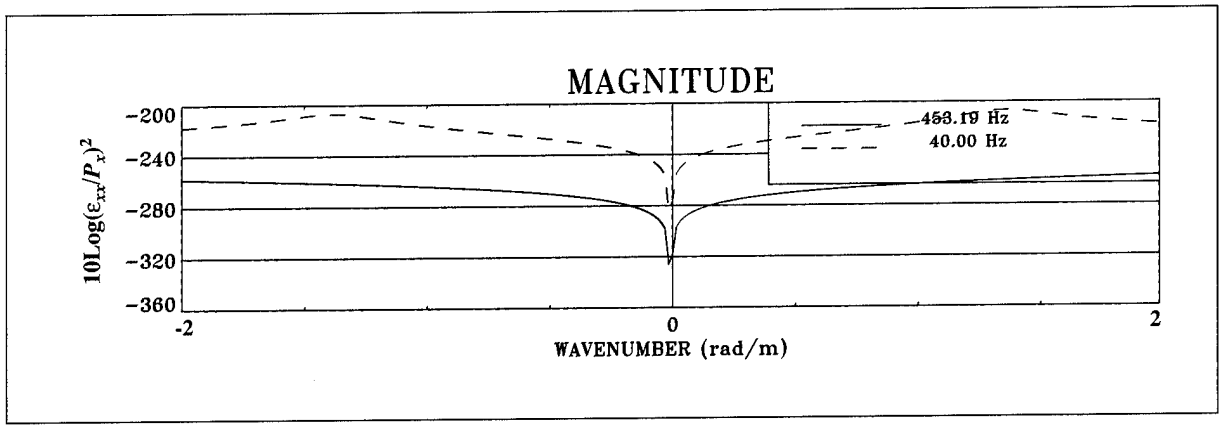


**Figure 55. Frequency Cut at 453.19 Hz Through the Magnitude Surface of Figure 54**

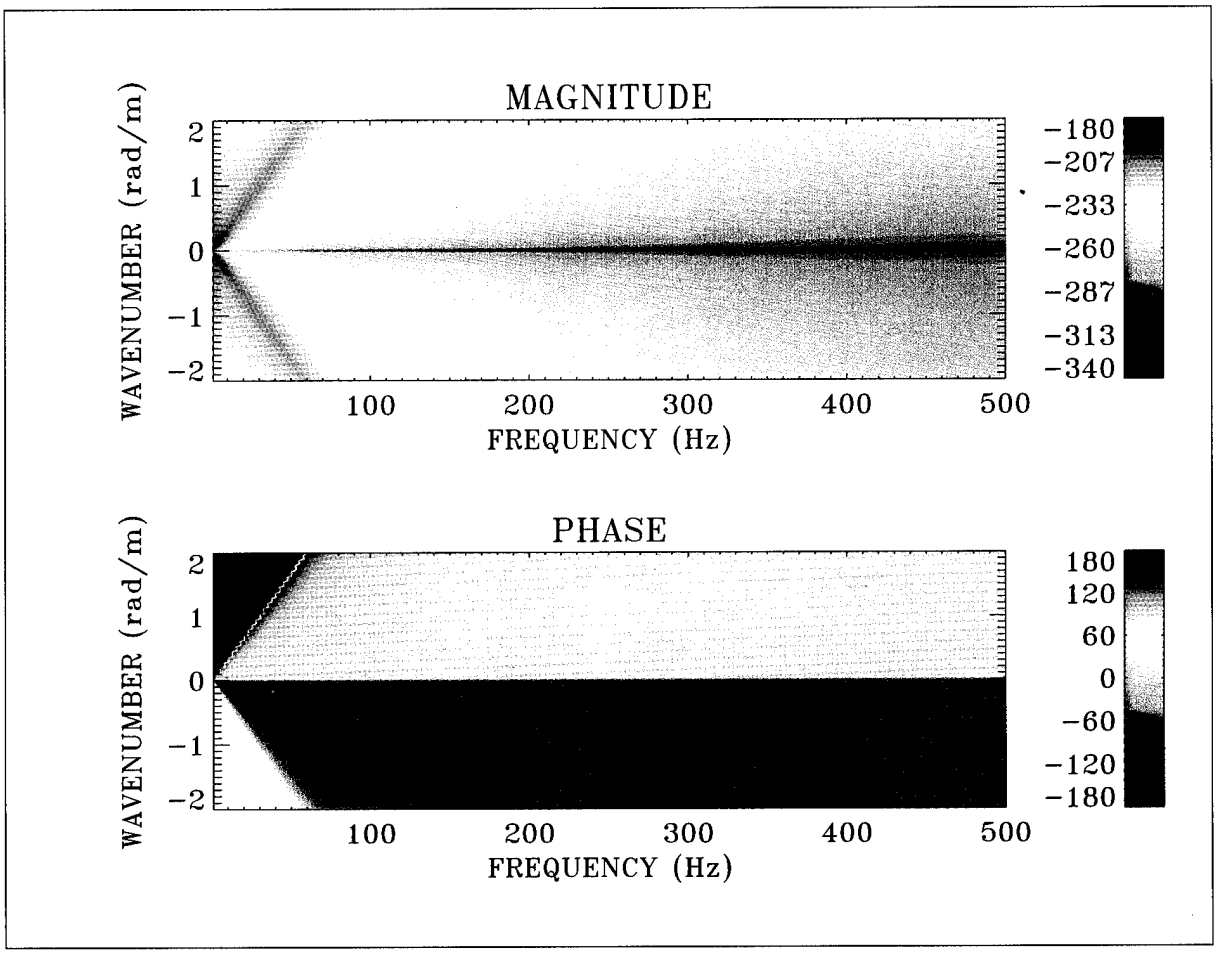


**Figure 56. Optical Phase Sensitivity Strain Transfer Surface: Magnitude = 10Log($\Delta\phi/\phi/P_x$)$^2$ and Phase in Degrees (Two Layers, $n$ = 0)**

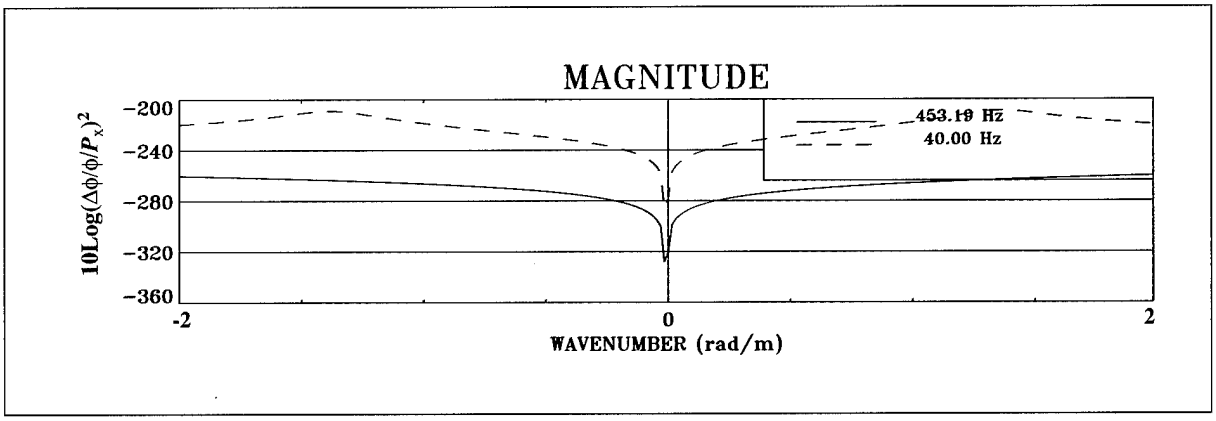


**Figure 57. Frequency Cut at 453.19 Hz Through the Magnitude Surface of Figure 56**

*Comparison of $P_o$ and $P_x$ Optical Phase Sensitivities (n = 0)*

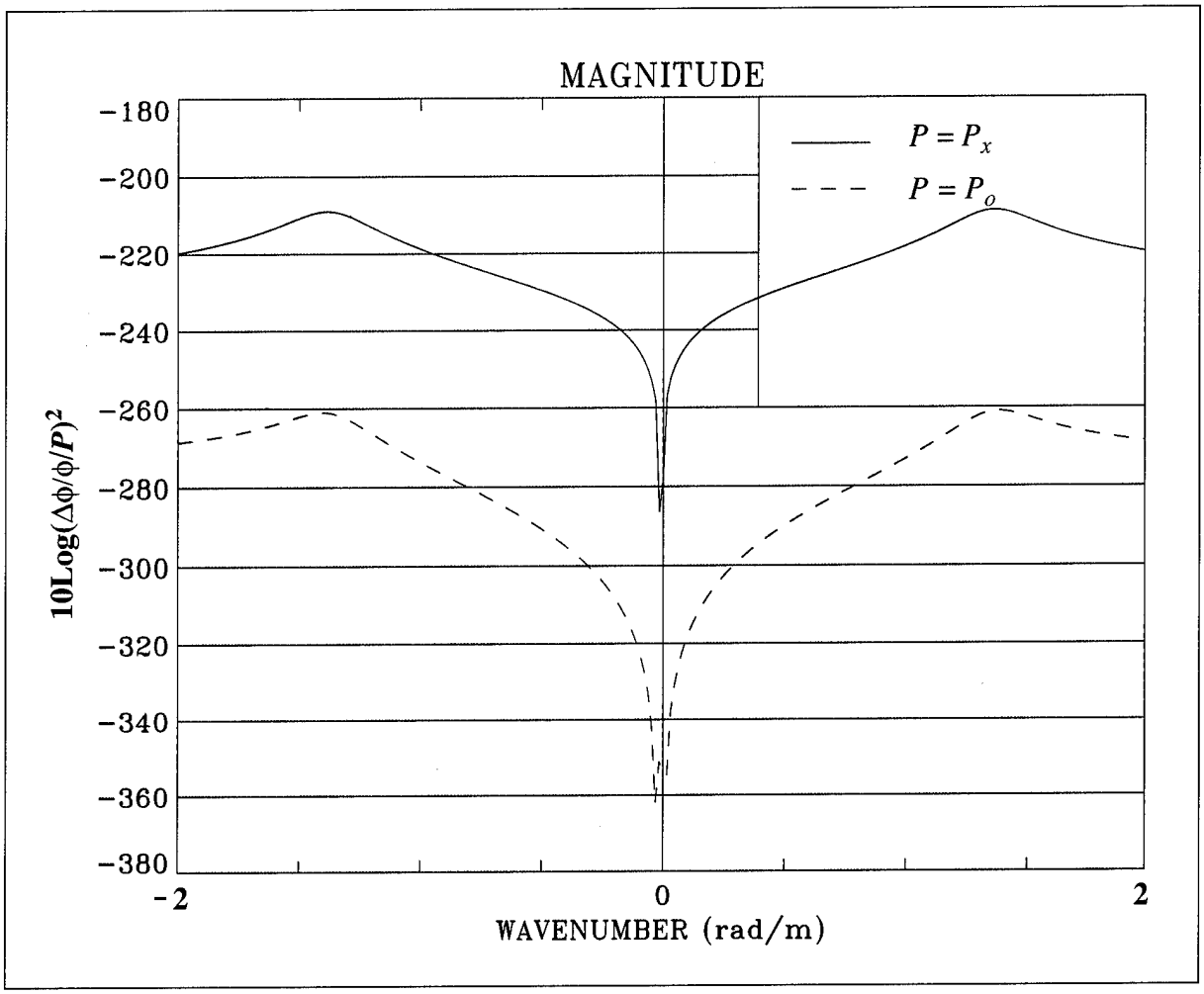


**Figure 58. Comparison of $\Delta\phi/\phi/P_x$ and $\Delta\phi/\phi/P_o$ at 40 Hz**

*Nonaxisymmetric Radial Pressure Excitation (n = 1), Two Layers*

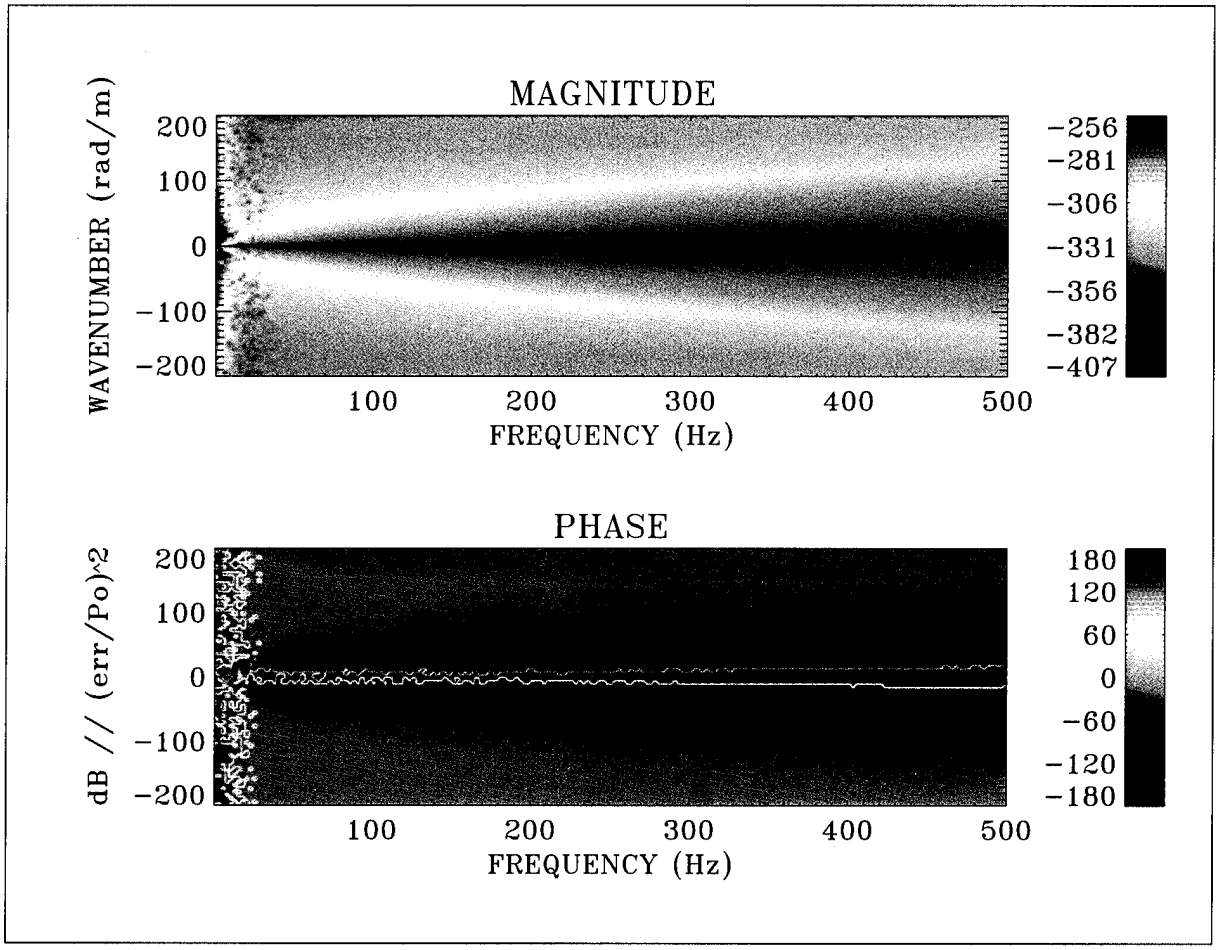


**Figure 59. Radial Strain Transfer Surface: Magnitude = 10Log($\varepsilon_{rr}/P_o$)$^2$ and Phase in Degrees (Two Layers, $n$ = 1)**

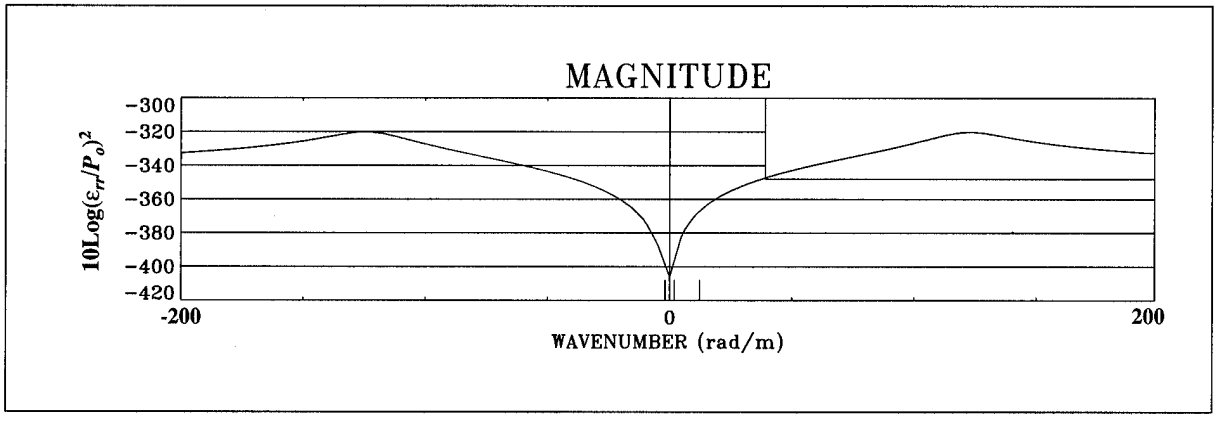


**Figure 60. Frequency Cut at 453.19 Hz Through the Magnitude Surface of Figure 59**

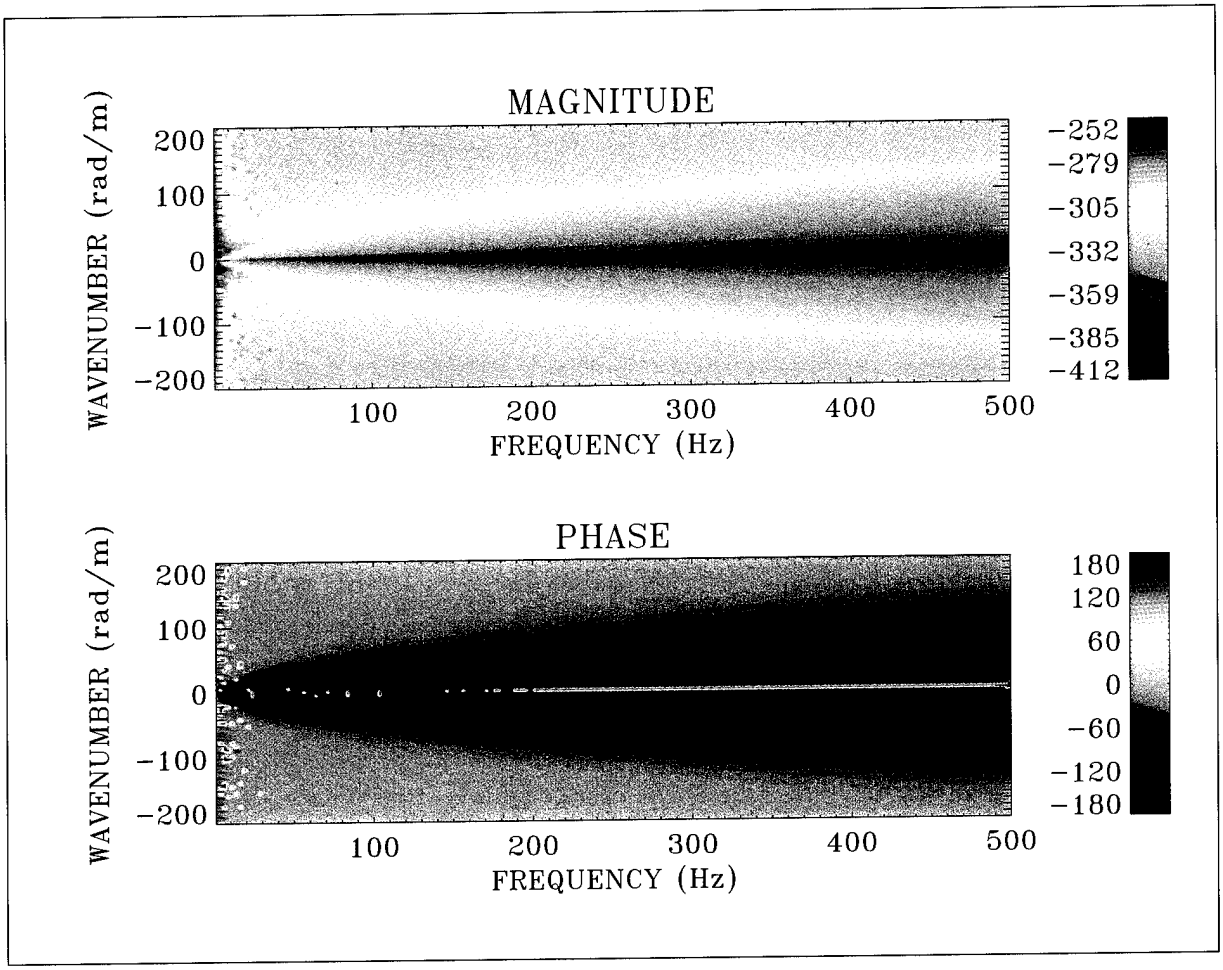


**Figure 61. Circumferential Strain Transfer Surface: Magnitude = $10\text{Log}(\varepsilon_{\theta\theta}/P_o)^2$ and Phase in Degrees (Two Layers, $n$ = 1)**

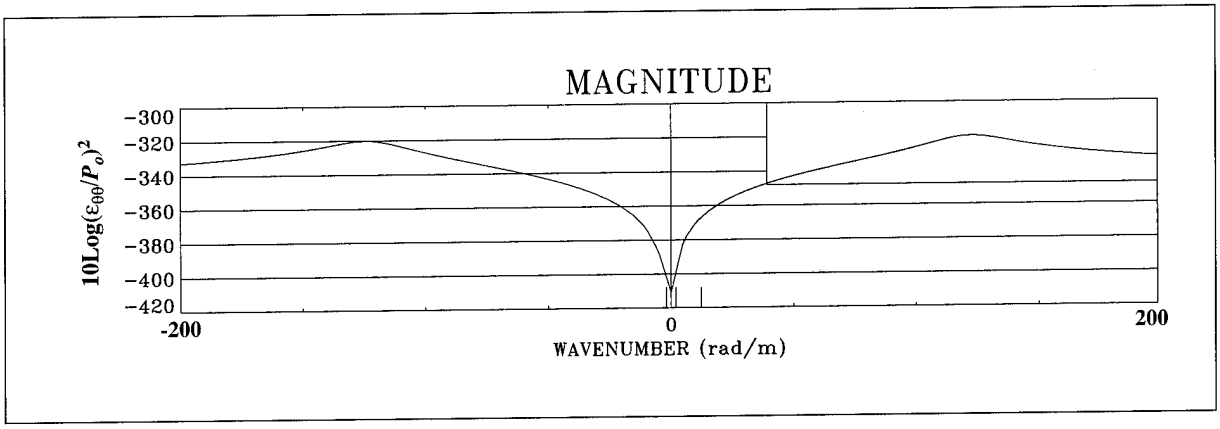


**Figure 62. Frequency Cut at 453.19 Hz Through the Magnitude Surface of Figure 61**

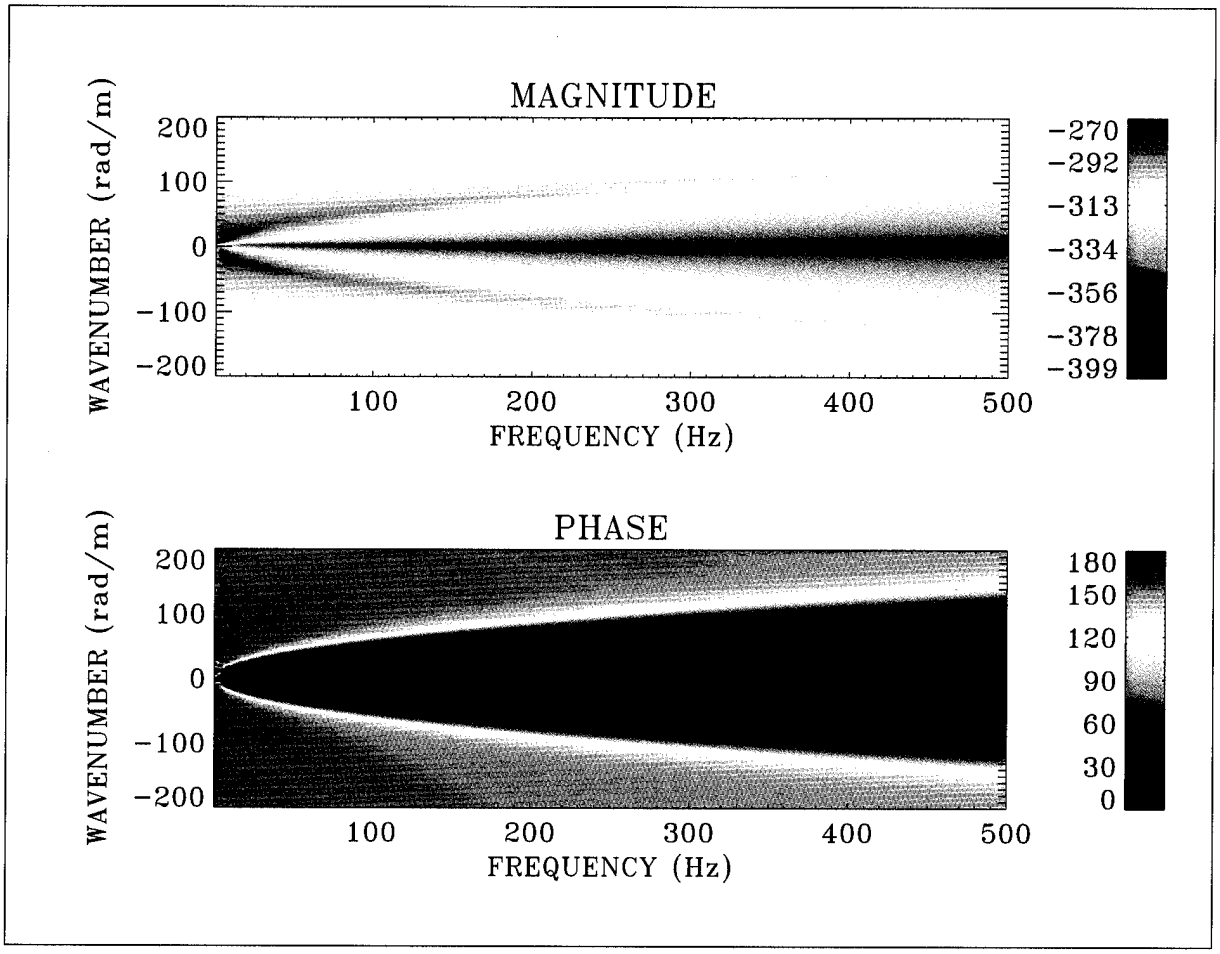


**Figure 63. Longitudinal Strain Transfer Surface: Magnitude = 10Log($\varepsilon_{xx}/P_o$)$^2$ and Phase in Degrees (Two Layers, $n$ = 1)**

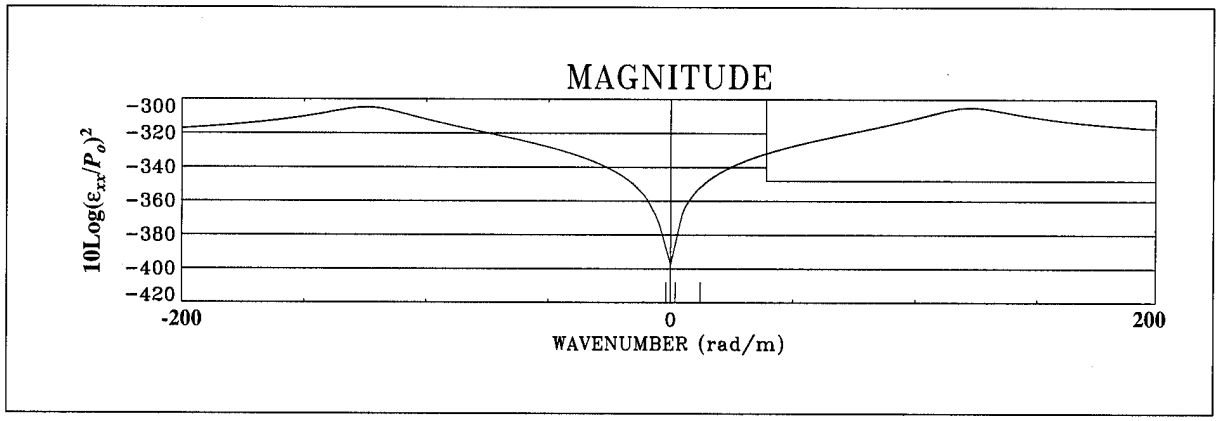


**Figure 64. Frequency Cut at 453.19 Hz Through the Magnitude Surface of Figure 63**

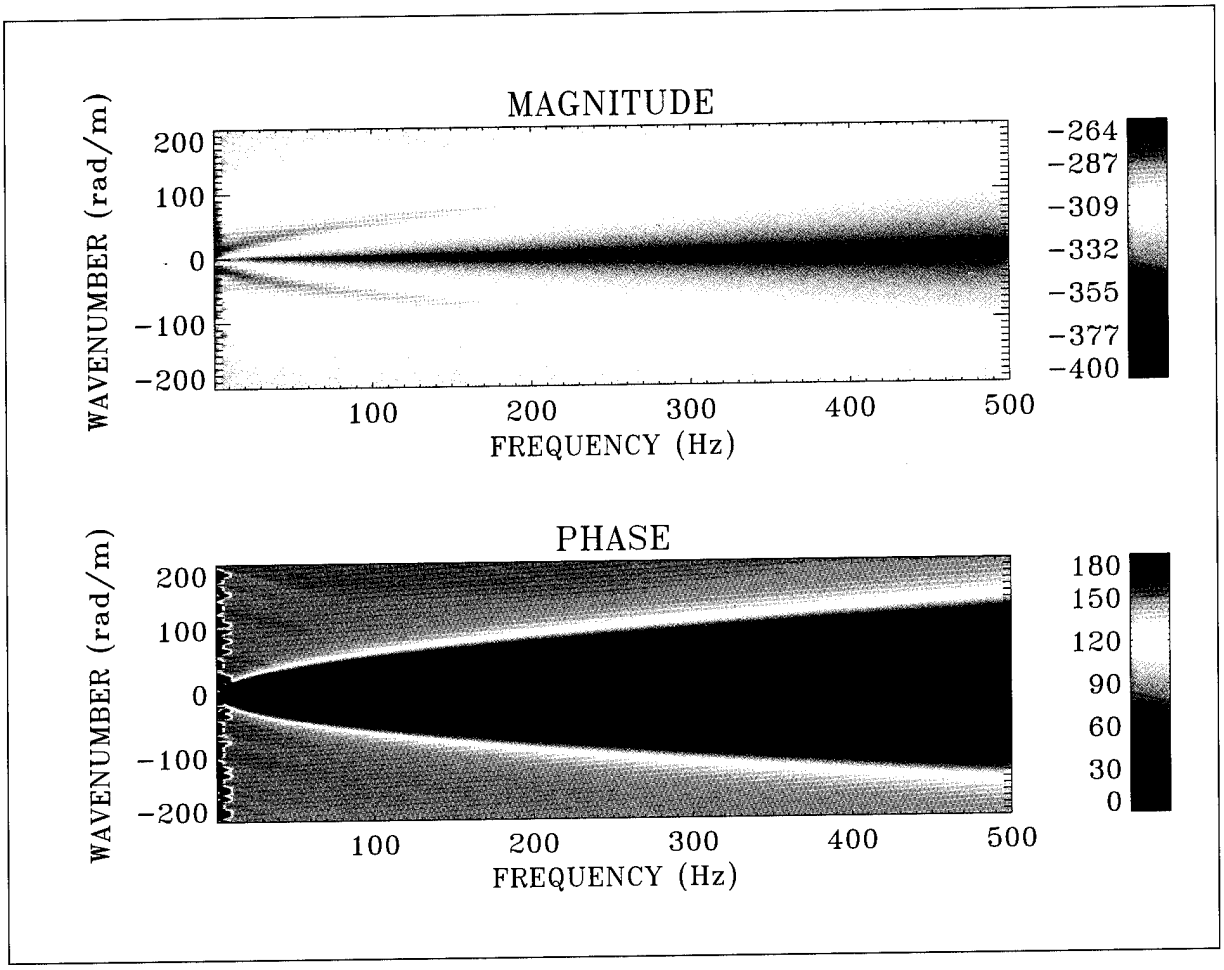


**Figure 65. Optical Phase Sensitivity Transfer Surface: Magnitude = 10Log($\Delta\phi/\phi/P_o$)$^2$ and Phase in Degrees (Two Layers, $n$ = 1)**

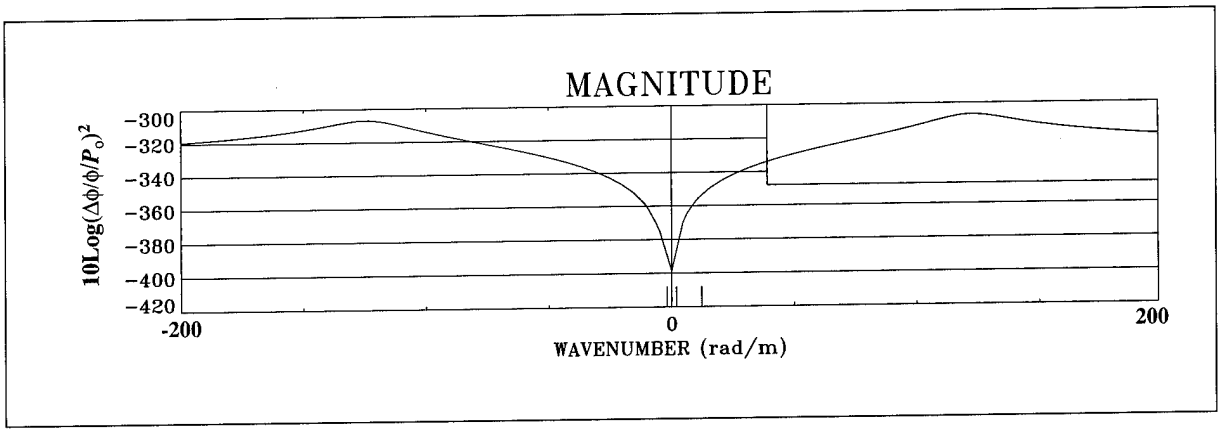


**Figure 66. Frequency Cut at 453.19 Hz Through the Magnitude Surface of Figure 65**

*Nonaxisymmetric Longitudinal Shear Stress Excitation (n = 1), Two Layers*

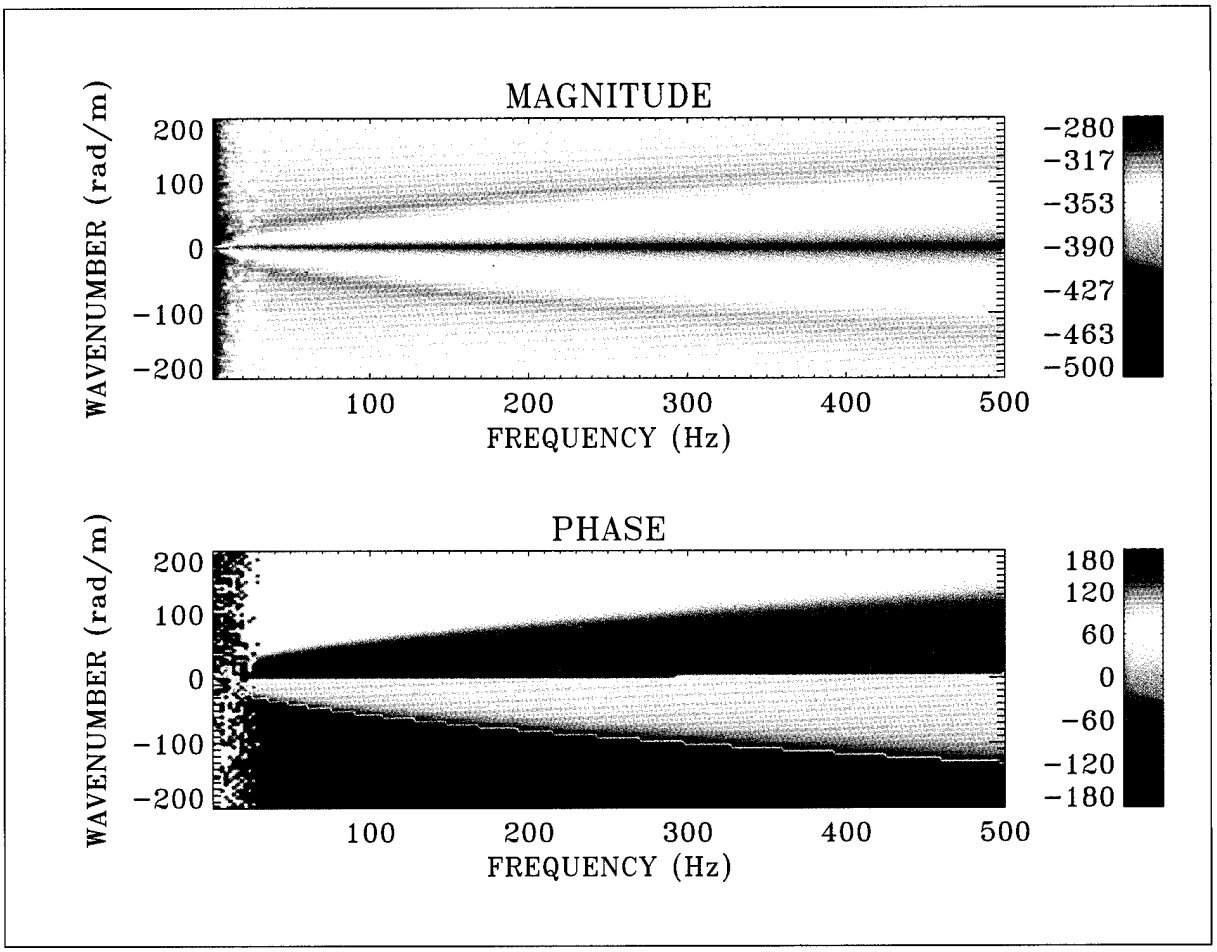


**Figure 67. Radial Strain Transfer Surface: Magnitude = 10Log($\varepsilon_{rr}/P_x$)$^2$ and Phase in Degrees (Two Layers, $n$ = 1)**

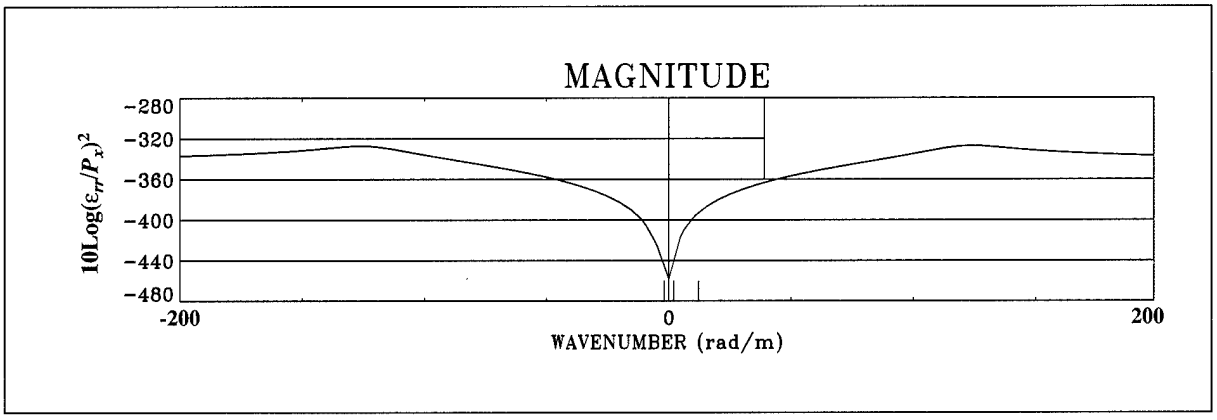


**Figure 68. Frequency Cut at 453.19 Hz Through the Magnitude Surface of Figure 67**

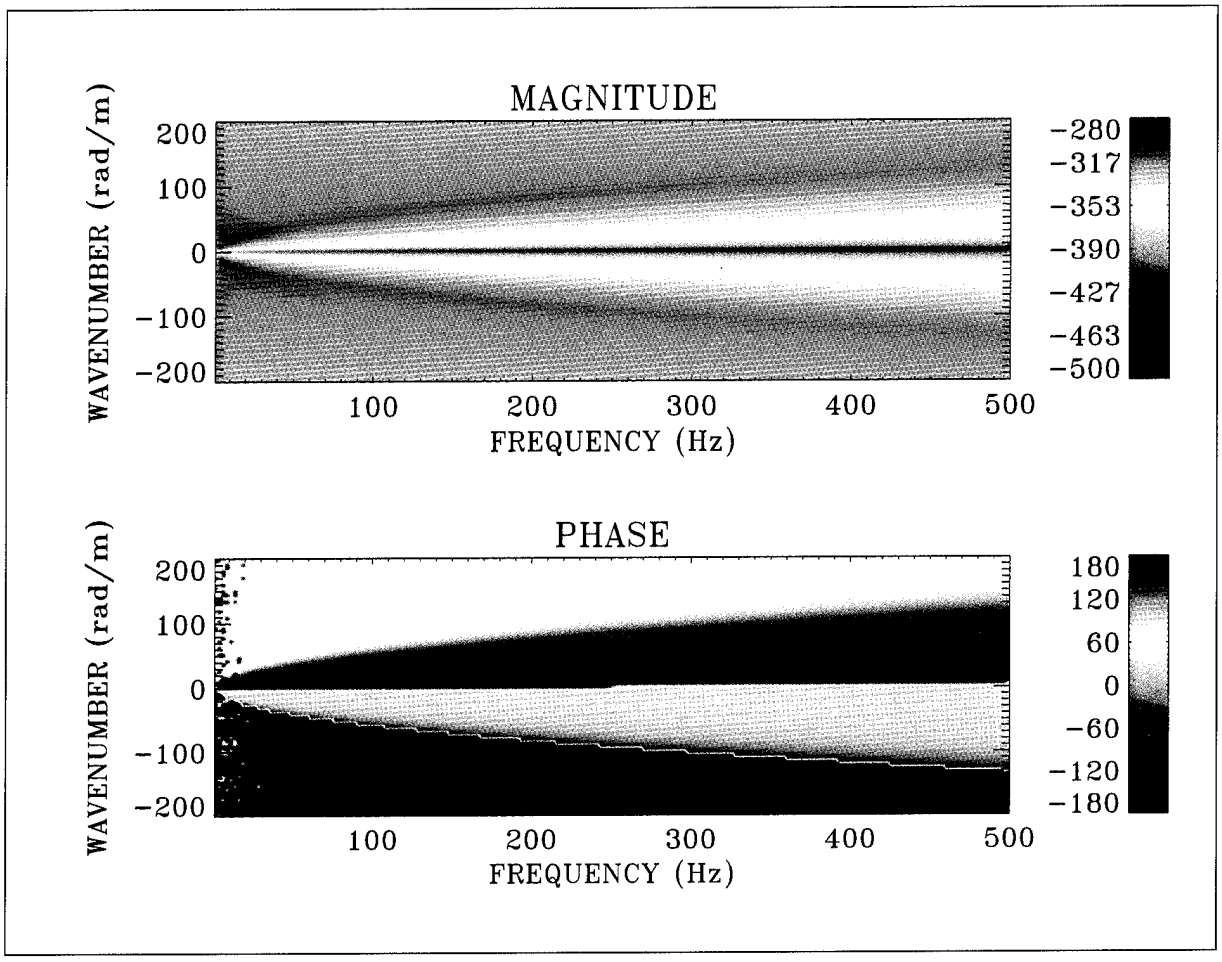


**Figure 69. Circumferential Strain Transfer Surface: Magnitude = 10Log($\varepsilon_{\theta\theta}/P_x$)$^2$ and Phase in Degrees (Two Layers, $n$ = 1)**

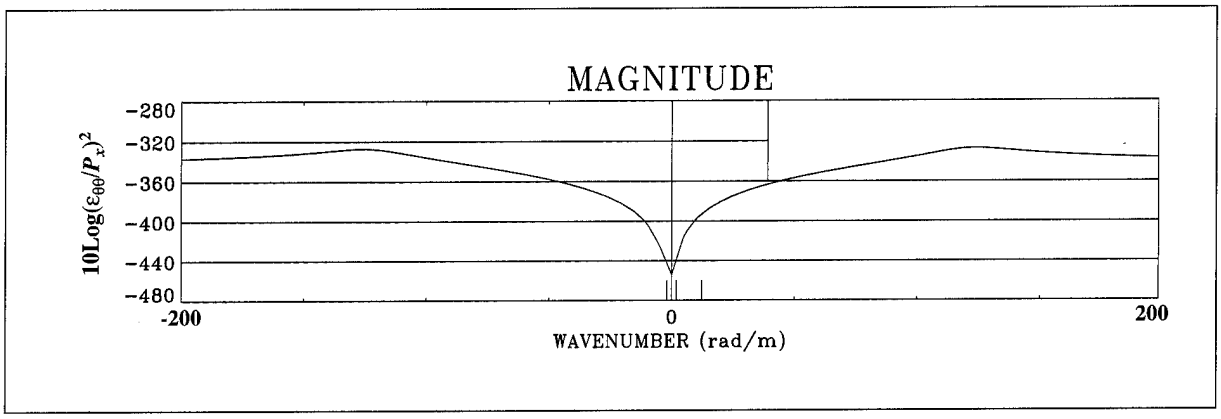


**Figure 70. Frequency Cut at 453.19 Hz Through the Magnitude Surface of Figure 69**

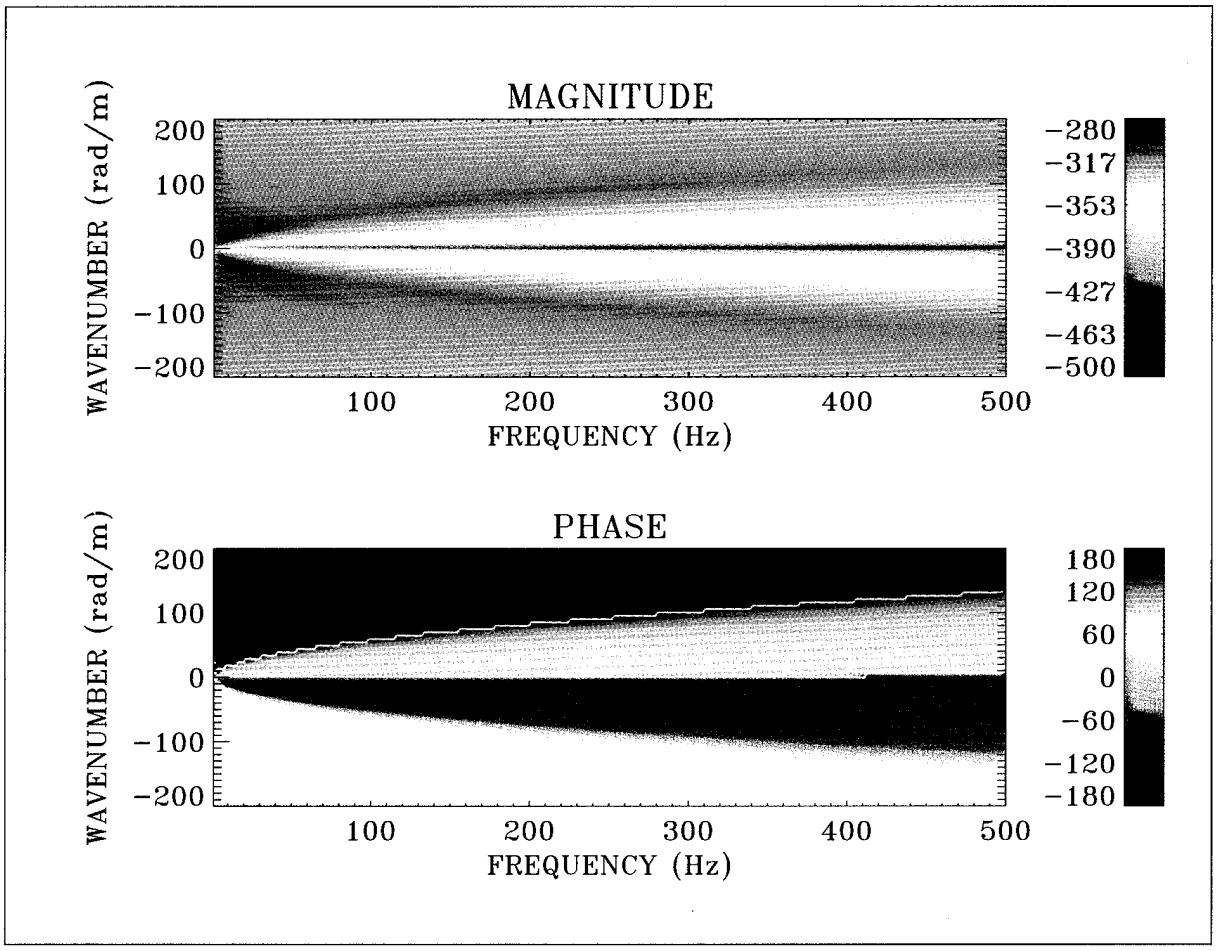


**Figure 71. Longitudinal Strain Transfer Surface: Magnitude = 10Log($\varepsilon_{xx}/P_x$)$^2$ and Phase in Degrees (Two Layers, $n$ = 1)**

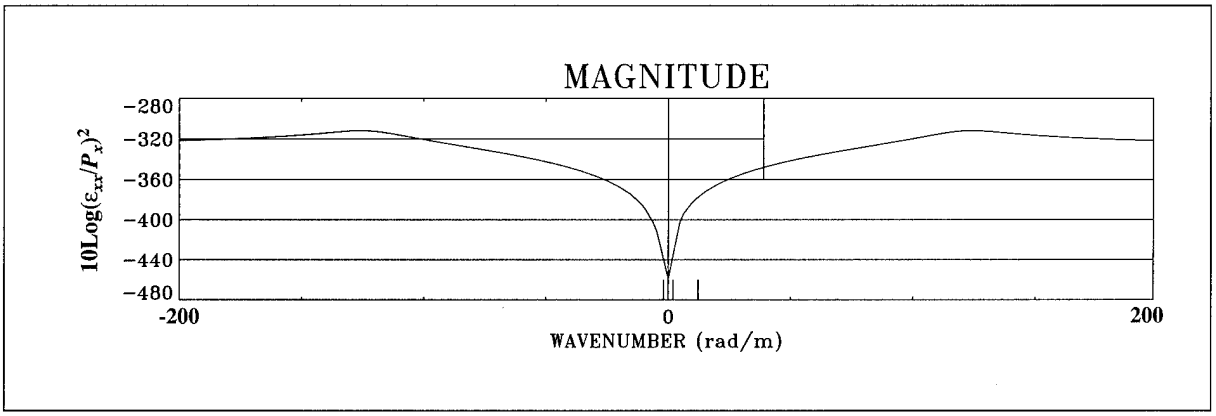


**Figure 72. Frequency Cut at 453.19 Hz Through the Magnitude Surface of Figure 71**

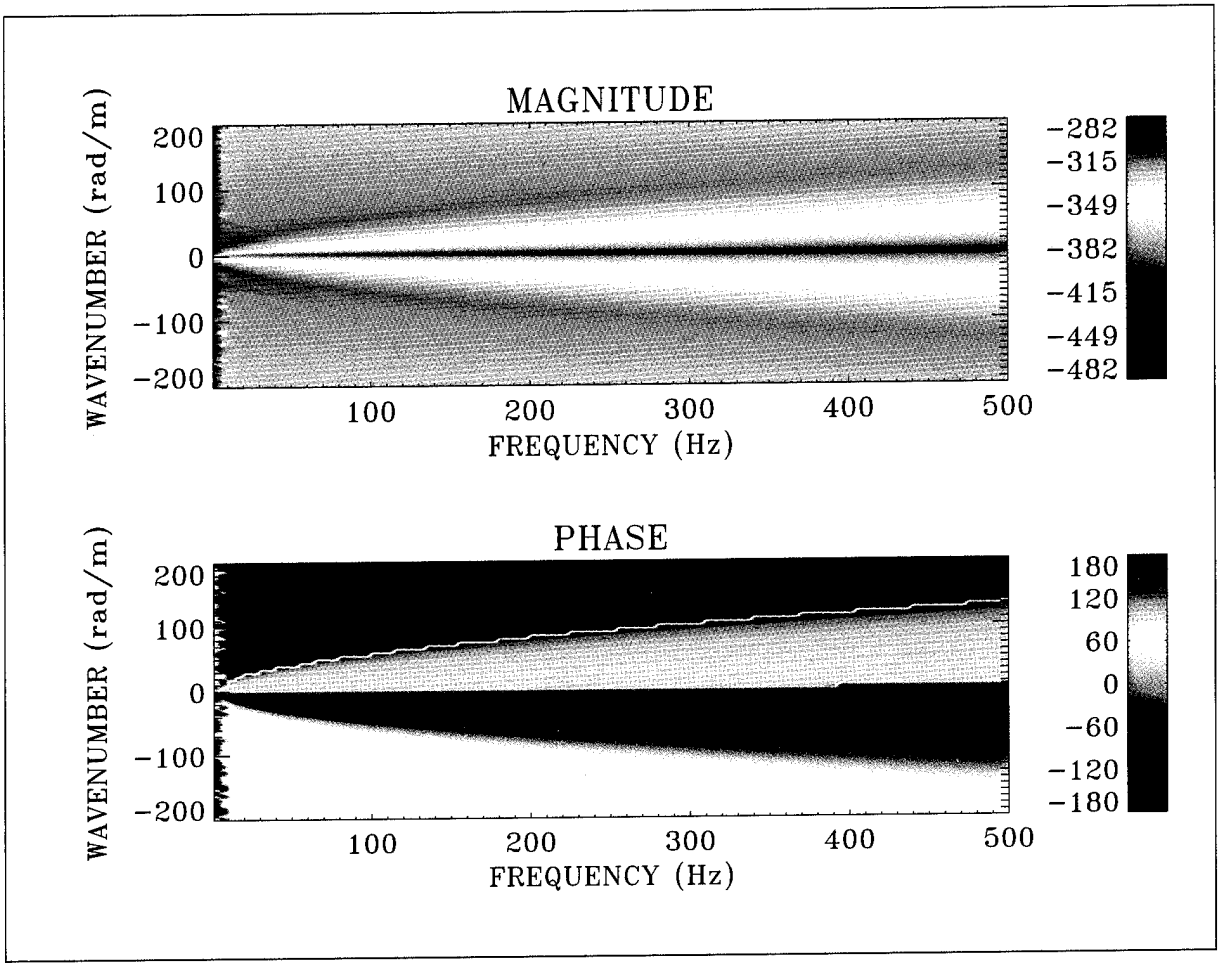


**Figure 73. Optical Phase Sensitivity Strain Transfer Surface: Magnitude = $10\text{Log}(\Delta\phi/\phi/P_x)^2$ and Phase in Degrees (Two Layers, $n = 1$)**

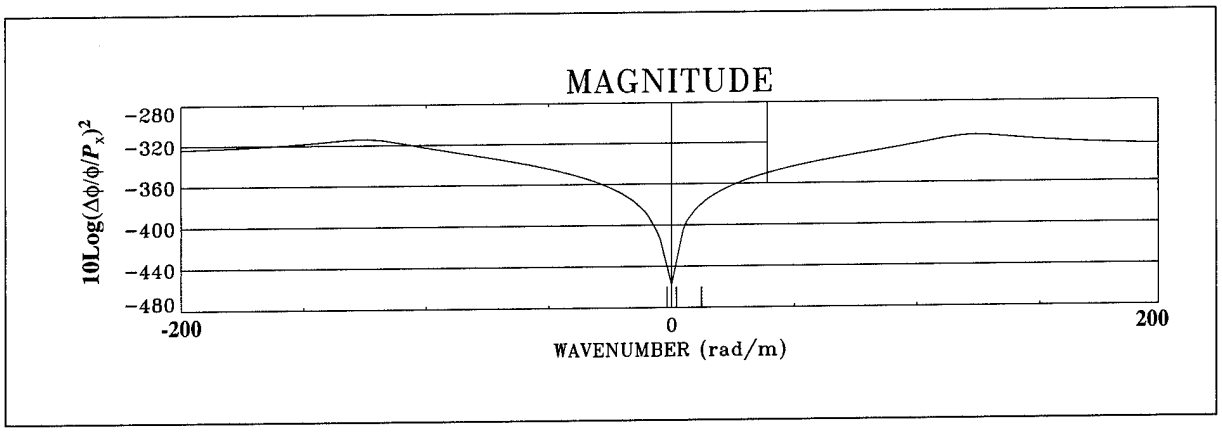


**Figure 74. Frequency Cut at 453.19 Hz Through the Magnitude Surface of Figure 73**

*Nonaxisymmetric Circumferential Shear Stress Excitation (n = 1), Two Layers*

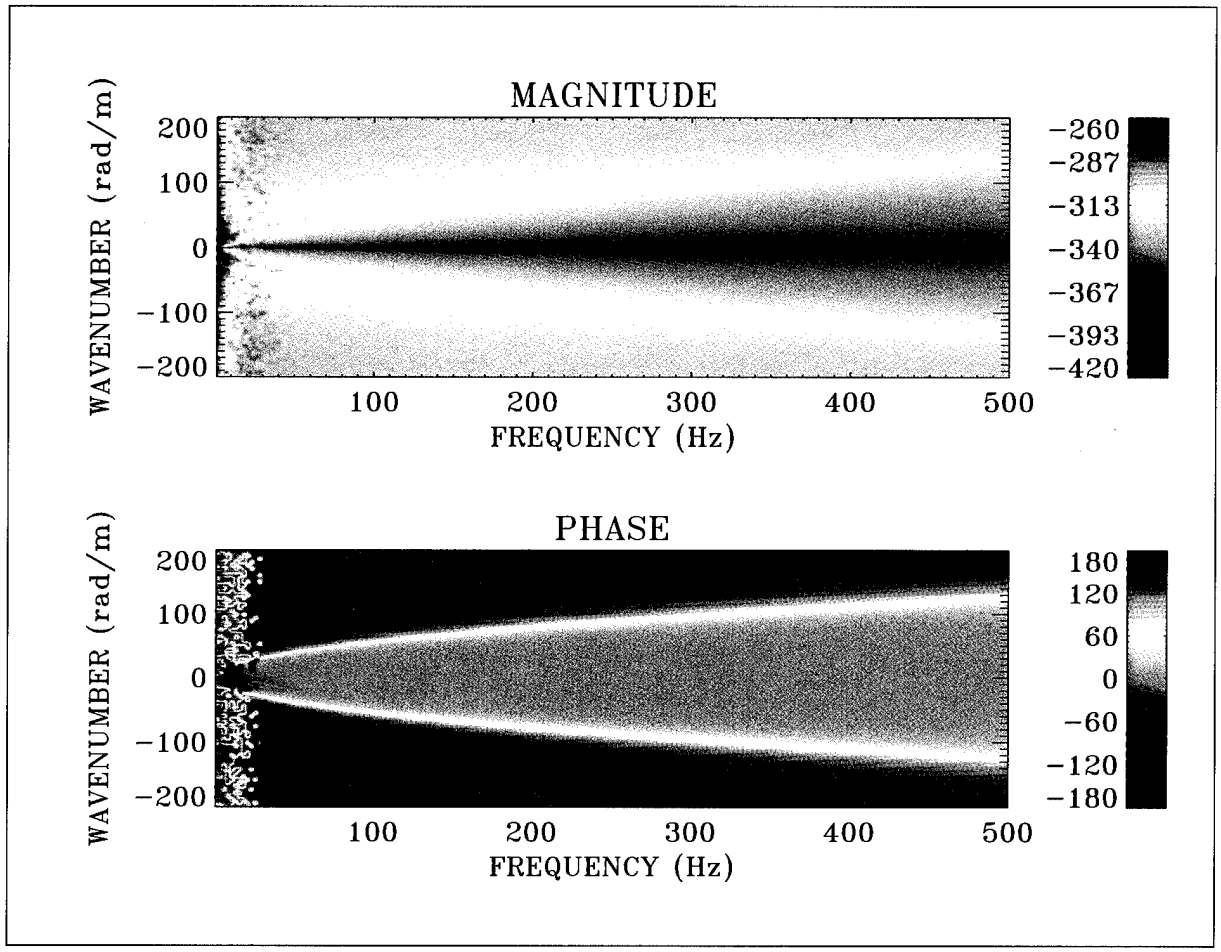


**Figure 75. Radial Strain Transfer Surface: Magnitude = 10Log($\varepsilon_{rr}/P_\theta$)$^2$ and Phase in Degrees (Two Layers, $n$ = 1)**

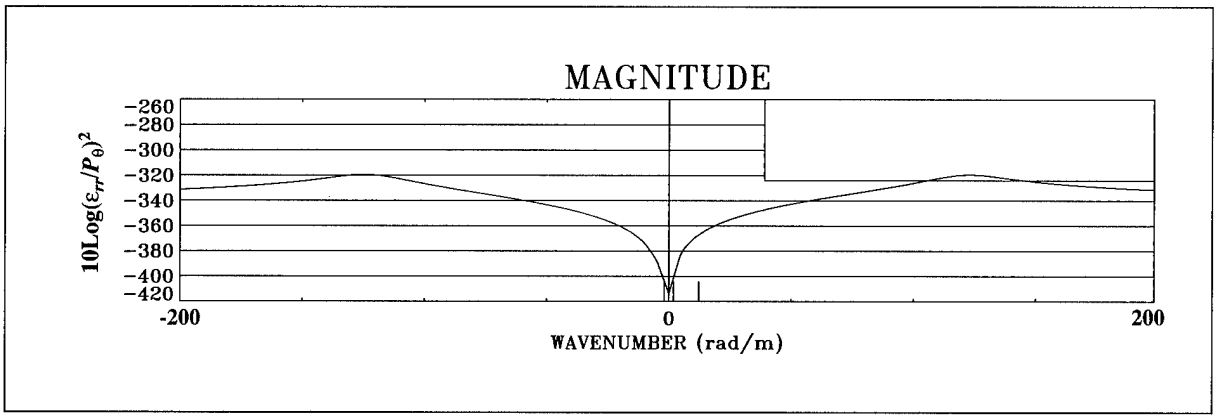


**Figure 76. Frequency Cut at 453.19 Hz Through the Magnitude Surface of Figure 75**

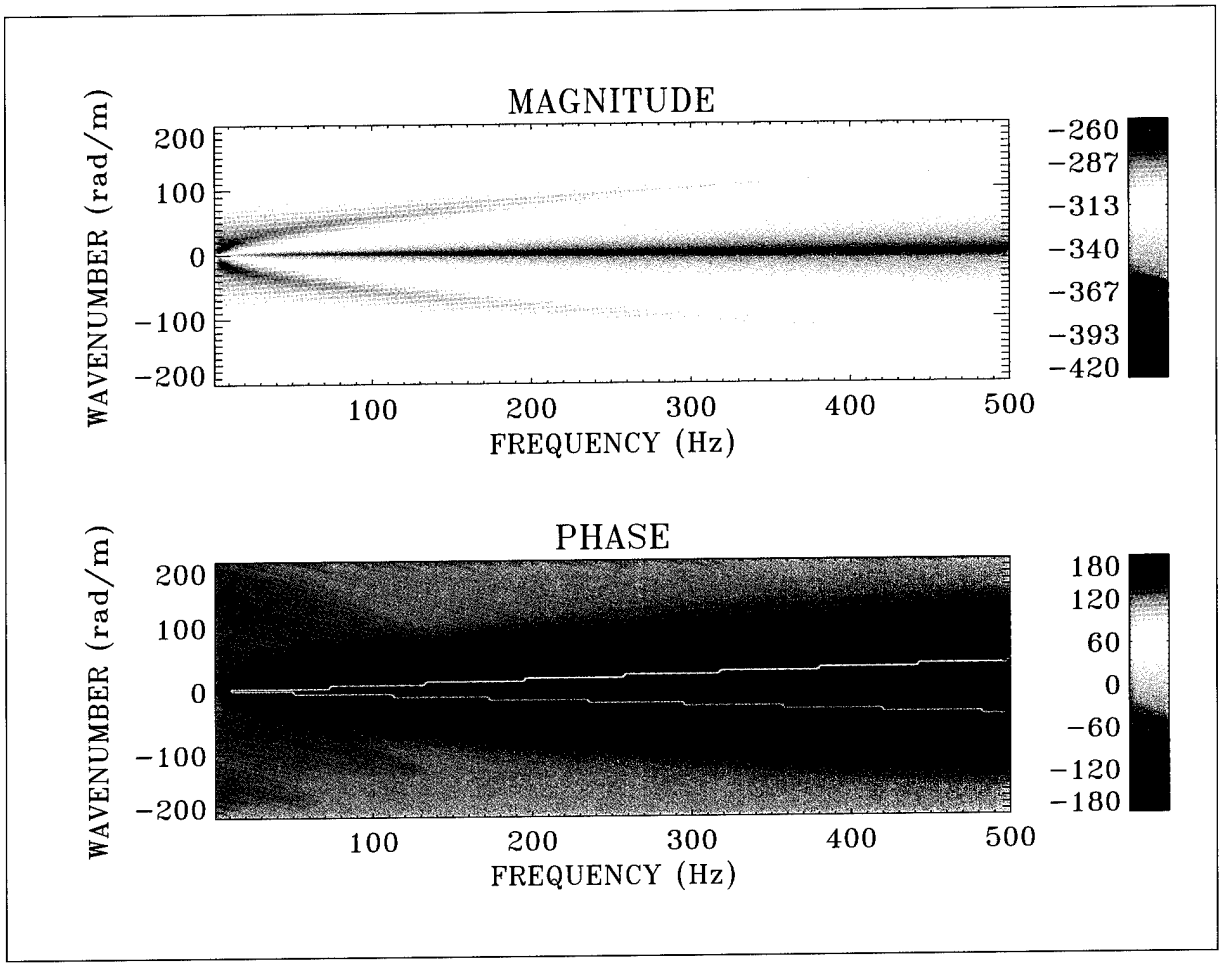


**Figure 77. Circumferential Strain Transfer Surface: Magnitude = $10\text{Log}(\varepsilon_{\theta\theta}/P_\theta)^2$ and Phase in Degrees (Two Layers, $n$ = 1)**

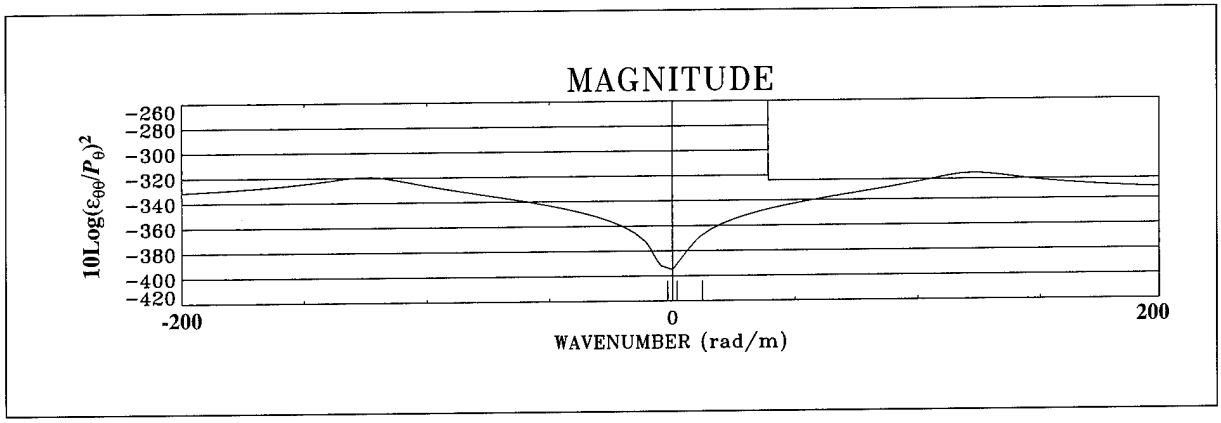


**Figure 78. Frequency Cut at 453.19 Hz Through the Magnitude Surface of Figure 77**

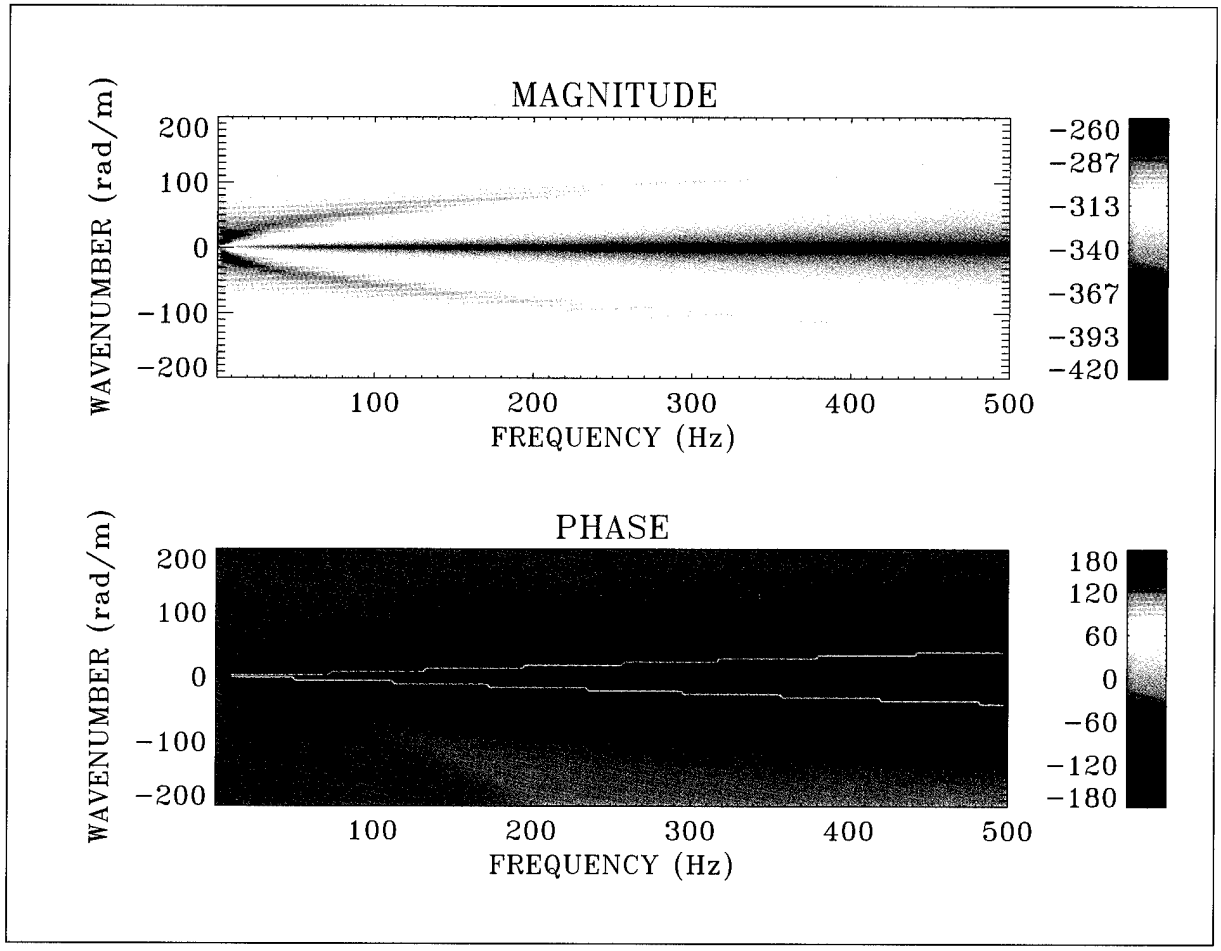


**Figure 79. Longitudinal Strain Transfer Surface: Magnitude = 10Log($\varepsilon_{xx}/P_0$)$^2$ and Phase in Degrees (Two Layers, $n$ = 1)**

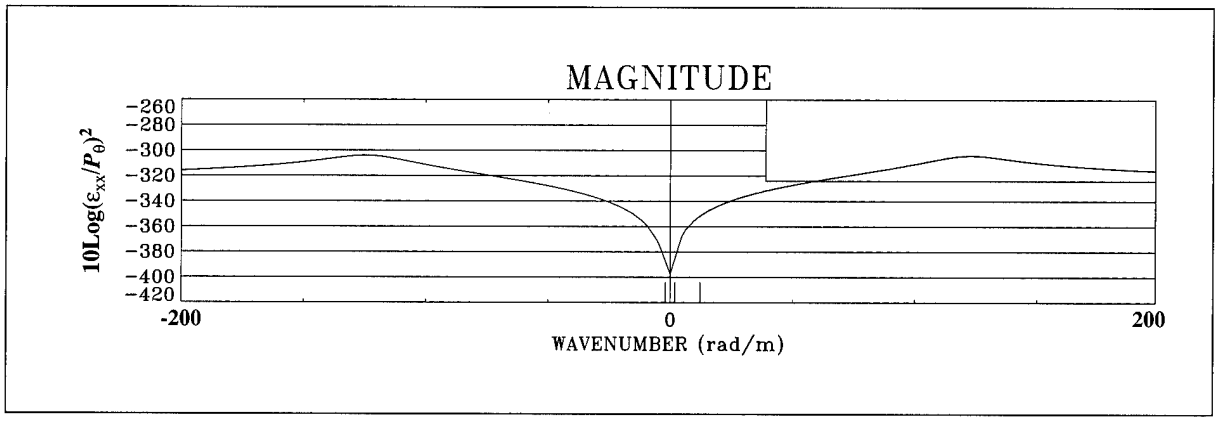


**Figure 80. Frequency Cut at 453.19 Hz Through the Magnitude Surface of Figure 79**

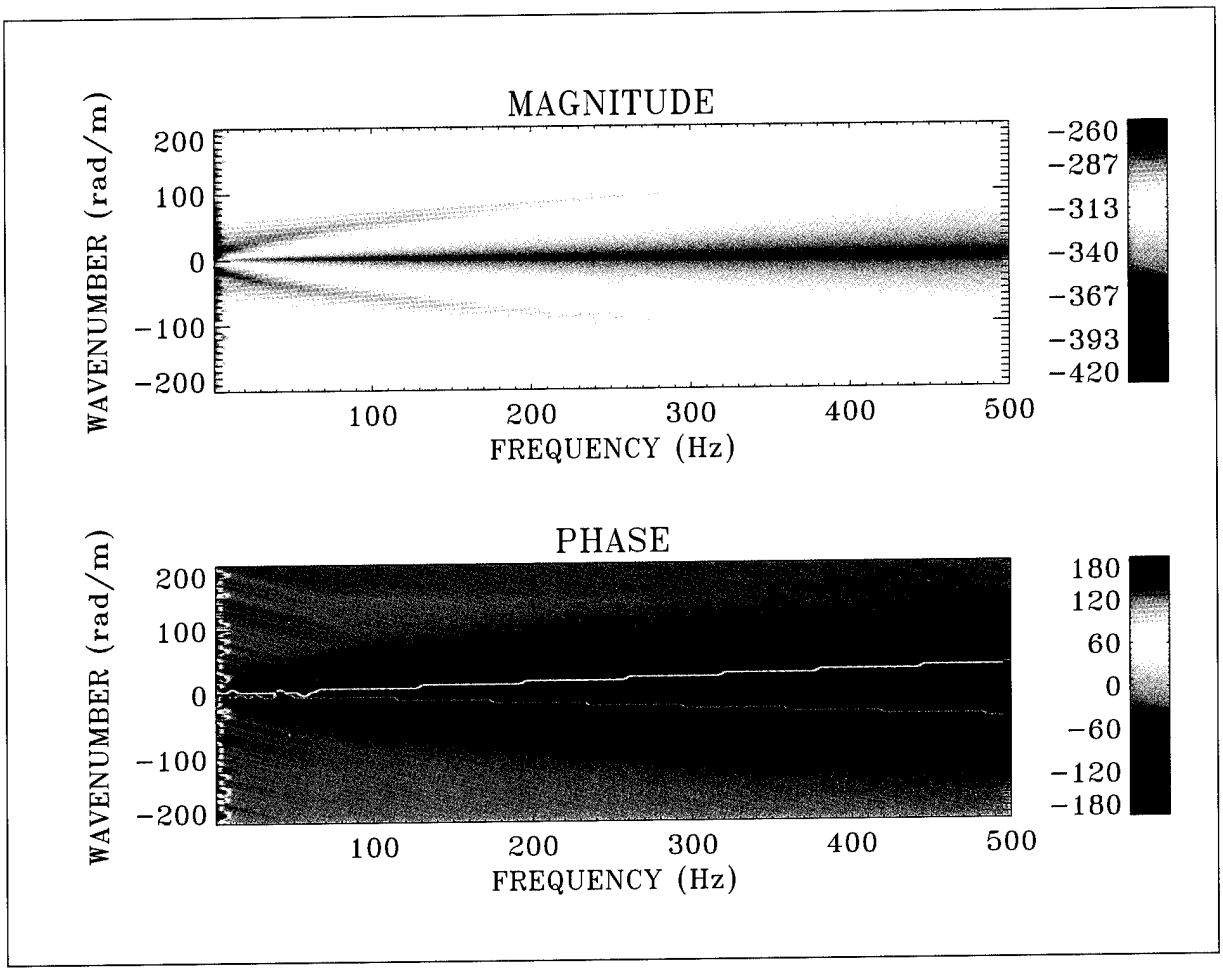


**Figure 81. Optical Phase Sensitivity Transfer Surface: Magnitude = $10\text{Log}(\Delta\phi/\phi/P_\theta)^2$ and Phase in Degrees (Two Layers, $n$ = 1)**

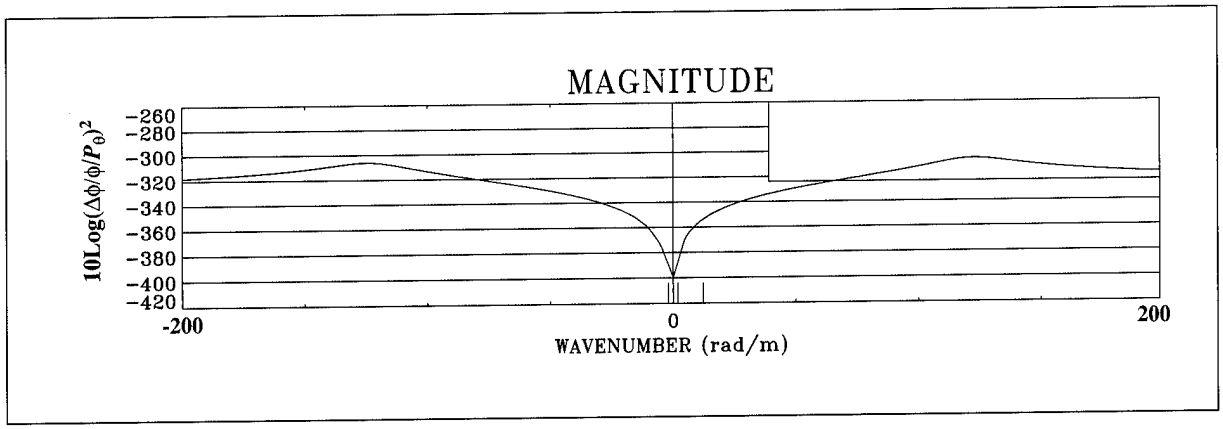


**Figure 82. Frequency Cut at 453.19 Hz Through the Magnitude Surface of Figure 81**

## EFFECTS OF THE SECOND LAYER

We will now consider the effects of a coating on the optical phase sensitivity of a bare and coated optical fiber subject to a harmonic radial pressure excitation $P_o$. The application of a coating results in an effect that is similar to what occurs when there is a variation in Poisson ratio (figure 41).

Figure 83 compares the optical phase sensitivity for a bare and coated optical fiber by overlaying cuts through figures 15 and 48 at 40 Hz. The wavenumbers corresponding to acoustic propagation speeds for directions parallel to the longitudinal axis of the fiber are indicated on figure 83 for both air and water. The foremost effect of the coating is to increase the

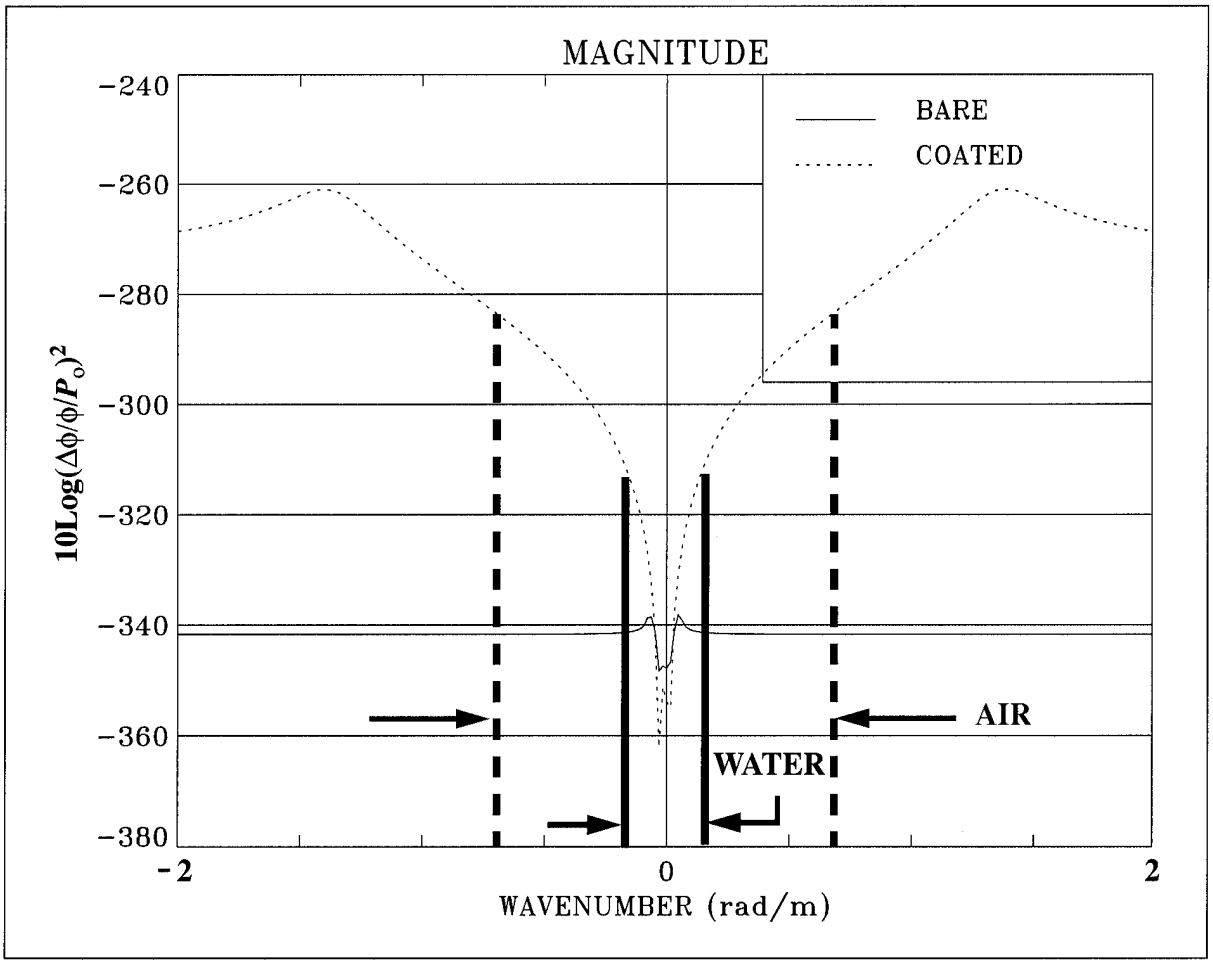


**Figure 83. Comparison of Optical Phase Sensitivity for a Bare and Coated Fiber at 40 Hz**

optical phase sensitivity of the optical fiber in the region of the extensional wave resonance. The optical phase sensitivity is much lower, approximately 80 dB, in the wavenumber region corresponding to that of the bare optical fiber extensional wave. The choice of optical phase sensitivity for this discussion is arbitrary; the comments are equally valid for any one of the strain components since the optical phase sensitivity depends on the strains as given by equation (198).

# CONCLUSIONS

From first principles, in the field of dynamic elasticity, a model has been derived for the steady state response of a two-layer infinite elastic solid cylinder in contact with an infinite outer fluid subject to forced harmonic excitation at the solid/fluid interface. The cylinders are treated as viscoelastic solids, and the fluid is treated as an inviscid ideal fluid. Both axisymmetric and nonaxisymmetric excitations are included in the analysis.

The solution is a closed form analytical result to the point of assembly of the dynamic system matrix. The system matrix is evaluated numerically at each discrete point in the wavenumber-frequency domain for the field parameters, displacements, strains, stresses, velocities, and fluid pressure. The elasticity model used for the cylinder is quite robust and will accurately describe the behavior of a wide class of materials whose mechanical properties can be described by two of the following macroscopic material properties: Young's modulus, Poisson ratio, or shear modulus. These materials range from closed-cell foam to optical glass fiber.

The simulations presented are for the single cylinder with an outer fluid and a double cylinder with an outer fluid. The simulations for the single cylinder were performed using material properties consistent with those of optical glass fiber. Two excitations ($P_o$ and $P_x$) were used for these simulations at two different circumferential order numbers ($n$ = 0 and $n$ = 1). The first branch of wave propagation supported by the single cylinder of optical glass fiber is the extensional wave, with energy propagating at a phase velocity of 5571 m/sec. From these simulations, it is evident that the strain and optical phase sensitivity (in the fiber) to longitudinal shear stress is 30 to 110 dB greater than the fiber sensitivity to radial pressure excitation. At the extensional wave resonance peak, the shear stress sensitivity is in excess of 110 dB. At the edge of the acoustic cone, the shear stress sensitivity is in excess of 70 dB, and at broadside ($k$ = 0), this excess is 30 dB. This analysis states that the sensitivity of the optical fiber to shear stress is five orders of magnitude higher than its sensitivity to radial pressure. Therefore, the radial pressure response will be dominated by the response to shear stress.

Two nonaxisymmetric simulations have been performed for circumferential order number

$n = 1$: $P_o$ and $P_x$. These excitations result in branches of dispersive wave propagation. Energy propagating in the $n = 1$ branches travels at a much slower rate than energy propagating in the $n = 0$ branches. For the $n = 1$ case, the phase velocity ranges from 12 to 20 m/sec over the frequency range from 1 to 500 Hz. The $n = 1$ excitations produce a deformation, principally in the $rx$-plane of the cylinder, whereas the principal deformation of the $n = 0$ excitation is in the longitudinal $x$-direction. For the $n = 1$ case, the magnitude of the strains produced by the longitudinal shear stress excitation is 20 to 100 dB smaller than the magnitude of the strains produced by the $n = 1$ radial pressure excitation.

The simulations performed with the double cylinder model were used to analyze the dynamic response of the optical glass fiber coated with ALCRYN. The dynamic material properties for the Young's modulus of ALCRYN were measured with a Metravib dynamic mechanical analyzer at the Naval Undersea Warfare Center Detachment in New London, Connecticut. The $P_o$ and $P_x$ excitations at $n = 0$ produce extensional wave responses that have been slowed to 190 m/sec. The reduction in extensional wave speed occurs because the ALCRYN coating contributes mass with a negligible contribution to the stiffness of the composite. A comparison of the optical phase sensitivity to radial pressure and to longitudinal shear stress reveals a shear stress response 50 to 70 dB greater than the radial pressure response. This result is consistent with that for the bare fiber.

The Poisson ratio exerts an interesting effect on the dynamic behavior of the cylinder. As the value of the Poisson ratio increases, the relative difference between the value of $10\text{Log}(\varepsilon_{rr}/P_o)^2$ at $k = 0$ and the value of $10\text{Log}(\varepsilon_{rr}/P_o)^2$ above the extensional wave resonance (flat plateau) increases (figure 41). In the limit of $\nu_c = 0$, the extensional wave vanishes under a $P_o$ excitation. This behavior is consistent with the fact that the $P_o$ excitation develops an extensional wave response, which is a transverse response to the applied force, only when there is a means of coupling energy from one direction into the corresponding perpendicular direction.

Similar to the effect that an increasing value of the Poisson ratio has on the single cylinder, a second cylinder with differing material properties from the first serves to increase the strain and optical phase sensitivity in comparison to the bare optical fiber in the region of the extensional

wave resonance peak (figure 83). Very little change occurs near $k = 0$ for this infinite cylinder formulation.

# REFERENCES


1. A. N. Holden, "Longitudinal Modes of Elastic Waves in Isotropic Cylinders and Slabs," *Bell Systems Technical Journal*, vol. 30, 1951, pp. 956-969.

2. R. K. Kaul and J. J. McCoy, "Propagation of Axisymmetric Waves in a Circular Semi-Infinite Elastic Rod," *Journal of the Acoustical Society of America*, vol. 36, 1964, pp. 653-660.

3. N. Lagakos and J. A. Bucaro, "Pressure Desensitization of Optical Fibers," *Applied Optics*, vol. 20, no. 15, 1981, pp. 2716-2720.

4. A. J. Hull, "The Phase Sensitivity of an Infinite Length Optical Fiber Subjected to a Forcing Function at a Definite Frequency and Wavenumber," NUWC-NPT Technical Report 10,853 Naval Undersea Warfare Center Detachment, New London, CT, April 1995.

5. J. D. Achenbach, *Wave Propagation in Elastic Solids,* Elsevier Publishing Company, Inc., New York, 1990, pp. 55-56.

6. J. D. Achenbach, p. 65.

7. J. D. Achenbach, p. 54.

8. J. D. Achenbach, pp. 238-239.

9. J. D. Achenbach, pp. 239-240.

10. J. D. Achenbach, pp. 73-75.

11. J. D. Achenbach, p. 78.

12. W. M. Ewing, W. S. Jardetzky, and F. Press, *Elastic Waves in Layered Media*, Mc-Graw Hill Book Company, Inc., New York, 1957, p. 317.

13. M. C. Junger and D. Feit, *Sound, Structures and Their Interaction*, Cambridge, MA, The MIT Press, 1986, p. 167.

14. N. Lagakos and J. A. Bucaro, pp. 2716-2720.

15. M. S. Peloquin, "FORTRAN Algorithms for the Three-Dimensional Solution of Two-Layer Solid and Hollow Cylinder Dynamic Elasticity Problems With and Without Fluids," NUWC-NPT Technical Document 11,065 Naval Undersea Warfare Center Detachment, New London, CT (To Be Published).

# APPENDIX A

## BESSEL FUNCTIONS OF COMPLEX ARGUMENT, SERIES REPRESENTATION

The inclusion of structural damping in the cylinder necessitates the evaluation of Bessel functions of complex argument. The series representation of these functions is then required. From Abramowitz and Stegun,[1] equations (A-1) through (A-6) are used for complex argument $z$, where $z$ ranges from $0 \le z \le 3$. The circumferential order number $n$ appears in the equations as well.

The Gamma[2] function is given by

$$\Gamma(n+K+1) = (n+K)!. \tag{A-1}$$

The Psi[3] or Digamma function is

$$\psi(1) = -\gamma, \qquad \psi(n) = -\gamma + \sum_{k=1}^{n-1} k^{-1}, \qquad n \ge 2 . \tag{A-2}$$

The value used for Euler's constant is $\gamma = 0.57721566490153286060606512$.

The Bessel function of the first[4] kind is

$$J_n(z) = \left(\frac{z}{2}\right)^n \sum_{k=0}^{\infty} \frac{\left(\left(-\frac{1}{4}\right)z^2\right)^k}{k!\Gamma(n+k+1)}. \tag{A-3}$$

---

1. M. Abramowitz and I. A. Stegun, *Handbook of Mathematical Functions*, U.S. Government Printing Office, Washington, DC, June 1964.
2. M. Abramowitz and I. A. Stegun, p. 255, equation 6.1.6.
3. M. Abramowitz and I. A. Stegun, p. 258, equation 6.3.2.
4. M. Abramowitz and I. A. Stegun, p. 360, equation 9.1.10.

The Bessel function of the second[5] kind over the range $0 < z \leq 3$ is

$$Y_n(z) = \left(-\frac{\left(\frac{z}{2}\right)^n}{\pi}\right)\left(\sum_{k=0}^{n-1}\frac{(n-k-1)!}{k!}\right)\left(\frac{1}{4}z^2\right)^k + \frac{2}{\pi}\ln\left(\frac{z}{2}\right)J_n(z)$$

$$-\frac{\left(\frac{z}{2}\right)^n}{\pi}\sum_{k=0}^{\infty}\left(\psi(k+1)+\psi(n+k+1)\right)\frac{\left(\left(-\frac{1}{4}\right)z^2\right)^k}{k!\,(n+k)!}. \qquad \text{(A-4)}$$

The Hankel function[6] of the first kind is given by

$$H_n^{(1)}(z) = J_n(z) + iY_n(z). \qquad \text{(A-5)}$$

The expression[7] used for the modified Bessel function $I_n$ over the range $0 \leq z \leq 3$ is

$$I_n(z) = \left(\frac{z}{2}\right)^n\sum_{k=0}^{\infty}\frac{\left(\left(\frac{1}{4}\right)z^2\right)^k}{k!\,\Gamma(n+k+1)}. \qquad \text{(A-6)}$$

The expression[8] used for the modified Bessel function $K_n$ over the range $0 < z \leq 3$ is

$$K_n(z) = \frac{1}{2}\left(\frac{1}{2}z\right)^{-n}\left(\sum_{k=0}^{n-1}\frac{(n-k-1)!}{k!}\right)\left(\left(-\frac{1}{4}\right)z^2\right)^k + (-1)^{n+1}\ln\left(\frac{z}{2}\right)I_n(z)$$

$$\left(+(-1)^n\left(\frac{z}{2}\right)^n\right)\left(\sum_{k=0}^{\infty}\left(\psi(k+1)+\psi(n+k+1)\right)\right)\frac{\left(\frac{1}{4}z^2\right)^k}{k!\,(n+k)!}. \qquad \text{(A-7)}$$

---

5. M. Abramowitz and I. A. Stegun, p. 360, equation 9.1.11.
6. M. Abramowitz and I. A. Stegun, p. 358, equation 9.1.3.
7. M. Abramowitz and I. A. Stegun, p. 375, equation 9.6.10.
8. M. Abramowitz and I. A. Stegun, p. 375, equation 9.6.11.

For the argument range $3 < z < \infty$, asymptotic expansions are used from Korn and Korn:[9]

$$J_n(z) = \sqrt{\frac{2}{\pi z}}\left(A_n(z)\cos\left(z - \frac{n\pi}{2} - \frac{\pi}{4}\right) - B_n(z)\sin\left(z - \frac{n\pi}{2} - \frac{\pi}{4}\right)\right) \tag{A-8}$$

and

$$Y_n(z) = \sqrt{\frac{2}{\pi z}}\left(A_n(z)\sin\left(z - \frac{n\pi}{2} - \frac{\pi}{4}\right) + B_n(z)\cos\left(z - \frac{n\pi}{2} - \frac{\pi}{4}\right)\right), \tag{A-9}$$

where

$$A_n(z) = 1 - \frac{(4n^2-1)(4n^2-9)}{2!(8z)^2} + \frac{(4n^2-1)(4n^2-9)(4n^2-25)(4n^2-49)}{4!(8z)^4} \mp \ldots,$$

and

$$B_n(z) = \frac{4n^2-1}{8z} - \frac{(4n^2-1)(4n^2-9)(4n^2-25)}{3!(8z)^3} \pm \ldots \tag{A-10}$$

9. G. A. Korn and T. M. Korn, *Mathematical Handbook for Scientists and Engineers*, McGraw-Hill Book Company, New York, pp. 868-869, equations 21.8-44 and 21.8.45.

# APPENDIX B

## DERIVATIVES OF BESSEL FUNCTIONS

An expression for the first derivative of the Bessel functions needed for the evaluation of the displacement potentials is taken from Arpaci,[1] and is listed here as equations (B-1) and (B-2):

$$\frac{d}{dx}(Z_n(\alpha x)) = -\alpha Z_{n+1}(\alpha x) + \frac{n}{x}Z_n(\alpha x), \qquad Z = J, Y, K, H^{(1)}, H^{(2)} \tag{B-1}$$

and

$$\frac{d}{dx}(I_n(\alpha x)) = \alpha I_{n+1}(\alpha x) + \frac{n}{x}I_n(\alpha x) . \tag{B-2}$$

The argument of the Bessel functions is composed of $\alpha$ (a constant) and $x$ (a complex number).

An expression for the second derivative of the Bessel functions listed in equation (B-1) is derived by differentiating this equation again with respect to $x$, which requires the use of the product rule on the second term of the right-hand side of equation (B-1) and the following effect of the recursion relationships for Bessel functions:

$$\frac{d}{dx}(Z_{n+1}(\alpha x)) = -\alpha Z_{n+2}(\alpha x) + \frac{n+1}{x}Z_{n+1}(\alpha x), \qquad Z = J, Y, K, H^{(1)}, H^{(2)} \tag{B-3}$$

.

The final expression for the second derivative is

$$\frac{\partial^2}{\partial x^2}Z_n(\alpha x) = \frac{\alpha^2}{4}(Z_{n-2}(\alpha x) - (2Z_n(\alpha x) + Z_{n+2}(\alpha x))) \qquad Z = J, Y, K, H^{(1)}, H^{(2)} . \tag{B-4}$$

---

1. V. S. Arpaci, *Conduction Heat Transfer*, Addison-Wesley Publishing Company, Reading, MA, p. 139, equation (3-139).

# INITIAL DISTRIBUTION LIST

| Addressee | No. of Copies |
|---|---|
| Defense Technical Information Center | 12 |
| Office of Naval Research (Code 321SS: K. Dial, S. Littlefield, R. Varley) | 3 |
| Naval Research Laboratory (A. Dandridge, S. Vohra) | 2 |
| Cambridge Acoustical Associates (J. Garrelick, J. Cole III) | 2 |
| Applied Measurement Systems, Inc., New London (J. Diggs) | 1 |